The Pennsylvania State University

The Graduate School

Department of Civil and Environmental Engineering

SUSTAINABLE RESOURCE RECOVERY AND ENERGY CONVERSION PROCESSES USING MICROBIAL ELECTROCHEMICAL TECHNOLOGIES

A Dissertation in

Civil and Environmental Engineering

by

Matthew D. Yates

Submitted in Partial Fulfillment
of the Requirements
for the Degree of

Doctor of Philosophy

August 2014

The dissertation of Matthew Yates was reviewed and approved* by the following:

Bruce E. Logan
Kappe Professor of Environmental Engineering & Evan Pugh Professor
Dissertation Advisor
Chair of Committee

John M. Regan
Professor of Environmental Engineering

Christopher A. Gorski
Assistant Professor of Civil Engineering

Ming Tien
Professor of Biochemistry

Peggy Johnson
Professor of Civil Engineering
Head of the Department of Civil and Environmental Engineering

*Signatures are on file in the Graduate School

ABSTRACT

Microbial Electrochemical Technologies (METs) are emerging technological platforms for the conversion of waste into usable products. METs utilize naturally occurring bacteria, called exoelectrogens, capable of transferring electrons to insoluble terminal electron acceptors. Electron transfer processes in the exoelectrogen *Geobacter sulfurreducens* were exploited here to develop sustainable processes for synthesis of industrially and socially relevant end products. The first process examined was the removal of soluble metals from solution to form catalytic nanoparticles and nanoporous structures. The second process examined was the biocatalytic conversion of electrons into hydrogen gas using electrons supplied directly to an electrode.

Nanoparticle formation is desirable because materials on the nanoscale possess different physical, optical, electronic, and mechanical properties compared to bulk materials. In the first process, soluble palladium was used to form catalytic palladium nanoparticles using extracellular electron transfer (EET) processes of *G. sulfurreducens*, typically the dominant member of mixed-culture METs. *Geobacter* cells reduced the palladium extracellularly using naturally produced pili, which provided extracellular adsorption and reduction sites to help delay the diffusion of soluble metals into the cell. The extracellular reduction prevented cell inactivation due to formation of intracellular particles, and therefore the cells could be reused in multiple palladium reduction cycles.

A *G. sulfurreducens* biofilm was next investigated as a biotemplate for the formation of a nanoporous catalytic palladium structure. *G. sulfurreducens* biofilms have a dense network of pili and extracellular cytochromes capable of high rates of electron transfer directly to an electrode surface. These pili and cytochromes provide a dense number of reduction sites for nanoparticle formation without the need for any synthetic components. The cells within the biofilm also can act as natural agents for preventing agglomeration of nanoparticles, and subsequent decrease of

active surface area, on the electrode surface. The cell template was carbonized and removed via thermal treatments, leaving a catalytically active mesoporous palladium structure. The biotemplated mesoporous structure had a high surface area composed of nanoparticles, and a high pore volume and surface area. The biotemplated porous structure also exhibited an increased catalytic activity compared to an electroplated palladium electrode and an electrode coated with synthetically produced palladium nanoparticles attached to the surface with a Nafion binder. The biotemplated mesoporous structure was found to be an alternative process to form a porous structure directly on an electrode using only materials and processes that naturally occur in *G. sulfurreducens* biofilms.

Biotemplated catalytic structures are an alternative method to form a porous structure with high catalytic activity without using any synthetic compounds. However, their uses in large scale processes require that the catalyst layer be durable. The electrochemical and mechanical stability of biotemplated mesoporous structures was tested on different support materials (polished graphite, carbon paper, carbon cloth, and stainless steel) subjected to electrochemical and/or mechanical stress. Carbon paper was found to withstand the most electrochemical and mechanical stress of the four different support materials tested. Polished graphite was able to withstand electrochemical stress, but deteriorated under a combination of electrochemical and mechanical stress. Different readily available and inexpensive polymers (polyaniline and polydimethylsiloxane) were also tested against a widely used polymer (Nafion®) to stabilize the palladium catalyst on the polished graphite surface. The polyaniline was the most effective binder because it enhanced the catalytic activity and could be electropolymerized around the catalyst, giving the greatest amount of control over the thickness of the polymer layer.

The second process studied used exoelectrogenic bacteria in METs for the conversion of electrons to hydrogen via water electrolysis in a biocathodic system. Naturally occurring biocatalytic cell material on the cathode surface was used to lower the cathode overpotential.

Different cell cultures (*G. sulfurreducens*, *Methanosarcina barkeri*, and *Escherichia coli*) were tested for their effect on hydrogen formation using electrons supplied to an insoluble electrode. The mode of hydrogen production was investigated by monitoring hydrogen production over three to five months using *G. sulfurreducens* biofilms (pregrown under anodic conditions with acetate) that were: (1) not supplied with an organic carbon source for cell growth and maintenance, (2) killed with ethanol, or (3) supplied with lactate, an organic carbon source and electron donor for *G. sulfurreducens*. Hydrogen was produced at a rate 10–20 times higher over five months in reactors that were either not given organic carbon or killed with ethanol, compared to reactors with lactate added. The methanogen, *M. barkeri*, was also tested as a biocatalyst because it is able to grow autotrophically. However, *M. barkeri* cells did not grow in the reactor with the electrode potential poised, based on the lack of evidence for methane production. Despite the lack of cell activity, the rate of hydrogen production with *M. barkeri* was similar to the rate observed in killed *G. sulfurreducens* reactors. The addition of *E. coli*, a non-exoelectrogenic bacteria, resulted in an initial elevated hydrogen gas production, but hydrogen production rates similar to background levels after three months. No cells were detected on the electrode surfaces after five months using scanning electron microscopy and unique metals, such as iron, nickel, cobalt, and zinc, were detected on the electrode surfaces exposed to cells. The identifiable peptides extracted from the electrodes were found to be derived primarily from metalloproteins produced by *G. sulfurreducens* and *M. barkeri* cells. These findings show that hydrogen can be produced in a biocathodic system by abiotic cell material attached to a graphite electrode surface and that it does not require electron uptake by living cells.

TABLE OF CONTENTS

LIST OF FIGURES

LIST OF TABLES

ACKNOWLEDGEMENTS

I would first like to thank my advisor Bruce Logan for the past five years at Penn State. The knowledge and skillset I have gained and the opportunities available to me during my time at Penn State have made this a very rewarding overall experience. I appreciate all of the advice and direction Bruce provided, complimented with the freedom to explore my own interests throughout my degree programs. This combination of direction and freedom helped me build the confidence and skills necessary to do my own research, while also giving me valuable insights and a different perspective on my research ideas. I would also like to thank the other members of my dissertation committee, Jay Regan, Chris Gorski, and Ming Tien, for taking the time to provide comments and insight into my work.

I am also grateful to everyone in the Logan Lab for all of the memories, both inside and outside of the lab. I enjoyed getting to know everyone that I crossed paths with and I wish everyone the best in the future. I have learned so much from all of the unique skill sets and diverse personalities of everyone in the group and could not have asked for a better, more supportive group to work with over the last five years. I would especially like to thank David Jones for all of his help throughout my five year career at Penn State. I truly appreciate all that he does behind the scenes to keep the lab running safely, the equipment operational, and everything organized.

Last, but certainly not least, I would like to thank my family for all of their support and encouragement at every stage of my life, including this latest chapter. I especially want to thank my wife, Sarah, for her unending support. Completing this degree would have been immeasurably harder without her limitless support, understanding, encouragement, and love.

Chapter 1

General Introduction

Worldwide demand for energy, chemicals, and fuels is growing faster than the current supply can support [1], necessitating new technologies that can simultaneously recover materials from waste streams to help meet increased demands, while also treating these waste streams to mitigate their possible environmental impacts. Recent research reflects this interest in finding sustainable alternatives and "cradle to cradle" approaches that regard waste as an un-utilized resource [2]. Water and energy are two especially relevant (and inextricably linked [3]) commodities due to concerns over the future of water supplies [4, 5] and impacts of burning fossil fuels [6]. Contaminant recovery from industrial waste streams, such as industrial waste streams that contain a variety of heavy metals [7], is important to keep water supplies clean for public consumption and to mitigate environmental impacts of toxic constituents. Increased material recovery would alleviate extraction of these raw materials from the ground, and could potentially reduce treatment requirements before the waste stream can be discharged. Additionally, sustainable alternatives to burning of fossil fuels for energy would lessen the impact of carbon dioxide release into the atmosphere and also could lessen water use for energy production [8].

Microbial electrochemical technologies is an emerging platform that utilize natural processes to treat waste streams while producing valuable products such as electricity, energy storage compounds, or chemicals [9]. METs are similar to other electrochemical systems in that electrons are donated to the anode by an electron donor, and are accepted from the cathode by the electron acceptor. The unique attribute of METs is the use of microorganisms to reduce electrode overpotentials at one or both electrodes. These microorganisms, often referred to as exoelectrogens or electrotrophs, depending on the direction of electron flow, have naturally

developed the ability to transfer electrons outside of the cell to give them an advantage in their natural environment [10]. The extracellular electron transfer process has been exploited in different MET systems designed to yield different end products. The first MET, the microbial fuel cell (MFC), was designed to oxidize organics present in wastewater and use the liberated electrons to produce electricity that could be used to power a wastewater treatment plant [11], which would achieve a sustainable water treatment process. METs have since expanded to include hydrogen production with microbial electrolysis cells(MECs), [12] and chemical production using biocathodic systems that can take up electrons from an electrode to synthesize useful end products [13].

To date, few METs have been tested at larger scales for wastewater treatment [14] . The ability to transfer electrons extracellularly can be exploited to drive alternative processes. It is shown here that exoelectrogenic bacteria can be used for the sustainable formation of catalytic nanoparticles and nanoporous structures from a metal-containing solution. Microorganisms from different phylogenetic classifications are used to facilitate the transfer of electrons to protons to sustainably form hydrogen via water electrolysis over long periods of time with little input.

1.1 Dissertation Scope and Outline

The extracellular electron transfer capabilities of exoelectrogenic bacteria were used here to study the sustainable conversion of soluble metals to nanostructures, and the sustainable conversion of electrons to hydrogen gas.

In **Chapter 3**, I examined the potential for *G. sulfurreducens* to be used as a sustainable biocatalyst for soluble palladium reduction to nanoparticles. Nanoparticle formation is desirable because of the increased catalytic activity due to an increased surface area to volume ratio. Microorganisms represent a sustainable catalyst for the formation of nanoparticles from metal

solutions because they do not require any synthetic chemicals for nanoparticle dispersion or stabilization. Naturally produced extracellular materials (e.g. polysaccharides, proteins) function as capping agents and stabilizers to keep reduced metal (10–50 nm [15]) at the nanoscale. Additionally, only an electron donor is required to provide reducing power for nanoparticle formation instead of a harsh chemical reducing agent such as sodium borohydride. Dissimilatory metal reducing bacteria are good candidates for nanoparticle production because their respiration allows them to transfer electrons outside of the cell to various electron acceptors (soluble and insoluble). *G. sulfurreducens*, the dominant member of power producing METs, has been shown to reduce insoluble and soluble metals, such as uranium during bioremediation studies, but this strain had not been studied for the recovery of catalytically active metals such as palladium. The objective of this study was to determine the ability of *G. sulfurreducens* suspensions to form nanoparticles from different starting concentrations of palladium and with different electron donors. Additionally, the localization of the formed palladium nanoparticles was determined. The results of this chapter were summarized in a paper by Matthew D. Yates, Roland D. Cusick, and Bruce E. Logan entitled *"Extracellular palladium nanoparticle production using* Geobacter sulfurreducens*"* published in the journal *ACS Sustainable Chemistry and Engineering*. I conducted all experiments and wrote the first manuscript draft. R.D. Cusick assisted with the experimental design and analysis. All co-authors assisted in the preparation of the final manuscript.

In **Chapter 4**, I studied the ability of *G. sulfurreducens* to produce nanoparticles primarily extracellularly due to naturally occurring conductive pili (Chapter 3), in order to produce a catalytic nanoporous structure. A *G. sulfurreducens* biofilm was used as a biotemplate because it is able to grow directly attached to an electrode surface, and it produces a dense, conductive network of pili which act as sites for soluble palladium adsorption and reduction. The hypothesis of this study was that a *G. sulfurreducens* biofilm grown on an electrode would provide a

sustainable biotemplate for the *in situ* formation and dispersion of palladium nanoparticles without the use of any synthetic stabilizers or binders to disperse and attach the nanoparticles to the electrode surface. The results of this chapter were summarized in a paper by Matthew D. Yates, Roland D. Cusick, Ivan Ivanov and Bruce E. Logan entitled *"Exoelectrogenic biofilm as a template for sustainable formation of a catalytic mesoporous structure"* published in the journal *Biotechnology & Bioengineering*. I conducted all experiments and wrote the first manuscript draft. R.D. Cusick assisted with the experimental design and analysis. I. Ivanov assisted with electrochemical setup and experimentation. All co-authors assisted in the preparation of the final manuscript.

In **Chapter 5**, I investigated the stability of the biotemplated nanoporous structures (Chapter 4) when they were subjected to electrochemical and mechanical stress. Stability of catalysts is an important consideration for large scale processes. Therefore, electrode stability should be critically evaluated with relevant reactants to evaluate degradation of the catalyst layer. Electrodes formed by synthetic methods are often required to attach nanoparticles or nanostructure to electrode support materials using a synthetic binder, such as Nafion®. The binder inherently acts as a stabilizer that is able to resist/mitigate the degradation of the catalyst material subjected to electrochemical and mechanical stress. The advantage of biotemplated electrodes is that no synthetic materials are required to form a porous catalyst layer directly on a conductive support. However, the lack of a binder could lead to failure (loss of catalyst) when the electrode is subjected to stresses, so investigating the stability of the nanoporous catalyst formed via a biotemplating process is important for examining the process potential for larger scale applications. The objective of this study was to investigate the stability of biotemplated catalyst layers on different support materials. Low cost polymers were evaluated for their effectiveness in stabilizing the catalyst layer to a polished graphite surface. Accelerated electrochemical stability tests were carried out by potential cycling at high rates for 3000 cycles with reactant to mimic

corrosive conditions in a fuel cell setting. The electrodes were also tested for their resistance to mechanical shear by rotating the electrode during accelerated stability tests. Resistance to shear will help to guide design of processes that do not use gaseous reactants, such as formic acid or alcohol fuel cells or for treatment processes. The results of this chapter were summarized in a paper by Matthew D. Yates and Bruce E. Logan entitled *"Biotemplated Palladium Catalysts can be Stabilized on Different Support Materials"* published in the journal *ChemElectroChem*. I conducted all experiments and wrote the original draft manuscript. All co-authors participated in the preparation of the final manuscript.

In **Chapter 6**, I examined the production of hydrogen at the cathode from water electrolysis at the anode, using biological materials as cathode catalysts. The use of biological materials as catalysts for hydrogen production is desirable because it might enable replacing expensive precious metal catalysts with sustainable materials. Hydrogenases are the primary biocatalyst studied for hydrogen production because these enzymes naturally function to reversibly catalyze the redox reaction of protons and electrons to hydrogen gas [16]. Purified hydrogenases from different microorganisms have been attached to electrodes as a biological catalyst for hydrogen formation [17, 18]. However, these systems suffer from short lifetimes due to protein unfolding [19]. Pure or mixed culture whole cells on cathode surfaces, called biocathodes, have also been used to produce hydrogen in METs [20, 21]. The mechanism of hydrogen production has been thought to be electron uptake by the cell, and subsequent utilization by hydrogenase enzymes to produce hydrogen. However, alternatives to this hypothesis have not been adequately tested. Additionally, the durability (over time) of biocathodic systems for hydrogen production has not been previously examined. The objectives of this study were to address these knowledge gaps by using different pure cultures to investigate their impact on hydrogen production in biocathodic systems, and to evaluate the stability of biocathodic hydrogen production over an extended period of time (~5 months). The results of this chapter will be summarized in a paper by Matthew D.

Yates, Michael Siegert, and Bruce E. Logan entitled *"Hydrogen Evolution Catalyzed by Viable and Non-viable Cells on Biocathodes"*. I conducted the experiments, analyzed data, and wrote the first manuscript draft. M. Siegert assisted with data collection and experimental design. All co-authors will assist in the preparation of the final manuscript.

1.2 Additional Research Publications

The following list includes published research that I contributed to as a co-investigator, but is not included in this dissertation.

1. Siegert M, Yates MD, Call DF, Spormann A, Logan BE. *Methanobacterium* dominates biocathodes. In preparation.
2. Siegert M, Li XF, Yates MD, Logan BE. High archaeal diversity of the inoculum improves methane gas production in microbial electrolysis cells. In preparation.
3. Yan H, Yates MD, Regan JM. Constant versus dynamic anode potentials: Effects on microbial community development and composition. *Applied and Environmental Microbiology* (in review)
4. Sun D, Wang A, Cheng S, Yates MD, Logan BE. Geobacter anodireducens sp. nov., a novel exoelectrogenic microbe in bioelectrochemical systems. *International Journal of Systematic and Evolutionary Microbiology* (in review)
5. Siegert M, Yates MD, Call DF, Zhu X, Logan BE (2014). Comparison of non-precious cathode materials for methane production by electromethanogenesis. *ACS Sustainable Chemistry and Engineering* **2**(4): 910-917

6. Zhu X, Yates MD, Hatzell MC, Ananda Rao H, Saikaly PE, Logan BE (2014). Microbial community composition is unaffected by anode potential. *Environmental Science and Technology* **48**: 1352-1358
7. Zhu X, Yates MD, Logan BE (2012). Set potential regulation reveals additional oxidation peaks of *Geobacter sulfurreducens* anodic biofilm. *Electrochemistry Communications* **22**: 116–119.
8. Liu G, Yates MD, Cheng S, Call DF, Sun D, Logan BE (2011). Examination of microbial fuel cell start-up times with domestic wastewater and additional amendments. *Bioresource Technology* **102**: 7301-7306.

1.3 Literature Cited

1. Tietenberg, T. and L. Lewis, *Environmental & Natural Resource Economics*. 8th ed. 2008: Addison Wesley.
2. Braungart, M. and W. McDonough, *Cradle to Cradle: Remaking the Way We Make Things*. 2008: Tantor Media.
3. Schnoor, J.L., *Water–Energy Nexus*. Environmental Science & Technology, 2011. **45**(12): p. 5065-5065.
4. Kargbo, D.M., R.G. Wilhelm, and D.J. Campbell, *Natural Gas Plays in the Marcellus Shale: Challenges and Potential Opportunities*. Environmental Science & Technology, 2010. **44**(15): p. 5679-5684.
5. Scown, C.D., A. Horvath, and T.E. McKone, *Water Footprint of U.S. Transportation Fuels*. Environmental Science & Technology, 2011. **45**(7): p. 2541-2553.
6. *Fact Sheet: The need for mitigation*, 2009, United Nations Framework Convention on Climate Change.

7. Volesky, B. and Z.R. Holan, *Biosorption of heavy metals.* Biotechnology Progress, 1995. **11**(3): p. 235-250.

8. Blackhurst, B.M., C. Hendrickson, and J.S.i. Vidal, *Direct and Indirect Water Withdrawals for U.S. Industrial Sectors.* Environmental Science & Technology, 2010. **44**(6): p. 2126-2130.

9. Logan, B.E. and K. Rabaey, *Conversion of Wastes into Bioelectricity and Chemicals by Using Microbial Electrochemical Technologies.* Science, 2012. **337**(6095): p. 686-690.

10. Lovley, D.R., *Dissimilatory metal reduction.* Ann Rev Microbiol, 1993. **47**(1): p. 263-290.

11. Logan, B.E., *Microbial fuel cells*. 2008, Hoboken, NJ: John Wiley & Sons, Inc. 300.

12. Call, D. and B.E. Logan, *Hydrogen production in a single chamber microbial electrolysis cell (MEC) lacking a membrane.* Environmental Science & Technology, 2008. **42**(9): p. 3401-3406.

13. Rabaey, K. and R.A. Rozendal, *Microbial electrosynthesis--revisiting the electrical route for microbial production.* Nat Rev Microbiol, 2010. **8**(10): p. 706-716.

14. Cusick, R., et al., *Performance of a pilot-scale continuous flow microbial electrolysis cell fed winery wastewater.* Applied Microbiology and Biotechnology, 2011. **89**(6): p. 2053-2063.

15. De Windt, W., et al., *Biological control of the size and reactivity of catalytic Pd(0) produced by Shewanella oneidensis.* Anton Leeuw J Microb, 2006. **90**(4): p. 377-389.

16. Thauer, R.K., et al., *Hydrogenases from methanogenic Archaea, nickel, a novel cofactor, and H_2 storage.* Annu Rev Biochem, 2010. **79**(1): p. 507-536.

17. Gutiérrez-Sánchez, C., et al., *Oriented Immobilization of a Membrane-Bound Hydrogenase onto an Electrode for Direct Electron Transfer.* Langmuir, 2011. **27**(10): p. 6449-6457.

18. Rüdiger, O., et al., *Oriented immobilization of Desulfovibrio gigas hydrogenase onto carbon electrodes by covalent bonds for nonmediated oxidation of H2.* J Am Chem Soc, 2005. **127**(46): p. 16008-16009.

19. Armstrong, F.A., et al., *Dynamic electrochemical investigations of hydrogen oxidation and production by enzymes and implications for future technology.* Chem Soc Rev, 2009. **38**(1): p. 36-51.

20. Geelhoed, J.S. and A.J.M. Stams, *Electricity-assisted biological hydrogen production from acetate by Geobacter sulfurreducens.* Environ Sci Technol, 2010. **45**(2): p. 815-820.

21. Villano, M., et al., *Bioelectrochemical hydrogen production with hydrogenophilic dechlorinating bacteria as electrocatalytic agents.* Bioresource Technol, 2011. **102**(3): p. 3193-3199.

Chapter 2

Literature Review

2.1 Microbial Electrochemical technologies

2.1.1 Principles of Microbial Electrochemical Technologies

Microbial electrochemical technologies (METs) consist of the same basic components as other electrochemical energy conversion and storage systems, such as batteries and fuel cells, with the exception that microorganisms are used to lower electrode overpotentials and enable the transformation of many different fuels to or from electrical current. METs have an anode and a cathode connected together with an external circuit (Figure 2.1). Electrons are donated to the anode by exoelectrogenic bacteria capable of oxidizing organic matter and donating electrons to an insoluble terminal electron acceptor. The electrons then pass through the external circuit to the cathode where they can be used to form desired end products, or water if the desired product is electricity.

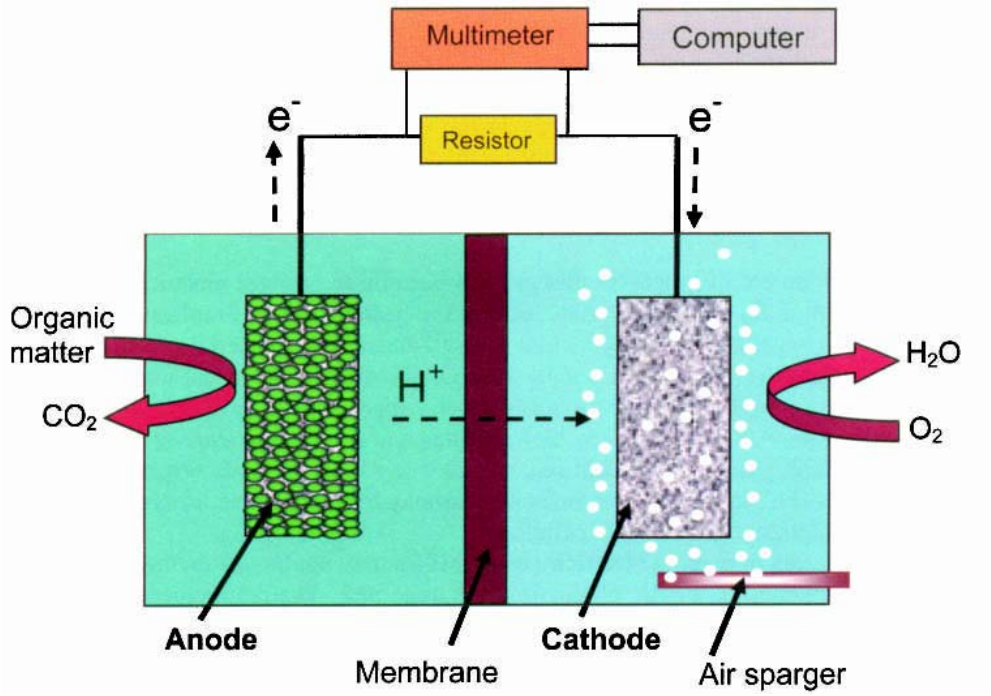

Figure 2.1. A schematic of a microbial fuel cell [1].

The first MET developed was the microbial fuel cell (MFC), which was designed to capture electrons as electrical energy through the oxidation of organics in wastewater. The utilization of electrons derived from the liberation of organics in wastewater could provide a method for simultaneous treatment of waste and harvesting of an under-utilized source of energy. The electrons captured as electrical energy could then be used to power pumps in the plant, decreasing the reliance of treatment plants on grid energy [1]. Electrons are transferred from organics to the anode by exoelectrogenic microorganisms. The transfer of electrons from organic material to the electrode via respiratory processes of exoelectrogenic bacteria generates a potential gradient between the anode and cathode, which can be captured in the form of usable energy. MFCs utilizing aceate as the electron donor and oxygen as the terminal electron acceptor at the cathode have a spontaneous flow of electrons from the anode to the cathode because the whole cell potential as calculated by the Nernst equation is positive at standard biological conditions (E_{anode}

= –0.279 V ; $E_{cathode}$ = 0.801 V, $E_{whole\ cell}$ = 1.1 V vs. standard hydrogen electrode [SHE]) [2]. Potential losses at the electrodes decrease the amount of energy that can be obtained compared to the theoretical whole cell potential. Potential losses at the anode (~0.1 V [3]) result from a portion of the substrate energy being used for growth and cell maintenance of the exoelectrogenic biofilm. Potential losses at the cathode are much larger (~0.5 V), and are the result of the catalyst and solution properties, including pH and conductivity [4]. These losses result in a typical experimental whole cell potential of 0.5-0.7 V [5].

Microbial electrolysis cells (MECs) are another type of MET with a similar set up as MFCs. MECs usually have a biotic anode that accepts electrons from the oxidation of organic matter by exoelectrogneic bacteria, an external circuit, and a cathode. However, the desired product of MECs is hydrogen gas production at the cathode, as opposed to electrical power production in MFCs. To achieve hydrogen production, the cathode chamber must be kept anaerobic, and therefore the potential at the cathode is different than when oxygen is present. The standard biological potential for hydrogen formation ($E_{cathode}$ = –0.414 V, [6]) is much lower than the oxygen reduction potential at an MFC cathode. In acetate oxidizing systems, this leads to a overall standard potential that is not thermodynamically spontaneous ($E_{whole\ cell}$ = –0.14). Additional energy must be provided in the form of an external power supply in order for the hydrogen evolution reaction to proceed. Theoretically, only 0.14 V must be supplied, but due to potential losses at the electrodes (called overpotentials) a practical potential of 0.6 V is often applied [1]. The potential applied to MECs is lower than the potential required for abiotic hydrogen formation via water electrolysis (1.23 V vs SHE). Although MECs require an input of energy, many systems use inexpensive materials as cathode catalysts, such as stainless steel [7], for hydrogen production compared to MFCs, which use platinum at the cathode to increase the kinetics of the oxygen reduction reaction. Inexpensive cathode catalyst for oxygen reduction, such as activated carbon, have been identified for MFCs [8]. Finding cheaper cathode materials

for METs, specifically MECs, is the subject of great research interest as the standard platinum cathode accounts for 47% of the cost of the system [9, 10].

The maximum amount of power or products that can be produced in METs changes with the introduction of a more complex substrate, such as wastewater. Most known exoelctrogenic bacteria are capable of oxidizing simple substrates, such as acetate, lactate and formate [11-13], but not complex organics substrates, such as proteins and sugars, forcing them to rely on different classes of microorganisms to break down more complex substrates to a usable form [14]. The reliance on fermentation of complex substrates makes this step the limiting step for the conversion of organics into electrons that can be captured as energy. Additionally, in mixed culture systems, the competition for simple fermentation end products between exoelectrogenic microorganisms and other members of the biofilm [15] becomes a consideration for the maximum amount of energy that can be extracted from a particular waste stream. Biodegradability of the substrates in the waste streams becomes more important when METs are adapted for the treatment of different industrial wastes, especially those with extreme pH, high organic loadings, or potentially toxic constituents [16], such as potato processing wastewater [17], winery wastewater [18], and others [19].

2.1.2 Anode materials

MET anodes can be made of any material that is able to provide attachment sites for exoelectrogenic microorganisms and conduct electrons to the external circuit. Carbon-based materials are the most often used because of their low cost and ease of production. Different materials such as carbon brushes, graphite granules, carbon paper, carbon cloth, graphite blocks, and graphite felt have all been utilized effectively as anodes. Anode surfaces have also been modified with different materials, such as carbon nanotubes [20] and amine functional groups

[21], or heat treated [22] to increase the conductivity of the electrode or enhance the attachment of microorganisms. Metals have also been investigated as an anode material because they have good conductivity. However, the metal used must be stable to be used in large scale industrial processes. Titanium [23] and stainless steel [24] are materials that meet this requirement and are used often in MET systems as current collectors.

2.1.3 Cathode Materials

The most commonly used cathode in MFCs is an air cathode [25]. The air cathode is often made of a carbon black/platinum active layer that is placed in contact with the solution to increase the rate of oxygen reduction to water. A PTFE diffusion layer is applied to the outside of the cathode to allow oxygen to passively diffuse into the reactor to eliminate the need for active aeration in the reactor. This design is effective, but the platinum layer is poisoned and the catalytic activity decreases considerably over a period of 6 months to 1 year [26]. Platinum is expensive and is a major cost in the system. Alternative materials, such as activated carbon [26], have been found to be viable alternatives to platinum, giving a similar catalytic activity to platinum while also lasting for a longer period of time before showing a substantial decrease in performance.

MECs originally used the same platinum-containing cathode as MFCs [27]. However, stainless steel has been more frequently used in current research as a standard cathode material in MECs [7, 28]. Stainless steel was found to have a similar performance as the standard platinum on carbon cloth cathode in MECs [7] while costing less.

Biocatalysts have also been explored on cathodes of METs. Biocathodes [29] are a low cost, sustainable alternative to precious metal catalysts in METs [30] in which naturally occurring microorganisms utilize electrons from the cathode and use them to reduce oxygen, protons, or

carbon dioxide. Biocathodes are more common in MECs than MFCs because of their versatility in producing different end products. Biocathodes are discussed in more detail in Section 2.3.

2.1.4 Extracellular Electron Transfer

Microorganisms on the anode surface are the driving force behind the energy producing capabilities of different MET systems. These microorganisms power the system by oxidizing organic material and donating the liberated electrons to an insoluble electron acceptor. Many microorganisms capable of extracellular electron transfer belong to a broad group of microorganisms called dissimilatory metal reducing bacteria (DMRB). DMRB utilize this capability for extracellular electron transfer in their natural environments to gain energy by oxidizing organic carbon and reducing abundant insoluble metals and minerals [31]. METs exploit this natural extracellular electron transfer by mimicking natural conditions in the MET reactor to induce electron transfer to the anode, which generates the necessary potential to produce the desired end product. Different classes of DMRB have developed different mechanisms for extracellular electron transfer to insoluble substrates (Figure 2.2). The most well-studied microorganisms in METs belong to the genera *Geobacter* and *Shewanella*.

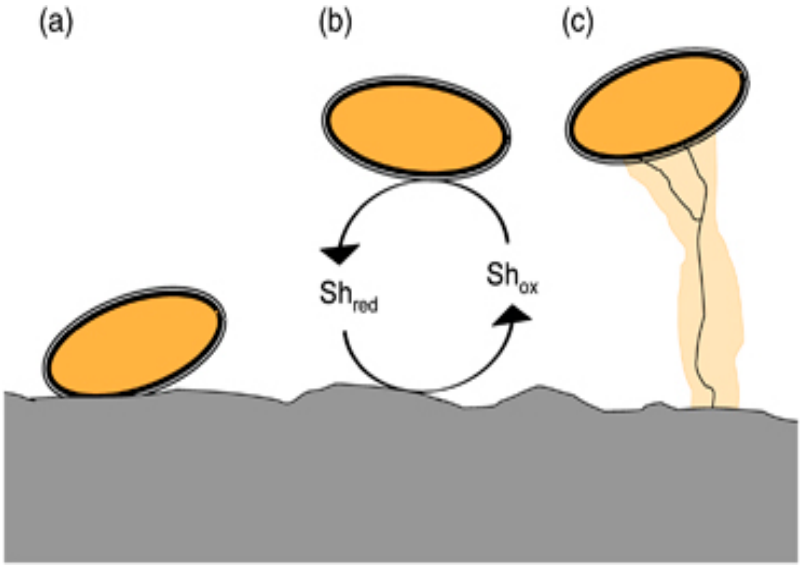

Figure 2.2. Different mechanisms for extracellular electron transfer. (A) Direct contact electron transfer, (B) electron shuttle mediated electron transfer, and (C) conductive appendages (nanowires) [32].

Geobacter is the most widely studied bacterium in METs because it is predominant in acetate-fed systems regardless of the inoculation source [33]. *Geobacter* is able to dominate in METs because it possesses physiological traits that give it a competitive advantage in this system. *Geobacter* is capable of transferring electrons extracellularly at the highest rate known among microorganisms [34], likely giving it the ability to respire more quickly than other microorganisms in the system. *Geobacter* is also able to grow at a wide range of potentials [35, 36], some very negative, making it resilient to changes in anode potential over the course of a batch cycle. Additionally, *Geobacter* sp. can create biofilms composed of conductive appendages that allow rapid extracellular electron transfer via outer membrane and extracellular cytochrome complexes [37, 38]. These appendages allow *Geobacter* biofilms to outcompete other microorganisms that do not possess this ability. The precise mechanism of electron transfer to the insoluble surface is still being debated. One proposed mechanism is that the pili conduct electrons via a metallic-like conductivity [39] using pi-pi stacking of aromatic amino acids side groups

along the pili [40]. A second proposed mechanism is that electrons are transferred to a surface via an electron hopping mechanism, where electrons hop between cytochromes within the biofilm along a potential gradient [41]. Pure culture *Geobacter* biofilms are able to grow to be approximately 50 μm thick, and cells on the outer edge of the biofilm are as metabolically active as those directly contacting the surface [42]. Additionally, the outer membrance cytochrome, *omc* Z, has been shown to localize at the solid surface of a *Geobacter* biofilm, suggesting that this protein facilitates electron transfer to a solid electrode [38]. The transfer of electrons through pili in a conductive biofilm allows *Geobacter* to be relatively far away from the surface of the electrode, while still remaining metabolically active, making this electron transfer mechanism very effective. Additionally, the available anodic sites for microbial reduction are independent of the surface area available for direct contact.

Shewanella is another exoelectrogenic genera studied in METs. *Shewanella* have been shown to produce conductive appendages that may function similarly to those produced by *Geobacter* spp. [43]. However, *Shewanella* use the Mtr pathway to transfer electrons to a surface [44, 45], which is distinct from that used by *Geobacter*. *Shewanella* are also able to transfer electrons to an insoluble surface through the production of soluble redox mediators called flavins [46]. Flavins are reduced internally and then excreted through the cell membrane. When a flavin comes into contact with a surface, the surface is reduced. It is possible for the flavin to diffuse back to the cell, but this does not necessarily occur because the process is diffusion controlled. This process is not as fast or as efficient as the direct contact mechanism utilized by *Geobacter*.

A third mechanism of extracellular electron transfer is through the direct contact of outer membrane proteins with a surface [32]. *Desulfovibrio* is thought to use this mechanism for extracellular electron transfer because it produces lower power in MFCs. The major limitation of the direct contact mechanism is that cells limited by the surface area provided since only a single

layer of cells can utilize the surface at a time [32]. *Shewanella* is also capable of extracellular electron transfer to surfaces by direct contact [47].

Many different microorganisms outside of the *Geobacter* and *Shewanella* genera are capable of extracellular electron transfer. Exoelectrogenic microorganisms isolated through 2008 were summarized in a review article, where a total of 21 exoelectrogens that do not require exogenous mediators were described [3]. Since 2008, other exoelectrogens have been isolated such as *Citrobacter* SX-1 [48], the enteric pathogen *Arcobacter butzleri* ED-1 [49], and the denitrifying bacterium *Comomonas denitrificans* [50]. More recently, exoelectrogens from extreme environments, such as the thermophilic bacterium *Thermincola ferroacetica* [51] and alkaliphilic bacterium *Geoalkalibacter* spp. [52] microorganims, have been isolated, suggesting that the ability to transfer electrons extracellularly is widespread among microorganisms in diverse environments.

2.2 Soluble Metal Removal and Recovery

2.2.1 Introduction

The demand for industrially important raw materials is increasing due to an increase in consumer demand for products of these materials, while the supply of many of these materials is steady or decreasing, largely due to the under-utilization of wastes as a resource [53]. A pertinent example of this gap between supply and demand is in the precious metals market. Precious metals, such as palladium, platinum, ruthenium, gold, and silver, are used in many industrial processes and consumer goods as catalytic and conductive materials [54]. However, many of these materials, especially platinum and palladium, are unable to be extracted at a rate necessary to meet demand [55]. The increasing emission standards for industrial processes and automobiles

as a result of concern over increasing levels of CO_2 [56] in the atmosphere have required an increase in the amount of catalytic materials in automotive catalytic converters [57]. Another consumer market that utilizes these precious metals is the electronics industry. Printed circuit boards in many electronics, especially high end electronics, make use of these precious metals due to their stability against corrosion and good conductivity [58]. However, after devices containing printed circuit boards become obsolete, they are often discarded into landfills or sent to scrap yards. As a result of decades of this practice, landfills with electronic wastes have high levels of unutilized precious metals [59]. Precious metals are also used as catalysts in other important industrial processes, such as hydrogenenation [60] and dehydrogenation reactions [61] to produce useful materials. There has been an increase of recycling of these precious metal containing materials in response to increasing market prices, but it has not been enough to bridge the gap in supply and demand for many of these materials [62]. The increase in demand for these raw materials necessitate new technologies able to recover and reuse materials found in waste streams in a sustainable way to minimize environmental impacts.

2.2.2 Treatment of Waste Streams to Remove Toxic Soluble Metals

Metals are commonly found in various industrial and municipal waste streams. Heavy metals, such as cadmium, chromium, lead, mercury, silver, and arsenic are often present in metal laden waste streams, which are toxic to humans and to other organisms in the environment [63]. The amount and type of metals present in different industrial waste streams depends on the industry.

Conventional removal of potentially harmful metals is often accomplished in water treatment plants by raising the pH using lime or sodium hydroxide to precipitate the metals out as hydroxides. However, the presence of metal complexing agents, such as natural organic matter, can keep heavy metals solubilized even at neutral or slightly basic pH [64] causing the effluent

water to fail to meet discharge limits set by regulatory agencies. Other chemicals can be added to overcome this limitation and further precipitate metals from solution [65], but the addition of many chemicals can be costly. Additionally, this process generates a sludge that contains high levels of toxic metals that then must be disposed as a hazardous material.

Biological materials have also been used to adsorb metal ions and remove them from solution [66]. Metal ions can adsorb to various proteins and extracellular polymeric substances produced by different microorganisms. Some microorganisms can reduce the toxic metals to an insoluble form after they are adsorbed to the cell [67-69]. The advantage of this method over chemical precipitation is that cell material is cheaper adsorbent and does not require that the bulk water characteristics be changed in order to remove the metals. However, using biological material to remove metals from suspensions also results in a heavy metal laden sludge that must be disposed of as a hazardous material.

2.2.3 Recovery of Soluble Metals as Nanomaterials using Synthetic Methods

In recent years, there has been increased interest in finding methods to recover soluble metals from waste streams in a usable form. The recovery of soluble metals as nanomaterials is desirable because nanomaterials have different optical and electronic properties compared with the same material in the bulk phase. Additionally, these materials have an enhanced catalytic activity due to an increased surface area to volume ratio [70]. When synthetic methods are employed, a strong reducing agent, such as sodium borohydride, is used to precipitate soluble metals out of solution. As the reaction proceeds, the nanoparticle “seed” continues to autocatalytically precipitate [71] additional soluble metal, and agglomerate with other particles until the particles form a bulk material. Stabilizing ligands and a capping agents composed of various polymers [72] are therefore required to prevent uncontrolled growth of the particle into the bulk phase. Empirically

determined ratios of soluble metal to stabilizing ligands have been developed so that the ligand envelopes the nanoparticle at a desired size to prevent further growth of the particle. In this way, nanoparticles with a narrow size range can be formed [73].

Nanoparticles possess a high surface area when they are stabilized in a suspension. However, nanoparticles aggregate when they are applied to supports for catalysis, which negates the surface area available for the reaction. Nanoparticles are often applied to surfaces using a drop-application procedure where they are applied directly to a surface and allowed to dry [74]. During this process, however, the surface tension of the water evaporating causes the particles to be drawn together on the surface and possibly into multiple layers, decreasing the available surface area [75]. Ideally, the nanoparticles would be organized into an ordered porous layer on the surface to maximize the activity and the material used, but this is difficult to achieve using a drop application process.

Different methods have been developed to prevent aggregation of nanoparticles on support materials. One method utilizes a chemically-modified electrode to provide adsorption sites for soluble metals [76]. The adsorbed metal ions can then be reduced with a strong reductant to form patterned nanoparticles on the surface of a support. This method allows for the controlled synthesis of dispersed nanoparticles in a single layer to maximize the surface area per weight of metal. However, only a single layer of ordered nanoparticles is formed on the support surface, which limits the available active surface area.

Another strategy for maximizing available surface area is by creating nanoporous materials that can be attached to a supports. Nanoporous materials are classified according to IUPAC nomenclature based on the average pore size diameter of the material (microporous material <2 nm pore diameter; mesoporous material 2-50 nm pore diameter; macroporous material >50 nm pore diameter). One common method of synthesizing mesoporous materials is using a block-co polymer assembly [70] (Figure 2.3). Block copolymer assemblies are made by first forming

nanoparticles using a functionalized polymer ligand. A secondary functionalized co-polymer is added to the suspension to interact with the functionalized nanoparticles to force them into an ordered structure. The polymers can then be carbonized by thermal processing and etched away with an acid solution, further thermal processing, or plasma treatment [77]. The resulting structure is an ordered mesoporous structure that can be attached to a support and used in catalysis. Mesoporous structures formed with block co-polymer assemblies have catalytic activities similar to bulk catalytic materials [77]. The disadvantage of using block co-polymer assemblies to form catalytic nanoporous materials is that the material is formed separate from the support, so it must be attached using a binder, which raises the cost of the process. Additionally, the process requires sacrificial functionalized polymers to create the ordered structure, which is both unsustainable and expensive.

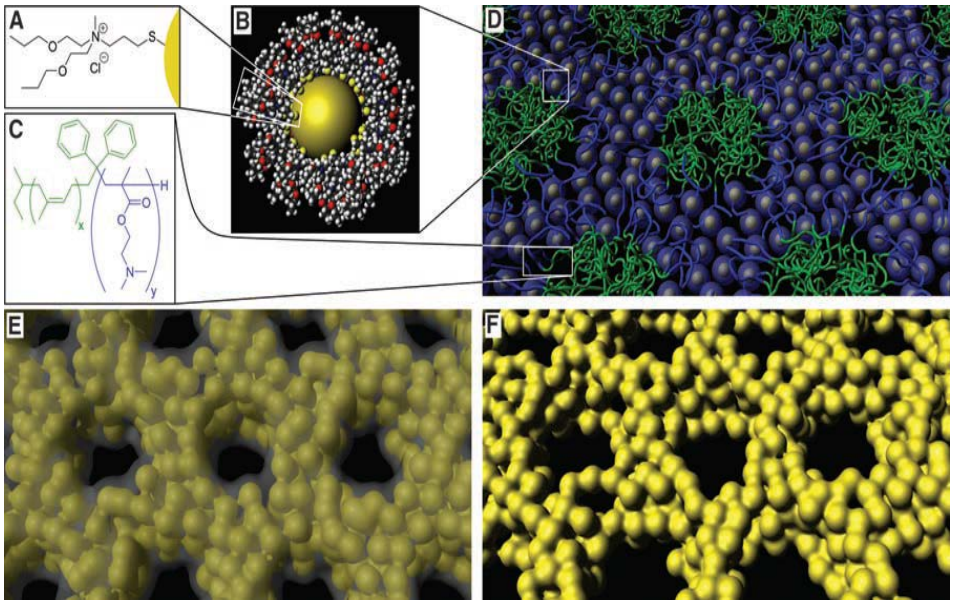

Figure 2.3. Schematic of a block co-polymer assembly for formation of a mesoporous structure [77].

Another technique for synthesis of porous materials is through a de-alloying process, which utilizes alloyed materials to form a porous structure on an electrode. One material acts as a

sacrificial template, while the other is the desired catalyst. The two materials are first electrodeposited onto a support in a desired ratio [78]. The template material is then etched away leaving a porous material behind [78]. This technique has the advantage that the resulting porous structure is synthesized directly on the support material without requiring a binder for attachment. However, the disadvantage is that a sacrificial material must be used and a chemical etching step is required. The chemicals used are often toxic and would require a treatment step if the process was scaled to an industrial size.

A fourth method to form porous materials is using a sol-gel synthesis process, which involves the use of a metal alkoxide precursor solution [79]. The precursor solution forms a diphasic liquid-solid sol-gel that can be processed in various ways to form different end products, often titanium and silicon based porous structures for dispersion of catalytic materials in the pores [80-82]. The advantage of this process is that it is very versatile and can form many different end products from similar starting materials by varying the treatment processes. The disadvantages are similar to the block co-polymer assembly process in which synthetic precursors are used that are discarded after formation of the end products, making the process effective, but not sustainable.

All of these methods are effective and have advantages and disadvantages. However, all of them require synthetic materials in the form of reducing agents, stabilizers, ligands, or binders. All of these synthetic materials decrease the sustainability of the overall process.

2.2.4 Biological Materials to Form Nanomaterials

In recent years, there has been a general shift toward investigating more sustainable approaches for metal recovery and catalyst formation to alleviate the demand for raw materials and reduce the volatility of the price for precious metals based on extraction rates. The major

biological material that is studied for the formation of nanomaterials is bacterial suspensions, although plant material [83] and fungi [84] are studied as well. Organisms such as *Shewanella oneidensis* [69], *Desulfovibrio desulfuricans* [85], *Geobacter sulfurreducens* [86], and *E. coli* [68] are species that have been used for soluble palladium reduction. The advantage of using bacteria to reduce soluble metals is that the catalyst is supported by the cell material when it is formed. The bio-catalyst can then be directly used in applications. A further advantage of using fermentative bacteria, such as *E. coli*, is that a fermentable substrate can be used to naturally produce hydrogen as a reductant for metal nanoparticle formation instead of adding an exogenous reductant. The primary focus of biological metal reduction has been on the formation of bio-palladium for use in reductive dechlorination reactions [69, 87]. Recovery of soluble metals from a mixed metal printed circuit board leachate has also been investigated [88].

The disadvantage of using cell material as a support for nanoparticles is that sulfur contained in cellular proteins can poison the catalyst, reducing the activity [76]. Nanoparticles formed by cell materials have been heat treated to remove the sulfur-containing protein material and maximize the catalytic activity [89]. The resulting nanomaterials can then be treated similarly to synthetically formed nanomaterials by forming a catalytic ink solution consisting of nanoparticles and a Nafion binder that is applied to electrodes for applications, such as hydrogen oxidation in fuel cells [90].

Biological materials have also been used as templates for formation of nanomaterials with different shapes. A genetically modified virus strain was used to form a tin nanoforest on an electrode for a high surface area battery electrode with high catalytic activity [91]. Bacterial flagella [92] have also been used as a sacrificial template to sustainably form nanomaterials. Biological materials represent a sustainable template because they take advantage of natural processes instead of synthetic materials to form a desired product. However, the disadvantage to

using biological materials is that the conditions are not as controlled or ordered as materials created with synthetic methods.

2.3 Bio-Electrochemical Energy Conversion

2.3.1 Introduction

Fossil fuels are the primary source of energy being used to meet the needs of society. Oil is primarily extracted and refined for use as an energy source in automotives [93]. Coal is extracted from the ground and burned in coal-fired power plants to produce grid energy [94]. Natural gas is also extracted from the ground (either as a co-product of oil extraction or as the only product) for use in vehicles, or burned in power plants [95]. Fossil fuels are desirable as an energy source because their energy density is higher than many other compounds, and they are stable at ambient conditions. However, stores of fossil fuels are finite [96] and cannot be easily replaced. Additionally, dependence on fossil fuels has resulted in political, economic, social, and environmental concerns among different groups. Therefore, alternative and renewable energy sources need to be found to alleviate dependence on fossil fuels.

Electricity supplied to the grid often comes from burning coal. Power plant operators have to produce a variable amount of electricity throughout the day due to variable demands based on time of day and the season, among other factors [97]. A variable amount of electricity demand often leads to an excess that is ultimately wasted [98], leading to a loss of potential energy that could be captured in a different medium, such as the formation of chemical bonds [99], the flux of ions in batteries [100], or the storage of charge in supercapacitors [101]. Wasting potential energy in the form of grounding excess electrons also occurs in sustainable energy sources, such

as wind farms [97]. Capturing otherwise unutilized electrons can enhance the economic viability of these processes by producing valuable co-products.

2.3.2 Conventional Synthesis of Energy Storage Compounds

Hydrogen is one potential alternative energy storage material because it has a high energy density per mass (100 kJ/g [102]) and it produces environmentally benign end products. However, the current method of hydrogen production relies on using fossil fuels. More than 95% of hydrogen is currently produced using fossil fuels, with methane accounting for ~45% of the hydrogen production (Figure 2.4). Methane is converted to hydrogen primarily using a stream reforming process [103]. During this process, methane is often reacted over a nickel catalyst at high temperatures with water vapor to form hydrogen and carbon monoxide [104]. The carbon monoxide can be used to produce more hydrogen by reacting with water vapor to form carbon dioxide and hydrogen in the water-gas shift reaction [105]. Using fossil fuels as a feedstock for hydrogen production represents an unsustainable energy conversion process and does not mitigate the production of carbon dioxide, even though the burning of hydrogen is clean. Additionally, hydrogen streams generated from fossil fuel often have low levels of impurities, such as carbon monoxide [106], which can poison precious metal catalysts in systems that utilize hydrogen as a feedstock for energy production, such as fuel cells [107].

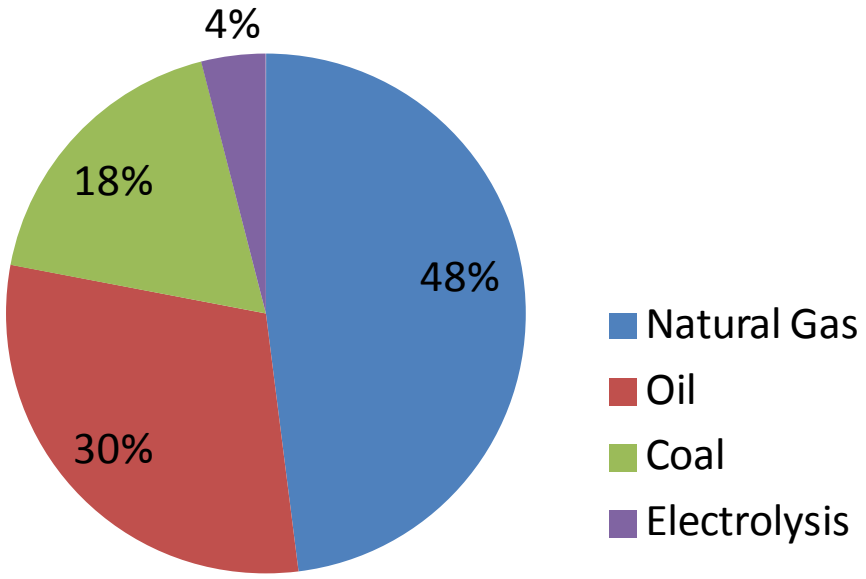

Figure 2.4. Percentage of hydrogen production from different feedstocks. Modified from [108].

Hydrogen can also be produced by water spitting, or electrolysis. Water electrolysis is a desirable route of hydrogen synthesis because water is an almost unlimited resource and produces clean hydrogen streams [109]. One major challenge with this approach is overcoming high electrode overpotentials. Overpotential is defined as the off-set potential needed to achieve a measurable catalytic effect compared to the theoretical potentials obtained from the Nernst equation. Overpotentials are often decreased using precious catalytic metals, such as platinum, to increase the rate of hydrogen production to make the process more economical. However, precious metals are easily poisoned by small concentrations of contaminants, such as sulfides [110], carbon monoxide [107], or alcohols [111], which limits the overall effectiveness of this process. Much research has focused on formation of catalysts for hydrogen generation without precious metals in response to this challenge [112-115].

Other chemicals are also commonly formed by electrosynthesis. Inorganic compounds such as hydrogen peroxide [116], and organic compounds, such as drug metabolites [117], are

common end products of electrosynthesis. Primary challenges associated with electrosynthesis of these compounds are the use of expensive catalysts and electrode product selectivity and stability [118].

2.3.3 Microbial Electrochemical Technologies for Hydrogen Production

Microbial electrochemical technologies (METs) can also be used to convert electrons generated in the process into valuable products. Microorganisms are used to lower electrode overpotentials as they can accept electrons directly from an insoluble electrode. The electrons are then converted into various products via different possible mechanisms [99] based on the microorganisms present in the system.

One product of microbial electrosynthesis that has been investigated is the formation of hydrogen. Using microorganisms as catalysts is advantageous because the catalyst material is inexpensive compared to precious metals as it is naturally produced by the biofilm. Additionally, hydrogen production from purified cell material, mainly hydrogenase enzymes [119], has been demonstrated. The use of purified enzymes for hydrogen production has two main challenges: the cost of purifying cell extracts [120] and the short lifetime of the system [121]. Using cathodic biofilms in METs for hydrogen production could be a more economical alternative because whole cell biocatalysts are used.

Both pure and mixed culture biofilms have been studied for hydrogen production. The majority of these studies utilize biofilms that are able to transfer electrons extracellularly. Pure culture *Geobacter sulfurreducens*[122] and *Desulfovibrio* sp. [123] biocathodes produced hydrogen at different rates, over a range of potentials, compared to abiotic electrodes. *Desulfovibrio sp*. were also identified as the dominant species in a mixed community biocathode producing hydrogen [124]. Other recent studies observed hydrogen production using mixed

culture biocathodes under mesophilic [125, 126] and thermophilic [127] conditions, and using a dechlorinating consortium[128].

2.3.4 Electrosynthesis of Other Compounds using Biocathodes

Biocathodes can be used to synthesize organic compounds, such as methane by using methanogens on a biocathode. Electromethanogenesis was first observed from a mixed culture biocathode in a microbial electrolysis cell [129] and has since been proposed as a method for conversion of carbon dioxide to methane in geological storage reservoirs [130]. Electromethanogenesis has also recently been shown to be catalyzed primarily by *Methanobacterium* sp. [131] using different cathode materials [132]. Recently, a mutant strain of the methanogen, *Methanococcus maripaludis*, with six deleted hydrogenases [133] was also shown to be able to produce methane directly from a cathode [134]. This was the first study to use a six hydrogenase-deleted mutant strain of an electrotrophic microorganism to show hydrogen-independent methane formation, although the rates of methane formation were ten times slower than the wild type. Hydrogen gas and formate accumulated in reactors when methanogenesis was inhibited with 2-bromoethanesulfonate, showing production of other small compounds with microbial electrosynthesis. Additionally, the hydrogenase deficient mutant strain increased the electrode overpotential compared to the abiotic control, while the wild type strain decreased the electrode overpotential [134], suggesting that interactions between cell proteins and the electrode surface was important for system performance.

Several different biocathodes have been used to form short chain organic carbon compounds from the reduction of CO_2. Pure culture biocathodes of different bacteria including *Sporomusa ovata*, *Clostridium ljundhalii*, and *Moorella thermoacetica* [135] produced acetate using a cathode as the sole electron donor. Biocathodes of *Sporomusa ovata* were able to produce acetate

using electrons provided by a solar cell [136], highlighting the potential to produce valuable products from sustainable sources of energy. Pure cultures of *Methanococcus maripaludis* produced formate using electrons from a cathode when methanogenesis was inhibited with 2-bromoethanesulfonate [134]. Mixed culture biocathodes have also been used for acetate production [137].

Biocathodes can also be utilized to increase the value of organic compounds by chain elongation reactions. Small chain organic compounds can be transformed into more valuable, longer chain carbon compounds such as caproic acid [138, 139].

2.3.5 Mechanisms of Microbial Electron Uptake

The mechanisms of electron uptake by microorganisms have been studied using different approaches. One approach is to investigate protein expression of cells utilizing electrons from an electrode to identify proteins relevant for electron uptake. Protein expression was monitored for *Geobacter sulfurreducens* biofilms under electron accepting (cathodic) and electron donating (anodic) conditions. Proteins expressed for electron transfer to an insoluble surface, such as outer surface cytochromes and pili, were not as highly expressed during biocathodic operation. Further, mutations for these proteins did not affect the level of current uptake by the biofilm, suggesting that the mechanism for electron uptake was likely different than the mechanism for electron transfer to an insoluble surface [140]. However, studies utilizing *Shewanella* at a biocathode have suggested that the same Mtr pathway that is utilized to release electrons to an anode, can be used to accept electrons from a cathode [141].

Another approach to investigate mechanisms of electron uptake for hydrogen gas production is using mutant strains of microorganisms. BESs using pure cultures of *G. sulfurreducens* that were operated under current consuming or current producing conditions had different

transcriptomic profiles, suggesting that the mechanism of current consumption was different than current production. Mutants with deleted genes encoding outer membrane cytochromes (Δ*omc* A, Δ*omc* B, Δ*omc* ST, Δ*omc* E, and Δ*omc* Z) or pilin proteins (Δ*pil*A) known to be important for current production had no effect on current consumption, confirming this different mechanism for the two different processes [140]. Another study utilized a hydrogenase deficient strain of the methanogen, *M. maripaludis* (described above), to show hydrogen independent formation of methane. However, no mechanism was proposed for this electron transfer [134].

In many microbial electrosynthesis studies sterile control electrodes are used that have never been exposed to cells. However, control electrodes exposed to inactivated cells are not evaluated under similar conditions as treatments, discounting potential effects of non-viable cell material on the properties and capabilities of the electrodes. Although different mechanisms of electron uptake from electrodes by microorganisms have been proposed using these different approaches, relatively little definitive evidence exists for the mechanism of electron transfer from a solid surface to microorganisms.

2.4 Literature Cited

1. Logan, B.E., *Microbial fuel cells*. 2008, Hoboken, NJ: John Wiley & Sons, Inc. 300.
2. Logan, B.E., et al., *Microbial fuel cells: methodology and technology*. Environmental Science & Technology, 2006. **40**(17): p. 5181-5192.
3. Logan, B.E., *Exoelectrogenic bacteria that power microbial fuel cells.* Nat Rev Microbiol, 2009. **7**(5): p. 375-381.
4. Rismani-Yazdi, H., et al., *Cathodic limitations in microbial fuel cells: An overview.* Journal of Power Sources, 2008. **180**: p. 683–694.

5. Cheng, S., H. Liu, and B.E. Logan, *Increased power generation in a continuous flow MFC with advective flow through the porous anode and reduced electrode spacing.* Environmental Science & Technology, 2006. **40**: p. 2426-2432.

6. Logan, B.E., et al., *Microbial electrolysis cells for high yield hydrogen gas production from organic matter.* Environmental Science & Technology, 2008. **42**(23): p. 8630-8640.

7. Call, D., M.D. Merrill, and B.E. Logan, *High surface area stainless steel brushes as cathodes in microbial electrolysis cells (MECs).* Environmental Science & Technology, 2009. **43**(6): p. 2179-2183.

8. Wei, B., et al., *Development and evaluation of carbon and binder loading in low-cost activated carbon cathodes for air-cathode microbial fuel cells.* RSC Advances, 2012. **2**(33): p. 12751-12758.

9. Zhang, F., et al., *Novel anti-flooding poly(dimethylsiloxane) (PDMS) catalyst binder for microbial fuel cell cathodes.* J Power Sources, 2012. **218**(0): p. 100-105.

10. Rozendal, R.A., et al., *Towards practical implementation of bioelectrochemical wastewater treatment.* Trends in Biotechnology, 2008. **26**(8): p. 450-459.

11. Caccavo, F., Jr, et al., *Geobacter sulfurreducens sp. nov., a hydrogen- and acetate-oxidizing dissimilatory metal-reducing microorganism.* Appl Environ Microbiol, 1994. **60**(10): p. 3752-3759.

12. Kim, H.-J., et al., *A microbial fuel cell type lactate biosensor using a metal-reducing bacterium, Shewanella putrefaciens.* Journal of Microbiology and Biotechnology, 1999. **9**(3): p. 365-367.

13. Clark, M.E., et al., *Temporal transcriptomic analysis as Desulfovibrio vulgaris Hildenborough transitions into stationary phase during electron donor depletion.* Applied and Environmental Microbiology, 2006. **72**(8): p. 5578-5588.

14. Sun, D., et al., *Syntrophic interactions improve power production in formic acid fed MFCs operated with set anode potentials or fixed resistances.* Biotechnology and Bioengineering, 2012. **109**(2): p. 405-414.

15. Ren, L., et al., *High current densities enable exoelectrogens to outcompete aerobic heterotrophs for substrate.* Biotechnol Bioeng, 2014. **In Press**.

16. Ren, L., et al., *Treatability studies on different refinery wastewater samples using high-throughput microbial electrolysis cells (MECs).* Bioresource Technology, 2013. **136**(0): p. 322-328.

17. Kiely, P.D., et al., *Anode microbial communities produced by changing from microbial fuel cell to microbial electrolysis cell operation using two different wastewaters.* Bioresource Technol, 2011. **102**(1): p. 388-394.

18. Cusick, R., et al., *Performance of a pilot-scale continuous flow microbial electrolysis cell fed winery wastewater.* Applied Microbiology and Biotechnology, 2011. **89**(6): p. 2053-2063.

19. Angenent, L.T., et al., *Production of bioenergy and biochemicals from industiral and agricultural wastewater*. Trends in Biotechnology, 2004. **22**(9): p. 477-485.

20. Mink, J.E., et al., *Vertically Grown Multiwalled Carbon Nanotube Anode and Nickel Silicide Integrated High Performance Microsized (1.25 μL) Microbial Fuel Cell.* Nano Letters, 2012. **12**(2): p. 791-795.

21. Zhu, N., et al., *Improved performance of membrane free single-chamber air-cathode microbial fuel cells with nitric acid and ethylenediamine surface modified activated carbon fiber felt anodes.* Bioresource Technology, 2011. **102**(1): p. 422-426.

22. Cheng, S. and B.E. Logan, *Ammonia treatment of carbon cloth anodes to enhance power generation of microbial fuel cells.* Electrochem Commun, 2007. **9**(3): p. 492-496.

23. Zhang, X., et al., *Scalable air cathode microbial fuel cells using glass fiber separators, plastic mesh supporters, and graphite fiber brush anodes.* Bioresource Technology, 2011. **102**(1): p. 372-375.

24. Dumas, C., et al., *Marine microbial fuel cell: Use of stainless steel electrodes as anode and cathode materials.* Electrochimica Acta, 2007. **53**: p. 468-473.

25. Cheng, S., H. Liu, and B.E. Logan, *Increased performance of single-chamber microbial fuel cells using an improved cathode structure.* Electrochem Commun, 2006. **8**: p. 489-494.

26. Zhang, F., et al., *Power generation using an activated carbon and metal mesh cathode in a microbial fuel cell.* Electrochemistry Communications, 2009: p. In press, doi:10.1016/j.elecom.2009.09.024.

27. Call, D. and B.E. Logan, *Hydrogen production in a single chamber microbial electrolysis cell (MEC) lacking a membrane.* Environmental Science & Technology, 2008. **42**(9): p. 3401-3406.

28. Selembo, P.A., M.D. Merrill, and B.E. Logan, *The use of stainless steel and nickel alloys as low-cost cathodes in microbial electrolysis cells.* Journal of Power Sources, 2009. **190**(2): p. 271-278.

29. He, Z. and L.T. Angenent, *Application of bacterial biocathodes in microbial fuel cells.* Electroanalysis, 2006. **18**(19-20): p. 2009-2015.

30. Clauwaert, P., et al., *Open air biocathode enables effective electricity generation with microbial fuel cells.* Environmental Science & Technology, 2007. **41**(21): p. 7564-7569.

31. Lovley, D.R., *Dissimilatory metal reduction.* Ann Rev Microbiol, 1993. **47**(1): p. 263-290.

32. Torres, C.I., et al., *A kinetic perspective on extracellular electron transfer by anode-respiring bacteria.* FEMS Microbiology Reviews, 2010. **34**(1): p. 3-17.

33. Yates, M.D., et al., *Convergent development of anodic bacterial communities in microbial fuel cells.* ISME J, 2012. **6**(11): p. 2002-2012.

34. Malvankar, N.S., M.T. Tuominen, and D.R. Lovley, *Biofilm conductivity is a decisive variable for high-current-density Geobacter sulfurreducens microbial fuel cells.* Energ Environ Sci, 2012. **5**(2): p. 5790-5797.

35. Zhu, X., et al., *Microbial community composition is unaffected by anode potential.* Environ Sci Technol, 2013.

36. Zhu, X., M.D. Yates, and B.E. Logan, *Set potential regulation reveals additional oxidation peaks of Geobacter sulfurreducens anodic biofilms.* Electrochem Commun, 2012. **22**(0): p. 116-119.

37. Kim, B.-C., et al., *OmcF, a putative c-type monoheme outer membrane cytochrome required for the expression of other outer membrane cytochromes in Geobacter sulfurreducens.* J Bacteriol, 2005. **187**(13): p. 4505-4513.

38. Inoue, K., et al., *Specific localization of the c-type cytochrome OmcZ at the anode surface in current-producing biofilms of Geobacter sulfurreducens.* Environ Microbiol Report, 2011. **3**(2): p. 211-217.

39. Lovley, D.R., *Live wires: direct extracellular electron exchange for bioenergy and the bioremediation of energy-related contamination.* Energy & Environmental Science, 2011. **4**(12): p. 4896-4906.

40. Vargas, M., et al., *Aromatic Amino Acids Required for Pili Conductivity and Long-Range Extracellular Electron Transport in Geobacter sulfurreducens.* mBio, 2013. **4**(2).

41. Bond, D.R., et al., *On electron transport through Geobacter biofilms.* ChemSusChem, 2012. **5**(6): p. 1099-1105.

42. Franks, A.E., et al., *Microtoming coupled to microarray analysis to evaluate the spatial metabolic status of Geobacter sulfurreducens biofilms.* ISME J, 2010. **4**(4): p. 509-519.

43. Gorby, Y.A., et al., *Electrically conductive bacterial nanowires produced by Shewanella oneidensis strain MR-1 and other microorganisms.* Proceedings of the National Academy of Science, 2006. **103**(30): p. 11358-11363.

44. Beliaev, A.S., et al., *MtrC, an outer membrane decahaem c cytochrome required for metal reduction in Shewanella putrefaciens MR-1.* Molecular Microbiology, 2001. **39**(3): p. 722-730.

45. Myers, C.R. and J.M. Myers, *MtrB Is required for proper incorporation of the cytochromes OmcA and OmcB into the outer membrane of Shewanella putrefaciens MR-1.* Applied and Environmental Microbiology, 2002. **68**(11): p. 5585-5594.

46. Marsili, E., et al., *Shewanella secretes flavins that mediate extracellular electron transfer.* Proceedings of the National Academy of Science, 2008. **105**(10): p. 3968–3973.

47. Myers, J.M. and C.R. Myers, *Role for outer membrane cytochromes OmcA and OmcB of Shewanella putrefaciens MR-1 in reduction of manganese dioxide.* Applied and Environmental Microbiology, 2001. **67**(1): p. 260-269.

48. Xu, S. and H. Liu, *New exoelectrogen Citrobacter sp. SX-1 isolated from a microbial fuel cell.* Journal of Applied Microbiology, 2011. **111**(5): p. 1108-1115.

49. Fedorovich, V., et al., *Novel Electrochemically Active Bacterium Phylogenetically Related to Arcobacter butzleri, Isolated from a Microbial Fuel Cell.* Appl. Environ. Microbiol., 2009. **75**(23): p. 7326-7334.

50. Xing, D., et al., *Isolation of the exoelectrogenic denitrifying bacterium Comamonas denitrificans based on dilution to extinction.* Appl Microbiol Biot, 2010. **85**(5): p. 1575-1587.

51. Parameswaran, P., et al., *Kinetic, Electrochemical, and Microscopic Characterization of the Thermophilic, Anode-Respiring Bacterium Thermincola ferriacetica.* Environmental Science & Technology, 2013. **47**(9): p. 4934-4940.

52. Badalamenti, J.P., R. Krajmalnik-Brown, and C.I. Torres, *Generation of High Current Densities by Pure Cultures of Anode-Respiring Geoalkalibacter spp. under Alkaline and Saline Conditions in Microbial Electrochemical Cells.* mBio, 2013. **4**(3).

53. Allen, D.T. and N. Behmanesh, *Wastes as Raw Materials*. The Greening of Industrial Ecosystems. 1994: National Acadamies Press.

54. *Johnson Matthey Platinum 2012 Interim Review.* 2012.

55. Marinho, R.S., J.C. Afonso, and J.W.S.D. da Cunha, *Recovery of platinum from spent catalysts by liquid–liquid extraction in chloride medium.* Journal of Hazardous Materials, 2010. **179**(1–3): p. 488-494.

56. Sullivan, J.L., et al., *CO2 Emission Benefit of Diesel (versus Gasoline) Powered Vehicles.* Environmental Science & Technology, 2004. **38**(12): p. 3217-3223.

57. Acres, G.J.K. and B. Harrison, *The Development of Catalysts for Emission Control from Motor Vehicles: Early Research at Johnson Matthey*. Topics in Catalysis, 2004. **28**(1-4): p. 3-11.

58. Park, Y.J. and D.J. Fray, *Recovery of high purity precious metals from printed circuit boards.* Journal of Hazardous Materials, 2009. **164**(2–3): p. 1152-1158.

59. Babu, B.R., A.K. Parande, and C.A. Basha, *Electrical and electronic waste: a global environmental problem.* Waste Management & Research, 2007. **25**(4): p. 307-318.

60. Tungler, A., et al., *Palladium-Mediated Heterogeneous Catalytic Hydrogenations.* Platinum Metals Review, 1998. **42**(3): p. 108-115.

61. Auer, E., et al., *Carbons as supports for industrial precious metal catalysts.* Applied Catalysis A: General, 1998. **173**(2): p. 259-271.

62. Johnson and Matthey, *Platinum 2012 Interim Review.* 2012.

63. Volesky, B. and Z.R. Holan, *Biosorption of heavy metals.* Biotechnology Progress, 1995. **11**(3): p. 235-250.

64. Reuter, J.H. and E.M. Perdue, *Importance of heavy metal-organic matter interactions in natural waters.* Geochimica et Cosmochimica Acta, 1977. **41**(2): p. 325-334.

65. Bhattacharyya, D., A.B. Jumawan, and R.B. Grieves, *Separation of Toxic Heavy Metals by Sulfide Precipitation.* Separation Science and Technology, 1979. **14**(5): p. 441-452.

66. van Hullebusch, E.D., M.H. Zandvoort, and P.N.L. Lens, *Metal immobilisation by biofilms: Mechanisms and analytical tools.* Rev Environ Sci Bio, 2003. **2**(1): p. 9-33.

67. Yong, P., et al., *Bioaccumulation of palladium by Desulfovibrio desulfuricans.* J Chem Technol Biot, 2002. **77**(5): p. 593-601.

68. Orozco, R.L., et al., *Towards an integrated system for bio-energy: hydrogen production by Escherichia coli and use of palladium-coated waste cells for electricity generation in a fuel cell.* Biotechnol Lett, 2010. **32**(12): p. 1837-1845.

69. Windt, W.D., P. Aelterman, and W. Verstraete, *Bioreductive deposition of palladium (0) nanoparticles on Shewanella oneidensis with catalytic activity towards reductive dechlorination of polychlorinated biphenyls.* Environ Microbiol, 2005. **7**(3): p. 314-325.

70. Mackay, M.E., et al., *General strategies for nanoparticle dispersion.* Science, 2006. **311**(5768): p. 1740-1743.

71. Law, N., et al., *Formation of nanoscale elemental silver particles via enzymatic reduction by Geobacter sulfurreducens.* Appl Environ Microbiol, 2008. **74**(22): p. 7090-7093.

72. Li, Y. and M.A. El-Sayed, *The effect of stabilizers on the catalytic activity and stability of Pd colloidal nanoparticles in the Suzuki reactions in aqueous solution†.* J Phys Chem B, 2001. **105**(37): p. 8938-8943.

73. Jana, N.R., L. Gearheart, and C.J. Murphy, *Seeding Growth for Size Control of 5−40 nm Diameter Gold Nanoparticles.* Langmuir, 2001. **17**(22): p. 6782-6786.

74. Sun, S., *Recent Advances in Chemical Synthesis, Self-Assembly, and Applications of FePt Nanoparticles.* Advanced Materials, 2006. **18**(4): p. 393-403.

75. Liu, S., et al., *Evaporation-induced self-assembly of gold nanoparticles into a highly organized two-dimensional array.* Physical Chemistry Chemical Physics, 2002. **4**(24): p. 6059-6062.

76. Rotaru, A.-E., et al., *Non-enzymatic palladium recovery on microbial and synthetic surfaces.* Biotechnol Bioeng, 2012. **109**(8): p. 1889-1897.

77. Warren, S.C., et al., *Ordered mesoporous materials from metal nanoparticle–block copolymer self-assembly.* Science, 2008. **320**(5884): p. 1748-1752.

78. Tominaka, S., et al., *Mesoporous PdCo sponge-like nanostructure synthesized by electrodeposition and dealloying for oxygen reduction reaction.* Journal of Materials Chemistry, 2010. **20**(34): p. 7175-7182.

79. Warren, S.C., et al., *A silica sol-gel design strategy for nanostructured metallic materials.* Nat Mater, 2012. **11**(5): p. 460-467.

80. Wang, C.-C. and J.Y. Ying, *Sol−Gel Synthesis and Hydrothermal Processing of Anatase and Rutile Titania Nanocrystals.* Chemistry of Materials, 1999. **11**(11): p. 3113-3120.

81. Lakshmi, B.B., C.J. Patrissi, and C.R. Martin, *Sol−Gel Template Synthesis of Semiconductor Oxide Micro- and Nanostructures.* Chemistry of Materials, 1997. **9**(11): p. 2544-2550.

82. Lakshmi, B.B., P.K. Dorhout, and C.R. Martin, *Sol−Gel Template Synthesis of Semiconductor Nanostructures.* Chemistry of Materials, 1997. **9**(3): p. 857-862.

83. Mohanpuria, P., N. Rana, and S. Yadav, *Biosynthesis of nanoparticles: technological concepts and future applications.* Journal of Nanoparticle Research, 2008. **10**(3): p. 507-517.

84. Mukherjee, P., et al., *Fungus-Mediated Synthesis of Silver Nanoparticles and Their Immobilization in the Mycelial Matrix: A Novel Biological Approach to Nanoparticle Synthesis.* Nano Letters, 2001. **1**(10): p. 515-519.

85. Baxter-Plant, V.S., I.P. Mikheenko, and L.E. Macaskie, *Sulphate-reducing bacteria, palladium and the reductive dehalogenation of chlorinated aromatic compounds.* Biodegradation, 2003. **14**(2): p. 83-90.

86. Pat-Espadas, A.M., et al., *Reduction of palladium and production of nano-catalyst by Geobacter sulfurreducens.* Appl Microbiol Biot, 2012: p. 1-8.

87. Hennebel, T., et al., *Biocatalytic dechlorination of trichloroethylene with bio-palladium in a pilot-scale membrane reactor*. Biotechnol Bioeng, 2009. **102**(4): p. 995-1002.

88. Mabbett, A.N., et al., *Biorecovered precious metals from industrial wastes: Single-step conversion of a mixed metal liquid waste to a bioinorganic catalyst with environmental application.* Environ Sci Technol, 2005. **40**(3): p. 1015-1021.

89. Yong, P., et al., *Biorefining of precious metals from wastes: an answer to manufacturing of cheap nanocatalysts for fuel cells and power generation via an integrated biorefinery?* Biotechnology Letters, 2010. **32**(12): p. 1821-1828.

90. Yong, P., et al., *From bio-mineralisation to fuel cells: biomanufacture of Pt and Pd nanocrystals for fuel cell electrode catalyst.* Biotechnol Lett, 2007. **29**(4): p. 539-544.

91. Liu, Y., et al., *Tin coated viral-nanoforests as sodium-ion battery anodes.* ACS Nano, 2013. **7**(4): p. 3627-3634.

92. Li, D., B. Mathew, and C. Mao, *Biotemplated synthesis of hollow double-layered core/shell titania/silica nanotubes under ambient conditions.* Small, 2012. **8**(23): p. 3691-3697.

93. *U.S. Energy Information Administration. 2012. Crude oil.*

94. *U.S. Energy Information Administration. 2012. Coal*.

95. *U.S. Energy Information Administration. 2010. Natural gas*.

96. Murphy, D.J. and C.A.S. Hall, *Energy return on investment, peak oil, and the end of economic growth.* Annals of the New York Academy of Sciences, 2011. **1219**(1): p. 52-72.

97. Denholm, P. and M. Hand, *Grid flexibility and storage required to achieve very high penetration of variable renewable electricity.* Energy Policy, 2011. **39**(3): p. 1817-1830.

98. Liu, C.-x., Q.-A. Zeng, and Y. Liu, *A Dynamic Load Control Scheme for Smart Grid Systems.* Energy Procedia, 2011. **12**(0): p. 200-205.

99. Rabaey, K. and R.A. Rozendal, *Microbial electrosynthesis--revisiting the electrical route for microbial production.* Nat Rev Microbiol, 2010. **8**(10): p. 706-716.

100. Teleke, S., et al., *Rule-Based Control of Battery Energy Storage for Dispatching Intermittent Renewable Sources.* Sustainable Energy, IEEE Transactions on, 2010. **1**(3): p. 117-124.

101. Zhang, L.L. and X.S. Zhao, *Carbon-based materials as supercapacitor electrodes.* Chemical Society Reviews, 2009. **38**(9): p. 2520-2531.

102. Dillon, A.C., et al., *Storage of hydrogen in single-walled carbon nanotubes.* Nature, 1997. **386**(6623): p. 377-379.

103. Ashcroft, A.T., et al., *Partial oxidation of methane to synthesis gas using carbon dioxide.* Nature, 1991. **352**(6332): p. 225-226.

104. Rostrup-Nielsen, J.R., *Sulfur-passivated nickel catalysts for carbon-free steam reforming of methane.* Journal of Catalysis, 1984. **85**(1): p. 31-43.

105. Xu, J. and G.F. Froment, *Methane steam reforming, methanation and water-gas shift: I. Intrinsic kinetics.* AIChE Journal, 1989. **35**(1): p. 88-96.

106. Vasudeva, K., et al., *Steam reforming of ethanol for hydrogen production: Thermodynamic analysis.* International Journal of Hydrogen Energy, 1996. **21**(1): p. 13-18.

107. Papageorgopoulos, D.C., et al., *CO tolerance of Pd-rich platinum palladium carbon-supported electrocatalysts: Proton exchange membrane fuel cell applications.* J Electrochem Soc, 2002. **149**(11): p. A1400-A1404.

108. Air Products and Chemicals, I. 2014; Available from: http://www.airproducts.com/industries/Energy/Power/Power-Generation/faqs.aspx.

109. Holladay, J.D., et al., *An overview of hydrogen production technologies.* Catalysis Today, 2009. **139**(4): p. 244-260.

110. Chin, D.-T. and P.D. Howard, *Hydrogen sulfide poisoning of platinum anode in phosphoric acid fuel cell electrolyte.* J Electrochem Soc, 1986. **133**(12): p. 2447-2450.

111. Ide, M.S., D.D. Falcone, and R.J. Davis, *On the deactivation of supported platinum catalysts for selective oxidation of alcohols.* J Catal, 2014. **311**(0): p. 295-305.

112. Sun, Y., et al., *Electrodeposited cobalt-sulfide catalyst for electrochemical and photoelectrochemical hydrogen generation from water.* J Am Chem Soc, 2013. **135**(47): p. 17699-17702.

113. Zhang, G., et al., *Stability of an H2-producing photocatalyst (Ru/(CuAg)0.15In0.3Zn1.4S2) in aqueous solution under visible light irradiation.* International Journal of Hydrogen Energy, 2013. **38**(3): p. 1286-1296.

114. Chen, W.-F., et al., *Biomass-derived electrocatalytic composites for hydrogen evolution.* Energ Environ Sci, 2013. **6**(6): p. 1818-1826.

115. Hu, H., Y. Fan, and H. Liu, *Non-precious metal catalysts (NiMo, NiW) for hydrogen production in single chamber tubular microbial electrolysis cells with cloth electrode assemblies* Water Research, 2009: p. Submitted.

116. Alcaide, F., P.-L. Cabot, and E. Brillas, *Fuel cells for chemicals and energy cogeneration.* Journal of Power Sources, 2006. **153**(1): p. 47-60.

117. Stalder, R. and G.P. Roth, *Preparative Microfluidic Electrosynthesis of Drug Metabolites.* ACS Medicinal Chemistry Letters, 2013. **4**(11): p. 1119-1123.

118. Couper, A.M., D. Pletcher, and F.C. Walsh, *Electrode materials for electrosynthesis.* Chemical Reviews, 1990. **90**(5): p. 837-865.

119. Armstrong, F.A., et al., *Dynamic electrochemical investigations of hydrogen oxidation and production by enzymes and implications for future technology.* Chem Soc Rev, 2009. **38**(1): p. 36-51.

120. Sané, S., et al., *Using planktonic microorganisms to supply the unpurified multi-copper oxidases laccase and copper efflux oxidases at a biofuel cell cathode.* Bioresource Technol, 2014. **158**(0): p. 231-238.

121. Gutiérrez-Sánchez, C., et al., *Oriented Immobilization of a Membrane-Bound Hydrogenase onto an Electrode for Direct Electron Transfer.* Langmuir, 2011. **27**(10): p. 6449-6457.

122. Geelhoed, J.S. and A.J.M. Stams, *Electricity-assisted biological hydrogen production from acetate by Geobacter sulfurreducens.* Environ Sci Technol, 2010. **45**(2): p. 815-820.

123. Aulenta, F., et al., *Linking bacterial metabolism to graphite cathodes: Electrochemical insights into the H_2-producing capability of Desulfovibrio sp.* ChemSusChem, 2012. **5**(6): p. 1080-1085.

124. Croese, E., et al., *Analysis of the microbial community of the biocathode of a hydrogen-producing microbial electrolysis cell.* Appl Microbiol Biotechnol, 2011. **92**(5): p. 1083-1093.

125. Batlle-Vilanova, P., et al., *Assessment of biotic and abiotic graphite cathodes for hydrogen production in microbial electrolysis cells.* Int J Hydrogen Energ, 2014. **39**(3): p. 1297-1305.

126. Rozendal, R.A., et al., *Hydrogen production with a microbial biocathode.* Environ Sci Technol, 2008. **42**(2): p. 629-634.

127. Fu, Q., et al., *Bioelectrochemical analyses of a thermophilic biocathode catalyzing sustainable hydrogen production.* Int J Hydrogen Energ, 2013. **38**(35): p. 15638-15645.

128. Villano, M., et al., *Bioelectrochemical hydrogen production with hydrogenophilic dechlorinating bacteria as electrocatalytic agents.* Bioresource Technol, 2011. **102**(3): p. 3193-3199.

129. Cheng, S., et al., *Direct biological conversion of electrons into methane by electromethanogenesis.* Environ Sci Technol, 2009. **43**(10): p. 3953-3958.

130. Sato, K., H. Kawaguchi, and H. Kobayashi, *Bio-electrochemical conversion of carbon dioxide to methane in geological storage reservoirs.* Energy Conversion and Management, 2013. **66**(0): p. 343-350.

131. Siegert, M., et al., *Methanobacterium dominates biocathodes.* ISME J, 2014. **In Review**.

132. Siegert, M., et al., *Comparison of non-precious metal cathode materials for methane production by electromethanogenesis.* ACS Sus Chem Eng, 2014.

133. Lie, T.J., et al., *Essential anaplerotic role for the energy-converting hydrogenase Eha in hydrogenotrophic methanogenesis.* Proceedings of the National Academy of Sciences, 2012.

134. Lohner, S.T., et al., *Microbial electrosynthesis by direct uptake and metabolism of cathodic electrons by the Archaeon Methanococcus maripaludis.* ISME J, 2014. **in press**.

135. Nevin, K.P., et al., *Electrosynthesis of organic compounds from carbon dioxide is catalyzed by a diversity of acetogenic microorganisms.* Appl Environ Microbiol, 2011. **77**(9): p. 2882-2886.

136. Nevin, K.P., et al., *Microbial Electrosynthesis: Feeding Microbes Electricity To Convert Carbon Dioxide and Water to Multicarbon Extracellular Organic Compounds.* mBio, 2010. **1**(2).

137. Marshall, C.W., et al., *Electrosynthesis of Commodity Chemicals by an Autotrophic Microbial Community.* Applied and Environmental Microbiology, 2012.

138. Agler, M.T., et al., *Chain elongation with reactor microbiomes: upgrading dilute ethanol to medium-chain carboxylates.* Energ Environ Sci, 2012. **5**(8): p. 8189-8192.

139. Van Eerten-Jansen, M.C.A.A., et al., *Bioelectrochemical Production of Caproate and Caprylate from Acetate by Mixed Cultures.* ACS Sustainable Chemistry & Engineering, 2013. **1**(5): p. 513-518.

140. Strycharz, S.M., et al., *Gene expression and deletion analysis of mechanisms for electron transfer from electrodes to Geobacter sulfurreducens.* Bioelectrochemistry, 2011. **80**(2): p. 142-150.

141. Ross, D.E., et al., *Towards electrosynthesis in Shewanella: Energetics of reversing the Mtr pathway for reductive metabolism.* PLoS ONE, 2011. **6**(2): p. e16649.

Chapter 3

Extracellular Palladium Nanoparticle Production Using *Geobacter sulfurreducens*

3.1 Abstract

Sustainable methods are needed to recycle precious metals and synthesize catalytic nanoparticles. Pd nanoparticles can be produced via microbial reduction of soluble Pd(II) to Pd(0), but in previous tests using dissimilatory metal reducing bacteria (DMRB), the nanoparticles were closely associated with the cells, occupying potential reductive sites and eliminating the potential for cell reuse. The DMRB *Geobacter sulfurreducens* was shown here to reduce soluble Pd(II) to Pd(0) nanoparticles primarily outside the cell, reducing the toxicity of metal ions and allowing nanoparticle recovery without cell destruction that has previously been observed using other microorganisms. Cultures reduced 50±3 mg/L Pd(II) with 1% hydrogen gas (v/v headspace) in six-hour incubation tests [100 mg/L Pd(II) initially], compared to 8±3 mg/L (10 mM acetate) without H_2. Acetate was ineffective as an electron donor for palladium removal in the presence or absence of fumarate as an electron acceptor. TEM imaging verified that Pd(0) nanoparticles were predominantly in the EPS surrounding cells in H_2-fed cultures, with only a small number of particles visible inside the cell. Separation of the cells and EPS by centrifugation allowed reuse of the cell suspensions and effective nanoparticle recovery. These results demonstrate effective Pd recovery and nanoparticle production using *G. sulfurreducens* cell suspensions and renewable substrates such as H_2 gas.

3.2 Introduction

Palladium is a precious metal commonly used in catalytic converters of automobiles to lower emissions of harmful pollutants, as well as in refining, electronics, dentistry, and catalysis [1, 2]. Palladium consumption has outpaced production rates in the last decade [2], increasing the need for more effective and sustainable methods for its recovery from waste streams. Bulk palladium recovery processes commonly involve dissolution of the metal using acids at high temperatures following separation of spent catalysts from other waste products. Strong reductants, such as sulfur dioxide or sodium borohydride, are then used to generate bulk insoluble palladium [3]. The production of palladium nanoparticle catalysts (0.1 – 100 nm in diameter) [4] has become favored over bulk production in order to take advantage of the unique physicochemical properties of these nano-sized particles [5]. Traditional chemical methods of palladium nanoparticle synthesis requires use of strong reducing agents, as well as ligand stabilizing polymers and capping agents to control particle size and dispersion [6]. These processes generate undesirable waste streams that need to be avoided.

There is growing interest in using microbiological methods to precipitate metals out of waste streams [7]. The major advantages of using bacteria is that the cells are the reducing agents, eliminating the need for chemical reducing agents (except for substrates for the bacteria), and the cells self-regulate particle growth so that they form only nano-sized particles. This strategy for nanoparticle synthesis avoids utilization of chemical reductants such as sodium borohydride [4] and expensive polymeric capping agents and stabilizers [8]. The catalytic activity of biologically-supported palladium nanoparticles for contaminant reduction has been compared to commercially available catalysts with mixed conclusions [6, 9, 10]. The formation of Pd nanoparticles on cell surfaces in high dry cell weight to palladium ratios has led to a decrease in catalytic activity due

to poisoning by sulfur compounds contained in cell proteins [6], making separation of nanoparticles from cells important to maintain catalytic activity.

Biological metal precipitation has been studied using various pure cultures [7], including *E. coli* [11], fermentative bacteria [12], and dissimilatory metal reducing bacteria (DMRB). Most of the work utilizing DMRB has focused on the *Shewanella* and *Desulfovibrio* genera [13, 14]. The primary route for nanoparticle synthesis by DMRB is through hydrogenases. In *Desulfovibrio* spp., different hydrogenases have been found in the periplasm, cytoplasm, and cytoplasmic membrane and have been shown to act as the nucleation and initiation point for metal reduction [15], with subsequent nanoparticle growth via autocatalytic reduction [14]. The nanoparticles formed in the periplasm and outer-membrane are naturally stabilized and capped with the native polymers, inhibiting aggregation and uncontrolled growth of the particles. Extracellular reduction also occurs in *Desulfovibrio* spp. during reduction of Au(III), but the mechanism, although not fully understood, is believed to differ from that of palladium [12, 16]. Outer membrane *c*-type cytochromes have also been shown to be a site for Pd(0) reduction in *Shewanella oneidensis* [17]. *Shewanella* and *Desulfovibrio* spp. can precipitate a broad range of metals (Fe, Mn, U, Cr, Te, Tc, Pd) [18, 19] using various electron donors (e.g. formate, pyruvate, or hydrogen). In addition, both *Desulfovibrio desulfuricans* (200 mg/L) and *Shewanella oneidensis* (1000 mg/L) can reduce high concentrations of soluble palladium to nanoscale particles. Nanoparticle formation by *Desulfovibrio* occurs primarily in the periplasm, which has the disadvantage of inactivating the cells by protruding through and rupturing the cell membrane, necessitating a new culture of bacteria for each reduction cycle [14]. Intracellular and periplasmic nanoparticle production also require additional procedures to access catalytically active sites [20]. The response of different microorganisms to Pd and other precipitated metals varies. *E. coli*, for example is able to perform enantioseletive deracemization reactions after being challenged with soluble palladium (~100 mg/L) [11] and fermentative bacteria are able to produce hydrogen after reduction of soluble

palladium (50 mg/L) [21]. Additionally, *Shewanella* cell suspensions have remained culturable after being challenged with low levels of soluble palladium (10 mg/L) [13], but cell culturability at elevated levels of Pd have not been tested. The viability of *Desulfovibrio* cells after palladium reduction has not been reported.

Geobacter are DMRBs that can reduce solid and insoluble metals extracellularly via multiple outer membrane cytochromes (e.g. OmcB, OmcC, OmcS, OmcF, OmcZ) [22, 23] or a *c*-type cytochrome that is excreted into solution [24]. *Geobacter* spp. also have multiple NiFe hydrogenase complexes (two membrane-bound periplasmic and two cytoplasmic hydrogenases) [25] with one essential periplasmic hydrogenase (Hyb) for respiration with hydrogen [26]. These microbes can reduce a variety of metals [27], including U(VI) to U(IV) [28] and amorphous Fe(III) to magnetite. Magnetite formed by *G. sulfurreducens* has been used as a nano-scale support for a palladium catalyst [29]. *G. sulfurreducens* has been shown to reduce Ag(I) to Ag(0) nanoparticles primarily via outer membrane *c*-type cytochromes during acetate oxidation and fumarate reduction [30]. Silver reduction occurred extracellularly with no evidence of reduction in the periplasm of the cells [30], suggesting that cells could remain viable, allowing for reuse of the cell suspension and recovery of nanoparticles without rupturing the cells. Recently, Pd(0) nanoparticle formation by *G. sulfurreducens* was shown for Cr(VI) reduction with formate as the electron donor, but only in the presence of a mediator (AQDS) [31]. The ability of *Geobacter* spp. to reduce palladium directly, or to use H_2 for metal nanoparticle formation, has not previously been examined.

The extent of Pd(II) reduction to Pd(0) nanoparticles was examined here using *Geobacter sulfurreducens* with hydrogen or acetate as electron donors, and the presence or absence of an alternate electron acceptor (fumarate). The potential for reusing the cell suspensions in successive reduction cycles was also examined following particle recovery by simple centrifugation. The

location of the particles (intracellular versus extracellular) was examined using electron microscopy.

3.3 Materials and Methods

3.3.1 Culturing Methods

Geobacter sulfurreducens PCA was obtained from frozen stocks (–80°C), and cultured in ATCC medium 1957 with 30 mM acetate at 30°C. Cells were anaerobically washed twice with ATCC medium 1957 (no electron donor or acceptor), and resuspended in sterilized anaerobic (80% CO_2/ 20% N_2) serum bottles at an OD_{610} of 0.5 ± 0.05.

3.3.2 Location of Palladium Reduction

Samples were collected and fixed in a 0.1 M sodium cacodylate buffer containing 2.5% glutaraldehyde and 1.5% paraformaldehyde in a 1:10 ratio of sample to fixative solution, and stored at 4°C. Samples for TEM analysis were prepared by either pelleting the cells (4500 × g for 10 minutes) before fixation, or by gravitational settling of the cells in fixative. Samples were analyzed with an environmental scanning electron microscope (E-SEM) (FEI Quanta 200) equipped with an electron dispersive X-ray spectroscopy (EDS) detector to confirm that the extracellular precipitates were palladium. Samples were also analyzed with a transmission electron microscope (TEM) (JEOL JEM 1200 EXII) to capture images of the extracellular palladium nanoparticles on the cell surface. Nanoparticle size was estimated by counting particles in TEM images using the Image J software. Samples were analyzed with a Live/Dead BacLight Bacterial Viability Kit (Invitrogen, USA) to determine the relative amount of cells that were alive

(based on having intact outer membranes) after palladization using an epifluorescent microscope (Olympus BX61).

To investigate the extent of extracellular palladium reduction, samples were fixed as described above and embedded in Eponate resin after staining with osmium tetroxide and uranyl acetate, and dehydrated in an ethanol and acetone series. The embedded sample was ultra-microtomed (Leica EM UC6 Microtome) into 70 nm slices and imaged using TEM.

3.3.3 Palladium Reduction Tests

To determine the optimal time for palladium reduction and nanoparticle formation, *G. sulfurreducens* cell suspensions and abiotic controls were incubated in 56 mL culture bottles (26 mL headspace) for 6, 12, and 24 hours (30°C) at a Pd(II) concentration of 100 mg/L. Culture incubation time was set to 6 hours to prevent excessive abiotic Pd reduction (Figure A.1). To determine the mass of palladium that *G. sulfurreducens* could reduce, cultures were incubated for 6 hours in solutions containing 5, 10, 50, 100, and 200 mg/L of Pd(II). The electron donors tested included hydrogen (headspace concentrations of 1, 2.5, and 5% v/v) and sodium acetate (10 mM). Sodium tetrachloropalladate (Na_2PdCl_4, Sigma-Aldrich, USA) was added to the cultures as the electron acceptor in all tests and sodium fumarate (40 mM) was added as an alternate electron acceptor in some tests with acetate as the electron donor. Negative controls were run for each condition using fresh, sterile medium. Killed controls for testing Pd removal were prepared by autoclaving cell suspensions at 121°C for 15 minutes. Any pressure in the serum bottles was released prior to addition of the electron donor. The reuse of cell suspensions examined using 2.5% H_2 in the headspace was also tested with sodium acetate (1 mM) as a carbon source. Tests were run in duplicate with abiotic controls. Cell suspensions reused in multiple reduction cycles were centrifuged, washed once with ATCC medium 1957 (no electron donor or acceptor), and

then re-suspended in fresh medium after each test. Subsequent tests were then conducted as above, with the indicated electron donor and 100 mg/L Pd(II) for 6 hrs at 30°C.

3.3.4 Palladium Analysis and Recovery

Soluble palladium (duplicates) was determined by filtering samples through 0.22 µm pore diameter filters followed by analysis using inductively coupled plasma emission spectrometry (ICP-AES) (Perkin-Elmer Optima 5300). Samples were acidified with 1 M nitric acid to prevent precipitation prior to analysis.

Particulate palladium recovery was examined using centrifugation and filtration. Cell suspensions were divided into three fractions: the supernatant containing no cells (Fraction 1), the cell fraction (Fraction 2), and the pellet that could not be resuspended by vortexing (Fraction 3). These fractions were obtained by first pelleting cells by centrifugation (4500 × g) for 10 minutes. The supernatant (Fraction 1) was decanted and centrifuged at 12,000 × g for 2 hr to concentrate suspended nanoparticles. The liquid was then placed in an oven set to 650°C for 2 hr to remove any organics and determine the mass of suspended palladium. Samples were stored at 4°C prior to further analysis. The cell fraction (Fraction 2) was then resuspended in bicarbonate buffer (described above) and filtered through 0.65 µm pore diameter centrifugal filters (Millipore, US) at 10,000 × g for 10 minutes in to test the efficacy of filtration on the separation of palladium nanoparticles from cells. The filtrate was centrifuged for an additional 2 hr at 12,000 × g to pellet any remaining particles and stored at 4°C. The pellet that could not be resuspended by vortexing (Fraction 3) was removed from the centrifuge tube, pyrolyzed at 650°C for 2 hours to remove organics, and weighed to determine the mass of palladium. A small portion (~200 µL) of these samples was taken to be analyzed by TEM to determine the size and morphology of the particles.

3.4 Results and Discussion

3.4.1 Extracellular Palladium Nanoparticle Formation

Palladium reduced with *G. sulfurreducens* cultures incubated with headspace hydrogen of 1 and 2.5% (v/v) and 10 mM acetate with fumarate produced nanoparticles on the surface of cells and in the EPS. Nanoparticles formed in solution were smaller and had less variation (14 ± 3 nm in diameter) than those closely associated with cells (25 ± 11 nm; Figure 3.1a), in agreement with previous reports for nanoparticle production with *Desulfovibrio* and *Shewanella* [13, 32]. Particles associated with the surface of cells were confirmed to be palladium using EDS (Figure A.2). Controlling palladium particle size and preventing aggregation is desirable because active surface area is maximized compared to larger, aggregated particles (1-10 μm) produced via abiotic reduction with H_2. There was little evidence of aggregation of the nanoparticles based on TEM images, highlighting the importance of palladium reduction in the presence of stabilizing ligands in the exopolymer matrix. Abiotic reduction of palladium occurred at an appreciable rate when the headspace H_2 (v/v) was above 2.5%, resulting in the growth of large and non-dispersed particles. Aggregates were apparent in the solution and microscopic analysis indicated the presence of many particles in the size range of 1-10 μm (Figure A.3).

Killed cells also removed palladium from solution (see below), but only a few extracellular nanoparticles were observed in TEM images (Figure 3.1f). The middle of the killed cells appeared dark relative to living cells in Pd reduction cultures, which indicated intracellular palladium accumulation. Palladium adsorption to biomass, and subsequent reduction by H_2, was likely the dominant mechanism of Pd removal in killed cell cultures. The internal reduction of palladium by autoclaved cells was observed in cross sections of resin embedded cells (Figure 3.2d). Cells were ruptured during the sterilization process allowing palladium to diffuse into the

cells and reduced. Metal adsorption to biomass is well known and can be used as a method of metallic ion removal from solution [33]. Dead biomass produced less nanoparticles because the extracellular and outer-membrane bound proteins were inactivated, inhibiting the normal cellular mechanisms of nanoparticle generation. Though removal of metals from waste streams by dead biomass is a viable option, live cells are better suited for concurrent removal and nanoparticle production that can be used for downstream applications.

Cross sections of resin embedded cells from live suspensions fed 1% H_2 showed primarily extracellular reduction (Figure 3.2a). Some periplasmic and intracellular reduction by *G. sulfurreducens* was also observed. It is possible that periplasmic reduction occurred due to oversaturation of extracellular reduction sites, allowing soluble palladium to diffuse into the periplasmic space where it could have been reduced via periplasmic hydrogenases [11]. Previously, periplasmic reduction of Ag(0) nanoparticles was not observed using *G. sulfurreducens* [30]. However, the Pd(II) concentration here was five times higher than the Ag(I) concentration in the previous study.

Palladium nanoparticle formation in solution was more evident when cells were gravity settled instead of centrifuged before TEM imaging (Figure 3.1c). Cells that were settled in fixative prior to imaging exhibited a noticeable increase in the amount of extracellular nanoparticles relatively far away (~200 nm) from cells. When cells were centrifuged before imaging, observed palladium nanoparticles were all very close to the cell surface (~20 nm). Centrifugation of cells to concentrate them before TEM imaging causes nanoparticles formed in solution to stick to the cell aggregates, which misrepresents the distribution of nanoparticles in different locations.

3.4.2 Palladium Reduction with Hydrogen or Acetate

Hydrogen was an effective electron donor for palladium reduction in cultures and controls. *G. sulfurreducens* cultures removed 51 ± 1 mg/L of a 100 mg/L Pd(II) solution, and 68 ± 1 mg/L of a 200 mg/L Pd(II) solution with 1% H_2 (v/v) in the headspace (Figure 3.3). Removal increased to 59 ± 1 mg/L [100 mg/L Pd(II)] when the headspace hydrogen was increased to 2.5% (v/v). Abiotic palladium reduction increased in the presence of high concentrations of H_2 (Fig. SI4). Pd(II) removal in abiotic controls was greater than in suspensions of *G. sulfurreducens* when H_2 concentrations were increased above 2.5% (v/v). However, the sizes of these particles could not be confined to the nanoparticle size range, and therefore they became much larger (tens of microns) than the bio-Pd nanoparticles, which is undesirable for downstream applications as less catalytic surface area is exposed.

Palladium removal by *G. sulfurreducens* using H_2 is low compared to other DMRB (Table 3.1). *Desulfovibrio* spp. were able to use hydrogen as an electron donor to remove 200 mg/L of soluble palladium in 30 min (*D. vulgaris*) [9] to 80 min (*D. fructosivorans*) [34] compared to 75% removal of a 50 mg/L solution by *G. sulfurreducens* in 360 min. *Shewanella oneidensis* MR-1 was able to use H_2 as an electron donor to reduce 90% of a 50 mg/L Pd(II) solution. However, the reduction reaction was allowed to proceed overnight, making the palladium removal rates by *S. oneidensis* MR-1 similar to those obtained in this study.

Acetate was ineffective as an electron donor for palladium reduction. The maximum palladium removal of *G. sulfurreducens* cultures fed sodium acetate (10 mM) was 15 ± 3 mg/L using a 50 mg/L Pd (II) solution (Figure 3.3). Removal decreased to 8 ± 3 mg/L Pd(II) when soluble palladium concentration was increased to 100 mg/L Pd(II). Cultures fed acetate and incubated with palladium as the sole electron acceptor produced few nanoparticles, as seen in TEM images (Figure 3.4a). Cross sections of resin embedded cells fed acetate showed an increase

of periplasmic palladium reduction compared to cells fed hydrogen (Figure 3.4f) Cell suspensions in a 100 mg/L Pd(II) solution given no electron donor removed a similar amount of palladium (6 ± 2 mg/L) as those fed acetate.

The inability of *G. sulfurreducens* to use acetate (its preferred electron donor) as an organic electron donor under anaerobic conditions for palladium reduction is different from other species of DMRB (Table 3.1). *S. oneidensis* MR-1 can effectively use organic electron donors such as formate, lactate, ethanol, and pyruvate and *D. vulgaris* was able to use formate to reduce palladium.

Killed cells removed a significant portion of the soluble palladium in solution, in agreement with previous studies [10, 12, 35]. In the presence of hydrogen, killed *G. sulfurreducens* cells removed 35 ± 1 mg/L (1% headspace H_2) and 42 ± 5 mg/L (2.5% headspace H_2) of a 100 mg/L Pd(II) solution.

3.4.3 Palladium Reduction with Fumarate

The addition of fumarate, as an alternate electron acceptor to acetate fed *G. sulfurreducens* cultures did not increase palladium reduction. Palladium removal was similar (8 ± 1 mg/L) upon the addition of fumarate to cultures with 100 mg/L Pd(II) in solution. No palladium reduction occurred in abiotic controls with acetate and fumarate. However, extracellular nanoparticles were produced with fumarate addition instead of intracellular accumulation (Figure 3.4c), similar to that observed in previous experiments on the reduction of soluble Ag(I) to Ag(0) nanoparticles in the presence of fumarate [30].

The limited ability of *G. sulfurreducens* to reduce palladium with acetate as the electron donor-suggests that the major pathway of Pd(II) reduction is via hydrogenase activity. However,

there are no extracellular hydrogenases identified in the genome of *G. sulfurreducens* [26]. With acetate as the electron donor, the expected mechanism of extracellular Pd(II) reduction is by cytochromes, but little extracellular reduction occurs with palladium as the sole electron acceptor, implying that soluble palladium could not be effectively used as a terminal electron acceptor. In tests with H_2 as the electron donor, palladium adsorbed to acid functional groups in the EPS are reduced to palladium nanoparticles, as shown in a similar test using carboxymethylcellulose as the ligand for nanoparticle formation [36]. However, acetate is unable to act as a reductant in the EPS, leading to a decrease in palladium reduction. When fumarate is present as the terminal electron acceptor, a portion of the electrons taken from acetate oxidation could be redirected to cytochromes for extracellular palladium reduction during respiration as a detoxification mechanism. The addition of fumarate increased nanoparticle formation, but did not increase the rate of palladium reduction, implying that acetate oxidation is the rate limiting step. The precise biological mechanism explaining the difference in palladium reduction by *G. sulfurreducens* when using hydrogen or acetate as the electron donor remains unclear.

3.4.4 Recycling of Cell Suspensions

Cultures were reused in successive reduction cycles for each electron donor with 100 mg/L of Pd(II) as the electron acceptor (Figure 3.5). Palladium removal was lower after the first cycle, but the percent removal was relatively stable thereafter. With 1% H_2 as the electron donor, 50 ± 1 mg/L of Pd(II) was removed during the initial cycle, and 26 ± 4 mg/L was removed during the next three cycles. Palladium removal increased to 55 ± 1 mg/L followed by 42 ± 1 mg/L for successive cycles with 2.5% H_2. Intracellular palladium accumulation in some cells in suspension, observed in the TEM images of embedded cells, could disrupt normal cellular processes and explain the drop in palladium removal after the first cycle.

The addition of low acetate concentrations (1 mM) as a carbon source for cell maintenance during reduction with 2.5% H_2 enhanced removal (58 ± 1 mg/L initially and 42 ± 3 mg/L for successive cycles). However, cultures with 10 mM acetate as the sole electron donor reduced only 8 ± 3 mg/L Pd during the first cycle, and there was no Pd(II) reduction in any of the three following cycles demonstrating acetate was an ineffective electron donor for Pd(II) reduction. Suspensions of *G. sulfurreducens* can be supplemented with acetate to provide a carbon source to support cellular maintenance while using a different electron donor (such as H_2) for palladium reduction, as acetate is ineffective as the sole electron donor for palladium reduction.

3.4.5 Palladium Recovery

Centrifugation was effective for palladium nanoparticle recovery from cell suspensions because nanoparticles were relatively far from the cell surfaces. Roughly 63 ± 5% of the initial soluble palladium added to the *G. sulfurreducens* cultures (1% H_2 in the headspace) was recovered as palladium particles by centrifugation. The centrifugation supernatant (Fraction 1) contained 13 ± 3% (0.4 ± 0.1 mg) of the initial palladium as palladium particles and the fraction of the cell pellet that could not be resuspended by vortexing (Fraction 3) contained 50 ± 1% (1.5 ± 0.3 mg) of the initial soluble palladium as particles. The remaining palladium remained attached to the cells or was lost in the solution. The palladium that remains attached to cells or inside the periplasm can be recovered once cell death and lysis occurs, allowing the palladium to be separated via centrifugation and recovered along with the palladium in solution. A continuous process would need to be employed to maintain an active, steady cell suspension. These results suggest that further optimization of nanoparticle separation and recovery via centrifugation is warranted to increase the overall efficiency of the process.

Filtration was ineffective at separating nanoparticles from cells. No palladium particles were detected in the cell fraction filtered by 0.65 μm centrifugal filters (Fraction 2). Filtration was a less effective separation technique because the EPS (and any nanoparticles in the EPS) was likely trapped by the filter material instead of passing through. Additionally, nanoparticles still attached to the cells or reduced inside the cells would not be passed through the filter.

3.5 Conclusions

G. sulfurreducens is able to reduce soluble Pd(II) into Pd(0) nanoparticles extracellulary, giving it potential application in the reclamation of palladium from waste streams. Hydrogen was an effective electron donor with an optimal headspace concentration of 1% (v/v) due to the low abiotic reduction. Acetate proved to be an ineffective electron donor when palladium was the sole electron acceptor and few nanoparticles were formed. The palladium reduction rate was further decreased when fumarate was added as an alternative electron acceptor, however nanoparticle production increased. The palladium could be recovered via centrifugation, but not filtration, after the reduction cycles. *G. sulfurreducens* also can be used multiple times for reduction despite some periplasmic reduction, enhancing its potential application for a sustainable method of palladium nanoparticle production.

3.6 Figures

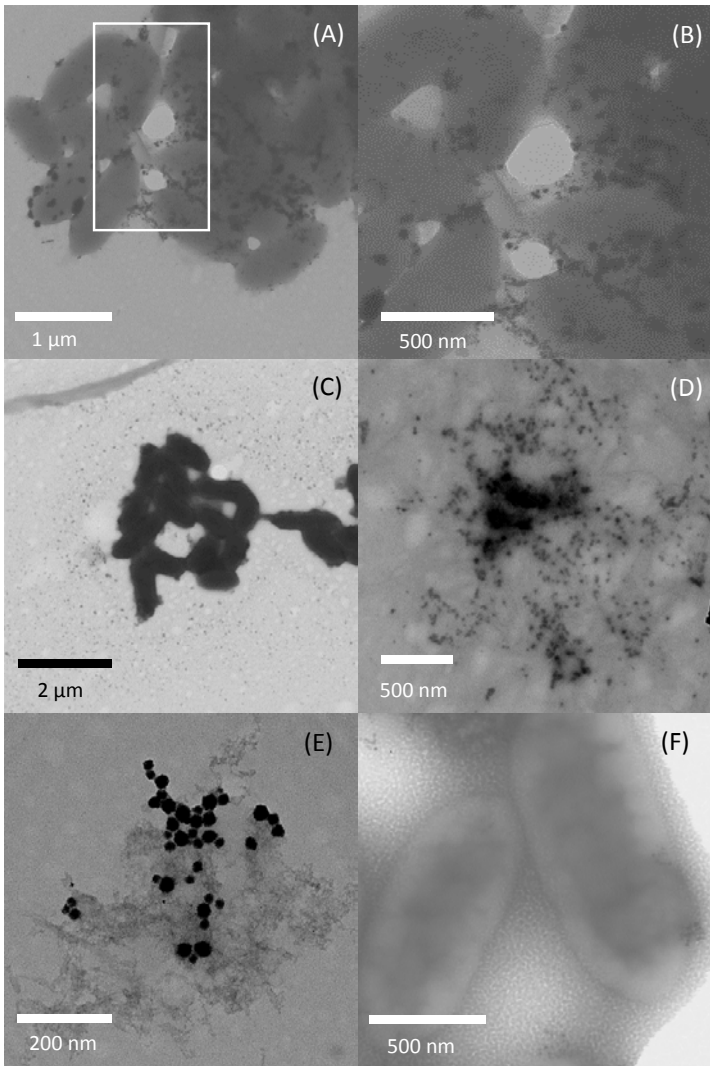

Figure 3.1. TEM images of palladium reduction with hydrogen as the electron donor. (A) palladium nanoparticles on the surface *G. sulfurreducens* and near the cell (expanded in (B)); (C) nanoparticles in the solution surrounding the cells; (D) magnification of particles in solution surrounding cells; (E) particles in centrifugation pellet; (F) autoclaved biomass with palladium as the sole electron acceptor exhibiting limited nanoparticle formation compared to viable biomass.

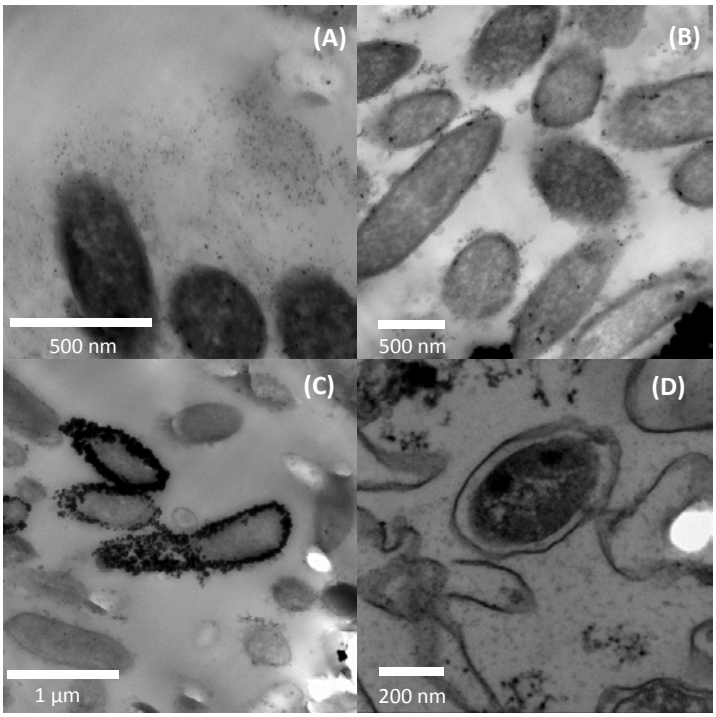

Figure 3.2. TEM images of ultra-microtomed cell pellet. (A) Extracellular reduction is seen in the space between the cells. (B) Cells exhibit some periplasmic and intracellular reduction. (C) A few cells exhibit buildup of palladium particles that cause cell death. (D) Killed cells fed hydrogen with increased intracellular palladium reduction due to membrane rupturing.

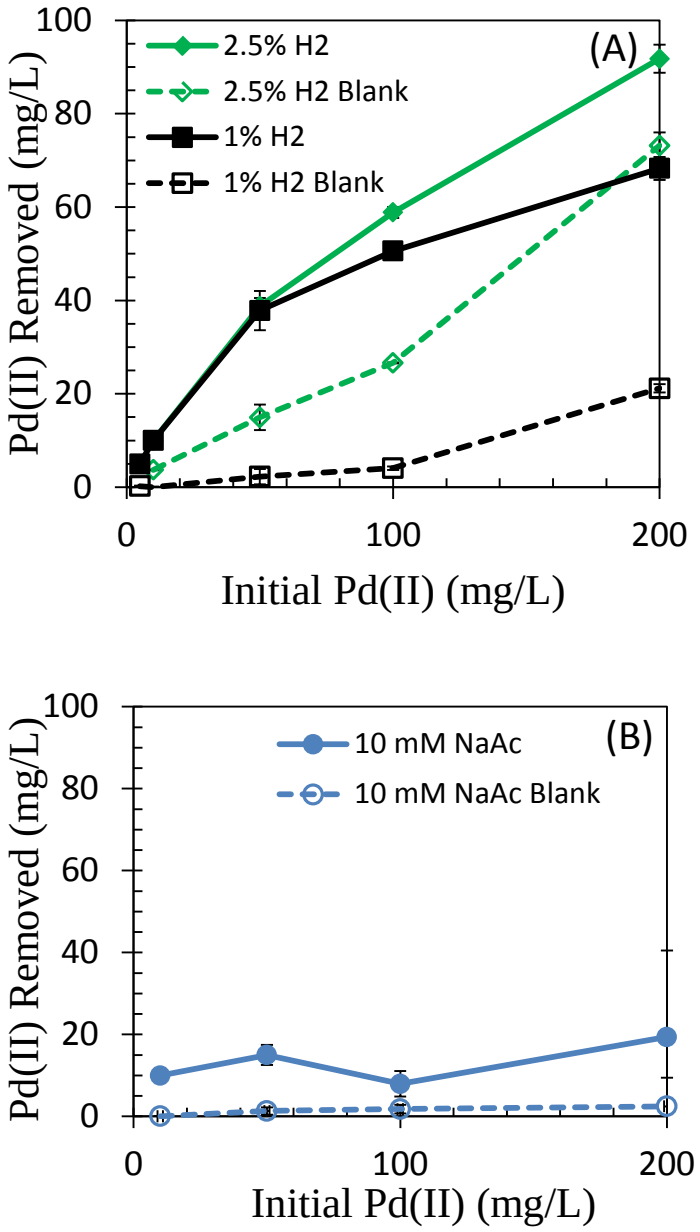

Figure 3.3. Palladium removal by *G. sulfurreducens* with (A) hydrogen or (B) acetate as the electron donor. Acetate was not an effective electron donor. Hydrogen was effective, but concentrations higher than 2.5% (v/v) in the headspace gave a large amount of abiotic reduction that confounded the amount of biological palladium removal. Reduction in abiotic tests is undesirable because particle growth and agglomeration is uncontrolled.

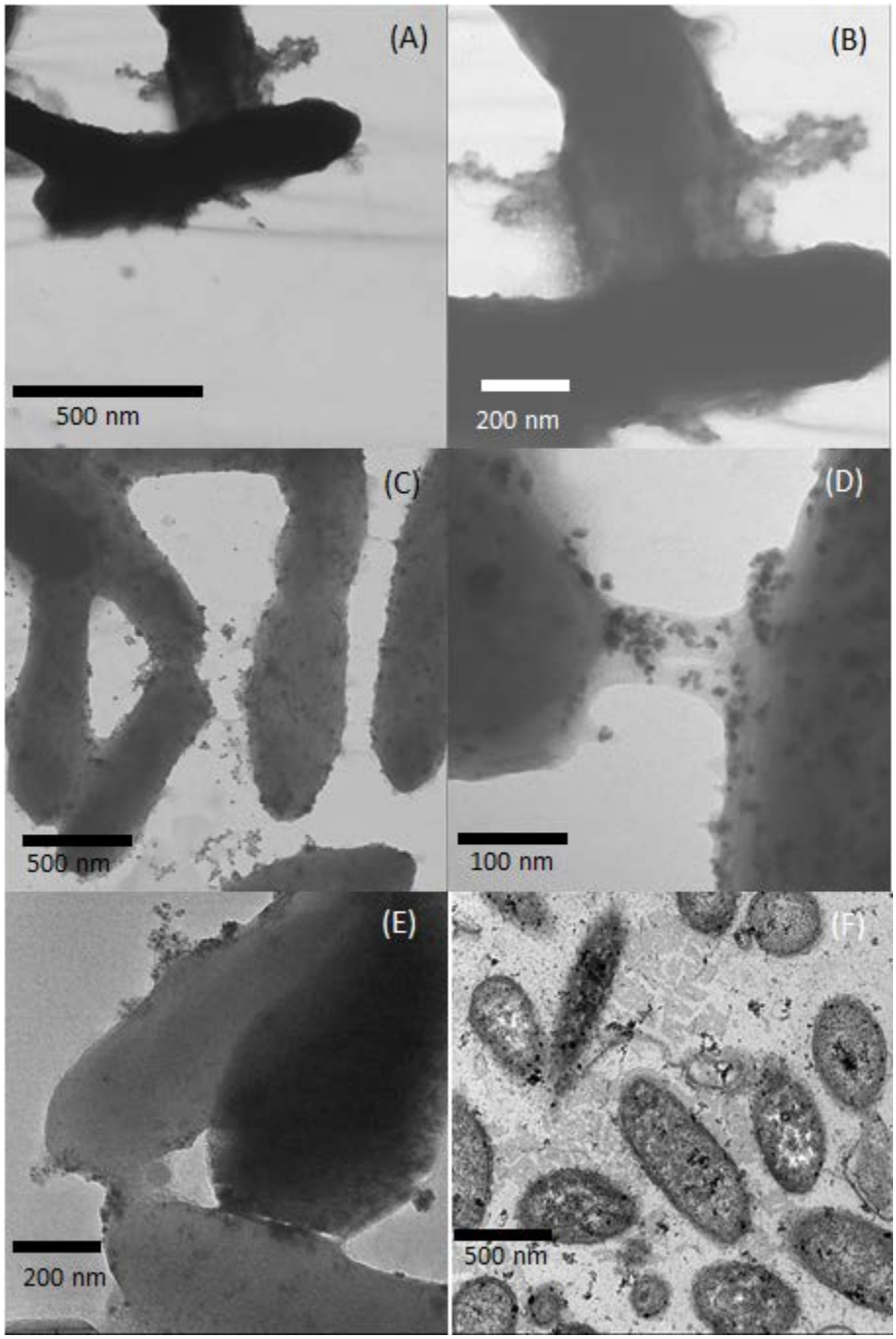

Figure 3.4. TEM images of palladium reduction with acetate as the electron donor. (A-B) Palladium as the sole electron acceptor; (C-D) palladium and fumarate as electron acceptors. (E) Viable cells with no electron donor and palladium as the sole electron acceptor exhibiting similar amounts of palladium reduction as suspensions containing acetate without fumarate. (F) Ultra-microtomed cells fed acetate with palladium as the sole electron acceptor. More periplasmic reduction occurs compared to cells fed hydrogen.

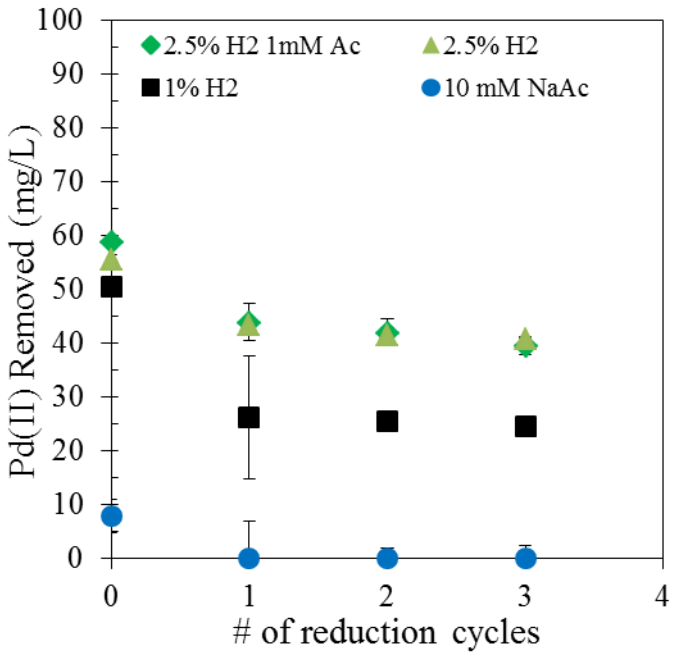

Figure 3.5. Successive cycles of palladium reduction by *G. sulfurreducens*. There is a decrease in efficacy between the first two cycles, but steady reduction between cycles 1 and 3 showing that cells are re-useable. Cultures with acetate as the electron donor could not be reused.

3.7 Tables

Table 3.1. Palladium removal by various bacterial species.

Organism	Cell OD_{610}	Pd(II) concentration (mg/L)	Reduction time (min)	Electron Donor	Removal (%)	Cells Recycled	Ref.
Desulfovibrio desulfuricans	0.7	200	2	H_2 formate	40 100	N	[14]
Desulfovibrio vulgaris	0.5	200	30	H_2	100	N	[9]
Desulfovibrio fructosivorans		200	80	H_2	100	N	[34]
Shewanella oneidensis MR-1	2	50	Overnight	H_2 formate pyruvate ethanol	90 95 75 75	N	[10]
Geobacter sulfurreducens	0.5	100 50 100	360	H_2 H_2 acetate	50 75 8	Y Y Y	This study

3.8 Literature Cited

1. Vlaar, T., E. Ruijter, and R.V.A. Orru, *Recent advances in palladium-catalyzed cascade cyclizations.* Adv Synth Catal, 2011. **353**(6): p. 809-841.
2. *Johnson Matthey Platinum 2012 Interim Review.* 2012.
3. Hoffmann, J.E., *Recovering platinum-group metals from auto catalysts.* JOM-J Met, 1988. **40**(6): p. 40-45.
4. *MSDS: Sodium borohydride. Revised: 11/21/2012. sigmaaldrich.com.*
5. Manocchi, A.K., et al., *Simple, readily controllable palladium nanoparticle formation on surface-assembled viral nanotemplates.* Langmuir, 2009. **26**(5): p. 3670-3677.
6. De Corte, S., et al., *Comparison of bacterial cells and amine-functionalized abiotic surfaces as support for Pd nanoparticle synthesis.* Colloid Surface B, 2013. **102**(0): p. 898-904.
7. Narayanan, K.B. and N. Sakthivel, *Biological synthesis of metal nanoparticles by microbes.* Adv Colloid Interface Sci, 2010. **156**(1–2): p. 1-13.
8. Ingham, B., et al., *How nanoparticles coalesce: An in situ study of Au nanoparticle aggregation and grain growth.* Chem Mater, 2011. **23**(14): p. 3312-3317.
9. Baxter-Plant, V.S., I.P. Mikheenko, and L.E. Macaskie, *Sulphate-reducing bacteria, palladium and the reductive dehalogenation of chlorinated aromatic compounds.* Biodegradation, 2003. **14**(2): p. 83-90.
10. Windt, W.D., P. Aelterman, and W. Verstraete, *Bioreductive deposition of palladium (0) nanoparticles on Shewanella oneidensis with catalytic activity towards reductive dechlorination of polychlorinated biphenyls.* Environ Microbiol, 2005. **7**(3): p. 314-325.
11. Coppi, M.V., *The hydrogenases of Geobacter sulfurreducens: a comparative genomic perspective.* Microbiology, 2005. **151**(4): p. 1239-1254.

12. Creamer, N.J., et al., *Palladium and gold removal and recovery from precious metal solutions and electronic scrap leachates by Desulfovibrio desulfuricans.* Biotechnol Lett, 2006. **28**(18): p. 1475-1484.

13. De Windt, W., et al., *Biological control of the size and reactivity of catalytic Pd(0) produced by Shewanella oneidensis.* Anton Leeuw J Microb, 2006. **90**(4): p. 377-389.

14. Yong, P., et al., *Bioaccumulation of palladium by Desulfovibrio desulfuricans.* J Chem Technol Biot, 2002. **77**(5): p. 593-601.

15. Yong, P., et al., *Biorefining of precious metals from wastes: an answer to manufacturing of cheap nanocatalysts for fuel cells and power generation via an integrated biorefinery?* Biotechnol Lett, 2010. **32**(12): p. 1821-1828.

16. Miretzky, P., A. Saralegui, and A. Fernández Cirelli, *Simultaneous heavy metal removal mechanism by dead macrophytes.* Chemosphere, 2006. **62**(2): p. 247-254.

17. Dantas, J.M., et al., *Solution structure of a mutant of the triheme cytochrome PpcA from Geobacter sulfurreducens sheds light on the role of the conserved aromatic residue F15.* Biochimica et Biophysica Acta (BBA) - Bioenergetics, (0).

18. Lovley, D.R., et al., *Reduction of uranium by cytochrome c3 of Desulfovibrio vulgaris.* Appl Environ Microbiol, 1993. **59**(11): p. 3572-3576.

19. Lovley, D.R., *Dissimilatory metal reduction.* Ann Rev Microbiol, 1993. **47**(1): p. 263-290.

20. Li, Y. and M.A. El-Sayed, *The effect of stabilizers on the catalytic activity and stability of Pd colloidal nanoparticles in the Suzuki reactions in aqueous solution†.* J Phys Chem B, 2001. **105**(37): p. 8938-8943.

21. Hamman, C.H., A. Hamnett, and W. Vielstich, *Electrochemistry*. 2007: Wiley-VCH Verlag GmbH & Co.

22. Zhou, M., et al., *Recent advances in microbial fuel cells (MFCs) and microbial electrolysis cells (MECs) for wastewater treatment, bioenergy and bioproducts.* Journal of Chemical Technology & Biotechnology, 2012: p. n/a-n/a.

23. Inoue, K., et al., *Specific localization of the c-type cytochrome OmcZ at the anode surface in current-producing biofilms of Geobacter sulfurreducens.* Environ Microbiol Report, 2011. **3**(2): p. 211-217.

24. Seeliger, S., R. Cord-Ruwisch, and B. Schink, *A periplasmic and extracellular c-type cytochrome of Geobacter sulfurreducens acts as a ferric iron reductase and as an electron carrier to other acceptors or to partner bacteria.* J Bacteriol, 1998. **180**(14): p. 3686-3691.

25. Singh, S., et al., *Bacterial synthesis of silicon/silica nanocomposites.* Journal of Materials Chemistry, 2008. **18**(22): p. 2601-2606.

26. Coppi, M.V., R.A. O'Neil, and D.R. Lovley, *Identification of an uptake hydrogenase required for hydrogen-dependent reduction of Fe(III) and other electron acceptors by Geobacter sulfurreducens.* J Bacteriol, 2004. **186**(10): p. 3022-3028.

27. Caccavo, F., Jr, et al., *Geobacter sulfurreducens sp. nov., a hydrogen- and acetate-oxidizing dissimilatory metal-reducing microorganism.* Appl Environ Microbiol, 1994. **60**(10): p. 3752-3759.

28. Cologgi, D.L., et al., *Extracellular reduction of uranium via Geobacter conductive pili as a protective cellular mechanism.* P Natl Acad Sci USA, 2011.

29. Coker, V.S., et al., *Microbial engineering of nanoheterostructures: Biological synthesis of a magnetically recoverable palladium nanocatalyst.* ACS Nano, 2010. **4**(5): p. 2577-2584.

30. Law, N., et al., *Formation of nanoscale elemental silver particles via enzymatic reduction by Geobacter sulfurreducens.* Appl Environ Microbiol, 2008. **74**(22): p. 7090-7093.

31. Schaak, R.E. and M.E. Williams, *Full Disclosure: The Practical Side of Nanoscale Total Synthesis.* ACS Nano, 2012. **6**(10): p. 8492-8497.

32. Sines, I.T., et al., *Synthesis of tetragonal mackinawite-type FeS nanosheets by solvothermal crystallization.* Journal of Solid State Chemistry, 2012. **196**(0): p. 17-20.

33. Nakamura, R., et al., *Biological Iron-Monosulfide Production for Efficient Electricity Harvesting from a Deep-Sea Metal-Reducing Bacterium.* ChemBioChem, 2010. **11**(5): p. 643-645.

34. Mikheenko, I.P., et al., *Bioaccumulation of palladium by Desulfovibrio fructosivorans wild-type and hydrogenase-deficient strains.* Appl Environ Microbiol, 2008. **74**(19): p. 6144-6146.

35. Müller, K., J. Geng, and W. Arlt, *Reversible vs. Irreversible Conversion of Hydrogen: How to Store Energy Efficiently?* Energy Technology, 2013: p. n/a-n/a.

36. Wu, X.-F., H. Neumann, and M. Beller, *Palladium-Catalyzed Oxidative Carbonylation Reactions.* ChemSusChem, 2013: p. n/a-n/a.

Chapter 4

Exoelectrogenic Biofilm as a Template for Sustainable Formation of a Catalytic Mesoporous Structure

4.1 Abstract

Mesoporous structures can increase catalytic activity by maximizing the ratio of surface area to volume, but current synthesis techniques utilize expensive polymers and toxic chemicals. A *Geobacter sulfurreducens* biofilm was used as a sustainable template to form mesoporous Pd structures while eliminating the need for synthetic chemicals. The bulk of the biofilm material was removed by thermal treatments after nanoparticle formation, producing a catalytic Pd mesoporous (pore size 9.7 ± 0.1 nm) structure attached to the graphite electrode with a 1.5–2 μm thick backbone composed of nanoparticles (~200 nm). A control electrode electrochemically plated with Pd in the absence of a biofilm exhibited a variable planar Pd base (~0.5–3 μm thick) with sporadic Pd extrusions (~2 μm across, 1–5 μm tall) from the surface. The bio-templated mesoporous structure produced 15–20% higher stable current densities during H_2 oxidation tests than the electrochemically plated control electrode, even though 30% less Pd was present in the biotemplated catalyst. These results indicate that electroactive biofilms can be used as a sustainable base material to produce nanoporous structures without the need for synthetic polymers.

4.2 Introduction

Nanoporous structures with high pore volumes can increase the catalytic activity of surfaces by maximizing the ratio of surface area to volume. Generating catalytic mesoporous structures [2–50 nm pore size; [1]] from stabilized nanoparticle suspensions and functionalized polymers in block co-polymer assemblies [2-4] minimizes the reduction of effective surface area due to agglomeration of nanoparticles during deposition directly onto supports [5]. Catalytic mesoporous structures are formed by removing the co-polymers and can subsequently be bound to an electrode and used in catalysis, such as H_2 oxidation [4, 6]. The usual synthesis methods for mesoporous structures are often environmentally unfriendly and costly because they require potentially hazardous strong reductants to precipitate soluble metals and synthetic polymers to form an ordered structure and bind it to an electrode. Other methods require electrodeposition onto supports and a subsequent dealloying procedure in an acidic environment to obtain porosity [7]. An alternative method to create a catalytic surface was developed here using biofilms of *Geobacter sulfurreducens*, eliminating the need for these synthetic chemicals and/or acidic conditions.

Dissimilatory metal reducing bacteria (DMRB), such as *G. sulfurreducens*, have been shown to sustainably reduce soluble metals from waste streams [8] to nanoparticles using naturally produced polymers as stabilizers and capping agents [9-12]. *G. sulfurreducens* produces electrically conductive pili [13], which increase the reduction rate of soluble metals [14] and enables attachment and extracellular electron transfer to insoluble electron acceptors at the highest known rates among microorganisms [15]. Nanostructure formation using biogenic templates has received increased interest recently as the development of green synthesis techniques become more desirable [16, 17]. Palladium catalysts formed by *Desulfovibrio desulfuricans* [18] and *Escherichia coli* [19] have been previously studied for hydrogen

oxidation. However, these studies use cell suspensions under a hydrogen atmosphere to form nanoparticles. The palladized cells are then carbonized and applied to an electrode using an expensive Nafion binder. Formation of mesoporous structures with a *G. sulfurreducens* biofilm allows direct synthesis on an electrode without the need for strong reductants or synthetic polymers and binders. These attributes make *G. sulfurreducens* an attractive, sustainable alternative for the formation of catalytic mesoporous structures.

Here, we report the *in situ* formation of palladium nanoparticles by a *G. sulfurreducens* biofilm attached to a polarized graphite electrode. The resulting nanoparticle-impregnated biofilm was then pyrolyzed and oxidized to remove the bulk of the cell material and expose a catalytic mesoporous Pd structure. The resulting structure was characterized electrochemically for H_2 oxidation and compared to control graphite electrodes electroplated with Pd or coated with a Pd black/Nafion suspension.

4.3 Materials and Methods

4.3.1 Reactor Construction

Two-chamber reactors (duplicates) with a Nafion 117 proton exchange membrane to separate the anode and cathode chambers were used for all tests. Graphite working electrodes (1 cm × 2 cm) were sanded with 400 and 1500 grit sandpaper, cleaned with 1 M HCl and de-ionized water and connected to a titanium wire. Electrodes had a contact resistance < 0.7 Ω. Working electrodes for rotating disk electrode (RDE) tests were prepared identically, but were cylindrical in shape (1.4 cm diameter) to fit onto the RDE apparatus. Counter electrodes were Pt wires (15 cm length x 0.25 cm diameter). Reference electrodes (Ag/AgCl, 3 M NaCl, +0.2 V vs SHE) were inserted into the working electrode chamber.

4.3.2 Culture Conditions and Operation

Geobacter sulfurreducens PCA was obtained from stocks frozen at –80°C. Stocks were cultured in ATCC medium 1957 with 30 mM acetate. Cultures were incubated at 30°C. The anode chambers of reactors were inoculated with 1:10 ratio of *G. sulfurreducens* culture to ATCC 1957 medium, excluding fumarate. Electrochemically plated graphite plates were run under the same conditions without inoculation of *G. sulfurreducens*. Anode potentials were set to –0.15 V (vs. SHE) with a potentiostat (Biologic, TN, USA) in a 30°C temperature controlled chamber. Anode chambers were stirred at ~200 rpm with a magnetic stir bar to help reduce diffusion limitations.

The biofilm was grown until current production began to decrease from its maximum (~5 days), when the medium was exchanged for fresh ATCC medium 1957, excluding fumarate, to remove cells in suspension. Sodium tetrachloropalladate (170 mg/L final concentration; Na_2PdCl_4, Sigma-Aldrich, USA) and sodium acetate (10 mM) were added to the working electrode chamber while the working electrode was set to –0.15 V (vs. SHE). Electrodes were disconnected from the potentiostat after one hour of incubation, removed from the reactor, and stored in anaerobic sodium bicarbonate medium at 4°C until pyrolysis (< 24 hrs). Control electrodes were subjected to identical potentiostatic control, but were not inoculated with *G. sulfurreducens*.

4.3.3 Thermal Treatments to Form Porous Structure

Electrodes were pyrolyzed in a Lindberg tube furnace (Thermo Scientific, USA) under an argon atmosphere. The furnace temperature was ramped at 5 °C/min to 450 °C and immediately

allowed to cool to ambient temperature to carbonize cell material. The carbon was then oxidized away at 450°C in air for two hours.

4.3.4 Electrochemical Characterization

Catalytic activity of electrodes for H_2 oxidation was evaluated using linear sweep voltammetry (LSV) in H_2 saturated 0.1 M H_2SO_4. The electrolyte was prepared by sparging 0.1 M H_2SO_4 with pure H_2 gas for at least 30 minutes. Electrochemical performance was tested using a rotating disk electrode (RDE) to decrease the effect of diffusion resistance. Tests were run with continuous H_2 or N_2 sparging to differentiate the catalytic currents gained by oxidizing H_2 from the background currents. Potentials were cycled between –0.1 to 0.4 V (vs SHE) at 1 mV/s during LSVs with an electrode rotation rate of 2000 or 1000 rpm to evaluate electrode performance. Current densities were normalized to the geometric surface area of the electrode. Data was recorded on a Solartron potentiostat (Solarton, USA). Pt wire counter electrodes and Ag/AgCl (3M NaCl) reference electrodes were used in all tests. Bare graphite electrodes and a Pd flag (Sigma-Aldrich, USA) connected to a titanium wire were also characterized electrochemically as controls. Electrical connectivity between the palladium layer and the graphite support was tested using prepared electrodes as hydrogen fuel cell anodes in two-chamber reactors with identical setup as described above for *G. sulfurreducens* growth.

4.3.5 Catalyst Layer Characterization

The electrode surface structure was examined using environmental scanning electron microscopy (E-SEM, FEI Quanta 200) equipped with electron dispersive X-ray spectrometry (EDS). Elemental spectra of the electrode surfaces were obtained after pyrolysis and after

oxidation using EDS. Particle sizes that composed the mesoporous structure were obtained with a field emission scanning electron microscope (FE-SEM, FEI NanoSEM 630) at high magnification (up to 100,000×). The height and evenness of the Pd layers was determined by measuring profile images along the edge of the structure with Image J software measuring tools. Thin sections (70 nm) of biofilms embedded in Eponate resin, after staining with osmium tetroxide and uranyl acetate and dehydrating in an ethanol and acetone series, were analyzed by TEM (JEOL JEM 1200 EXII) to show that the biofilm reduced the palladium to palladium nanoparticles in the extracellular space (Figure B.4).

Surface area, pore volume, and average pore size of the structures formed on the electrodes were obtained from N_2 adsorption/desorption isotherms with a Micromeritics ASAP 2000 (Micromeritics, GA, USA) analyzer using the Brunauer–Emmett–Teller (BET) gas adsorption method. The weight of palladium on the electrodes was determined gravimetrically by gently scraping the palladium layer off the graphite support with a clean scalpel and weighing it with a Mettler-Toledo UMT2 microbalance (Mettler-Toledo, Columbus,OH).

4.4 Results and Discussion

4.4.1 Electrochemical Analysis under Hydrogen or Nitrogen Sparging

A *G. sulfurreducens* biofilm grown on a polished, poised (–0.15 V vs SHE) graphite electrode (duplicates) was an effective template for the formation of a mesoporous structure with increased catalytic activity. The mesoporous Pd structure was formed by pyrolysis (450 °C in Ar, 5°C/min ramp followed by immediate cooling) and oxidation (450°C in air, 2 h) of the *G. sulfurreducens* template after *in situ* reduction of Pd(II) to Pd(0) nanoparticles (Figure 4.1). Some Pd(0) was likely converted to palladium oxide during the oxidation step of the process [20]. In H_2

oxidation tests, the bio-templated Pd structures produced higher catalytic current densities at 0.4 V during LSV scans (1 mV/s) in 0.1 M H_2SO_4 compared to the electro-plated electrodes (Figure 4.2) at rotation rates of 2000 rpm (3.5 vs. 2.7 mA/cm^2) and 1000 rpm (2.3 vs. 2.0 mA/cm^2) with continuous H_2 sparging. Current densities are compared at 0.4 V to account only for the catalytic current due to hydrogen oxidation and not include current from the large, non-catalytic oxidation peak. Catalytic current densities were 9–23% larger for biotemplated electrodes above 0.25 V during rotation and 75–100% larger above 0.08 V without rotation. Duplicate electrodes generally exhibited minimal variations in current density profiles (Figure B.1). In one case (biotemplated electrode at 0 rpm) the maximum current peak was three times larger than its duplicate, but it still exhibited a similar stable current density between 0.08 and 0.4 V. Voltammograms exhibited a current peak at ~0.15 V during H_2 sparging tests likely due to corrosion of the carbon support [21] or pyrolyzed carbonaceous cell material remaining in the structure. A polymeric binder was not needed for attachment of the biotemplated structure to the graphite electrode because carbonaceous cell material likely bonded the Pd structure to the graphite surface. It is possible that some of this carbonaceous material could have blocked active Pd sites, decreasing maximum attainable catalytic current by the biotemplated catalyst. The control electrode coated with a Pd black and Nafion suspension produced less current at 1000 rpm than both electrochemically formed electrodes (1.1 mA/cm^2), likely due to the diffusion resistance of H_2 through the Nafion binder. Biotemplated electrodes that were pyrolyzed, but not oxidized, produced approximately half the current density (1.2 mA/cm^2) at 0.4 V and 1000 rpm (Figure B.2) as electrodes that were both pyrolyzed and oxidized, likely because much of the palladium structure was encased in carbonized cell material. The graphite electrode control lacking a catalyst or binder produced negligible current (0.16 mA/cm^2, 1000 rpm). The current density of the bio-templated Pd structure (0.35 mA/cm^2) at 0.4 V obtained by LSVs without rotation was higher than the electrochemically plated graphite electrode (0.2 mA/cm^2) and a bulk Pd flag electrode (0.1

mA/cm^2). Electrical connectivity between the palladium layer and the graphite support was confirmed by current generation through hydrogen oxidation in a two-chambered fuel cell without potentiostatic control (Figure B.3).

Voltammograms generated with N_2 sparging of the solutions gave similar current densities in RDE tests at 1000 and 2000 rpm (0.43 ± 0.1 mA/ cm^2; Figure 4.2). A carbon corrosion peak was observed under N_2 sparging conditions, but it was shifted to a more negative potential of ~100 mV to 0.05 V, compared to H_2 sparging conditions. The presence and similar magnitude of peaks with both N_2 and H_2 sparging implies the peak is a result of a non-catalytic oxidation current, likely due to the corrosion of the graphite support (Figure B.4) or carbonized cell material that remained in the structure due to incomplete oxidation [22].

4.4.2 Electrode Surface Characterization with Microscopy

Mesoporous structures generated using a *G. sulfurreducens* biofilm as a template for Pd reduction had higher porosities than the electrochemically coated graphite electrode control. Interconnected Pd nanoparticles (~100–300 nm) produced by *G. sulfurreducens* formed the backbone (Fig. 3, Fig. SI5) of the structure, which resulted in increased void space after oxidation of the cell material. Sintering of Pd nanoparticles during oxidation at 450^{o}C likely influenced the final shape of the porous structure and can result in a decrease [20] of active surface area. However, removal of carbonized cell material at this temperature increased the catalytic current density and surface area (detailed below) versus the un-oxidized electrode by removing the bulk of the carbonized cell material to expose catalytically active sites within the porous Pd backbone. The electrode surfaces were composed of ~97% Pd (by weight) after pyrolysis and oxidation compared to 50% carbon and 50% Pd after pyrolysis alone, for areas analyzed with EDS (Figure B.6), highlighting the importance of the oxidation step. The mesoporous palladium layer formed

by *G. sulfurreducens* was ~3 µm thick after the cell material was removed (Figure 4.3). Electrochemically plated Pd control electrodes exhibited a variable planar base layer (~0.5 to 3 µm thick) with sporadic extrusions (~2 µm diameter, ~1–5 µm tall) from the surface (Figure 4.3) after undergoing similar thermal treatments. The structural difference between the two methods highlights the advantage of using a *G. sulfurreducens* biofilm as a template for the formation of a mesoporous structure composed of Pd nanoparticles with increased available catalytic surface area without the use of any synthetic chemicals.

4.4.3 Pore Volume Analysis of Palladium Layer

The surface area of the electrodes formed over a biotemplate or by electrochemical plating was quantified from N_2 adsorption/ desorption isotherms using the Brunauer–Emmett–Teller (BET) gas adsorption method (Figure B.7). The average BET surface area of the blank graphite electrodes before treatment was 0.65 ± 0.05 m^2/g (Table 4.1). The Pd structure formed over the *G. sulfurreducens* template exhibited an increased BET surface area (569 ± 75 m^2/g) and pore volume (1.4 ± 0.17 cm^3/g) compared to the electrochemically plated Pd electrode (330 ± 45 m^2/g and 0.9 ± 0.14 cm^3/g). The average pore size of the biotemplated structure (9.7 ± 0.1 nm) was similar to the electro-plated structure (11.1 ± 0.3 nm), and both structures are classified as mesoporous materials (2–50 nm pore size). Although an ordered mesoporous structure was not included as a control in this study, the surface area of the electroplated catalyst was similar to other chemically formed mesoporous palladium and carbon electrodes [345 m^2/g [23]; 241 m^2/g [24]]. The increase in surface area is likely due to the surface roughness of the carbon support, which could provide an irregular pattern and more facets for palladium growth compared to a smooth surface, such as a gold electrode.

The mass of Pd (normalized by electrode surface area) was determined by carefully removing the Pd film from the electrode surface and weighing. The biotemplated structure contained 33% less Pd (~0.23 ± 0.01 mg Pd/cm^2) than the electro-plated electrode (~0.35 ± 0.02 mg/cm^2). Normalizing the current density of the catalysts by the surface area and the mass of palladium in the catalyst layer results in a 47% higher current density for the biotemplated catalyst (14.8 mA/cm^2-mg Pd) compared to the electroplated catalyst (7.8 mA/cm^2-mg Pd) at 0.4 V and 2000 rpm.

4.5 Conclusions

These results show that exoelectrogenic biofilms of *G. sulfurreducens* served as a facile, sustainable biogenic template for the formation of catalytic mesoporous structures by producing a porous interconnected nanoparticle framework *in situ*. The mesoporous structure had an increased surface area and pore volume compared to an electrochemically coated Pd structure, resulting in higher stable current densities during H_2 oxidation tests despite having 33% less Pd in the catalyst layer. Although the process was not optimized here, the results indicate that *G. sulfurreducens* can successfully and sustainably form a mesoporous catalytic structure without addition of any chemical reductants or synthetic polymers. The ability for *G. sulfurreducens* to form a porous structure from soluble metals using only natural processes has implications for utilizing biofilms to recover and disperse metal as nanoparticles conductive surfaces to sustainably form porous catalysts tailored to different applications.

4.6 Figures

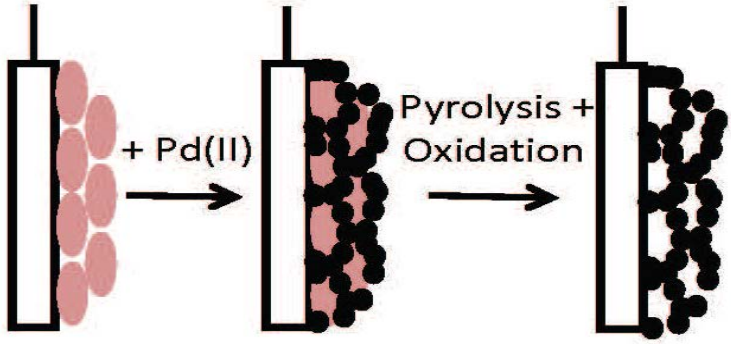

Figure 4.1. Schematic of the formation of a Pd mesoporous structure using a *G. sulfurreducens* biofilm as a bio-template. Pd(II) is reduced to Pd nanoparticles by the biofilm in situ. The cell material is then removed by pyrolysis and oxidation leaving a mesoporous structure.

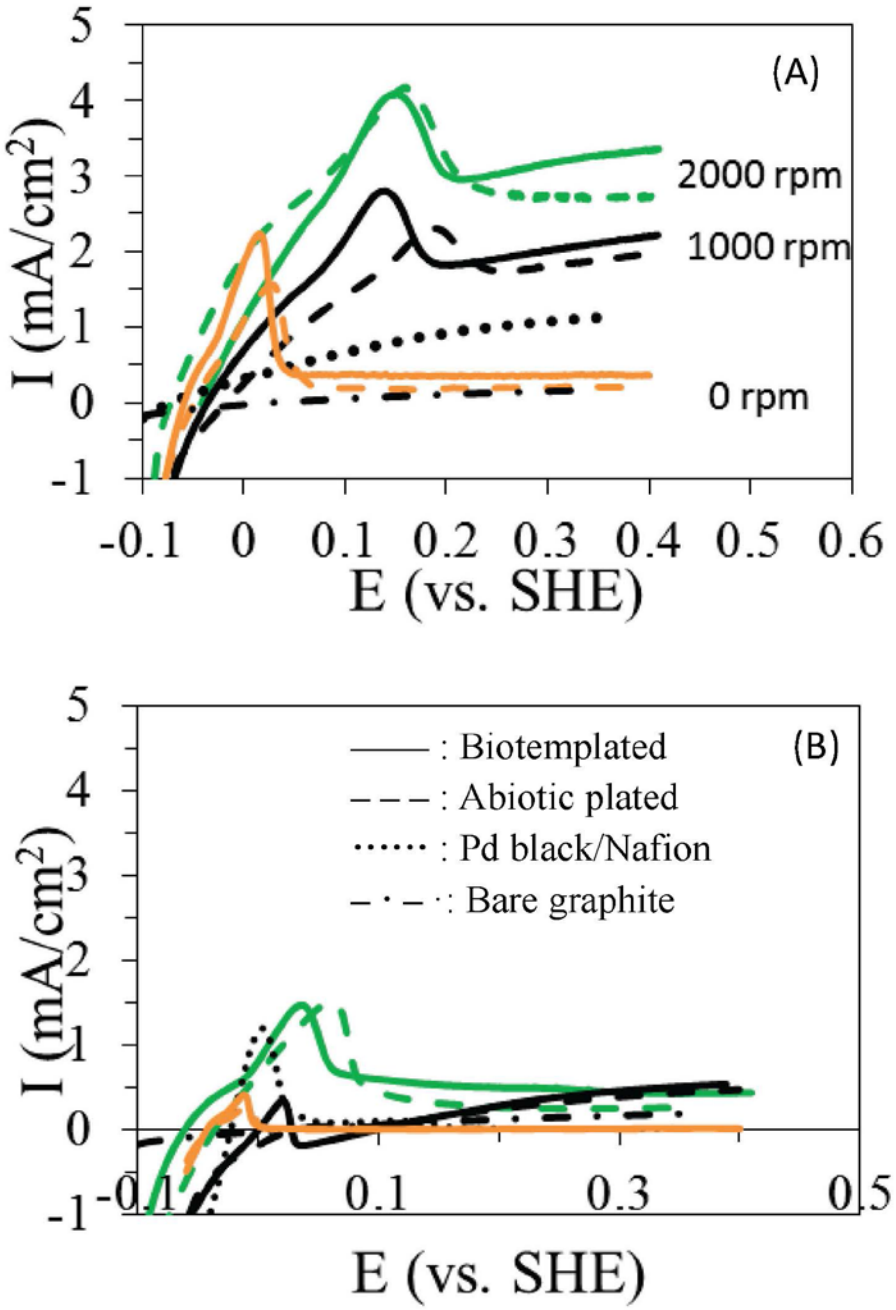

Figure 4.2. Average voltammograms of bio-templated porous electrodes (——), abiotic electrochemically plated graphite electrodes (- - - -), Pd nanoparticles bound to a graphite with Nafion (·····), and a bare graphite electrode (– · – · –) with continuous (A) H_2 or (B) N_2 sparging during rotating disk electrode tests at 2000 (green) and 1000 (black) rpm or without rotation (orange) in 0.1 M H_2SO_4. Nafion and bare graphite electrodes were only run at 1000 rpm. The bio-templated porous structure produced 15-20% more current density at 0.4 V under all H_2-sparged conditions. A characteristic carbon corrosion peak is present at ~0.15 V with H_2 sparging and ~0.05 V with N_2 sparging. Electrodes were fabricated and tested in duplicate (Figure B.1).

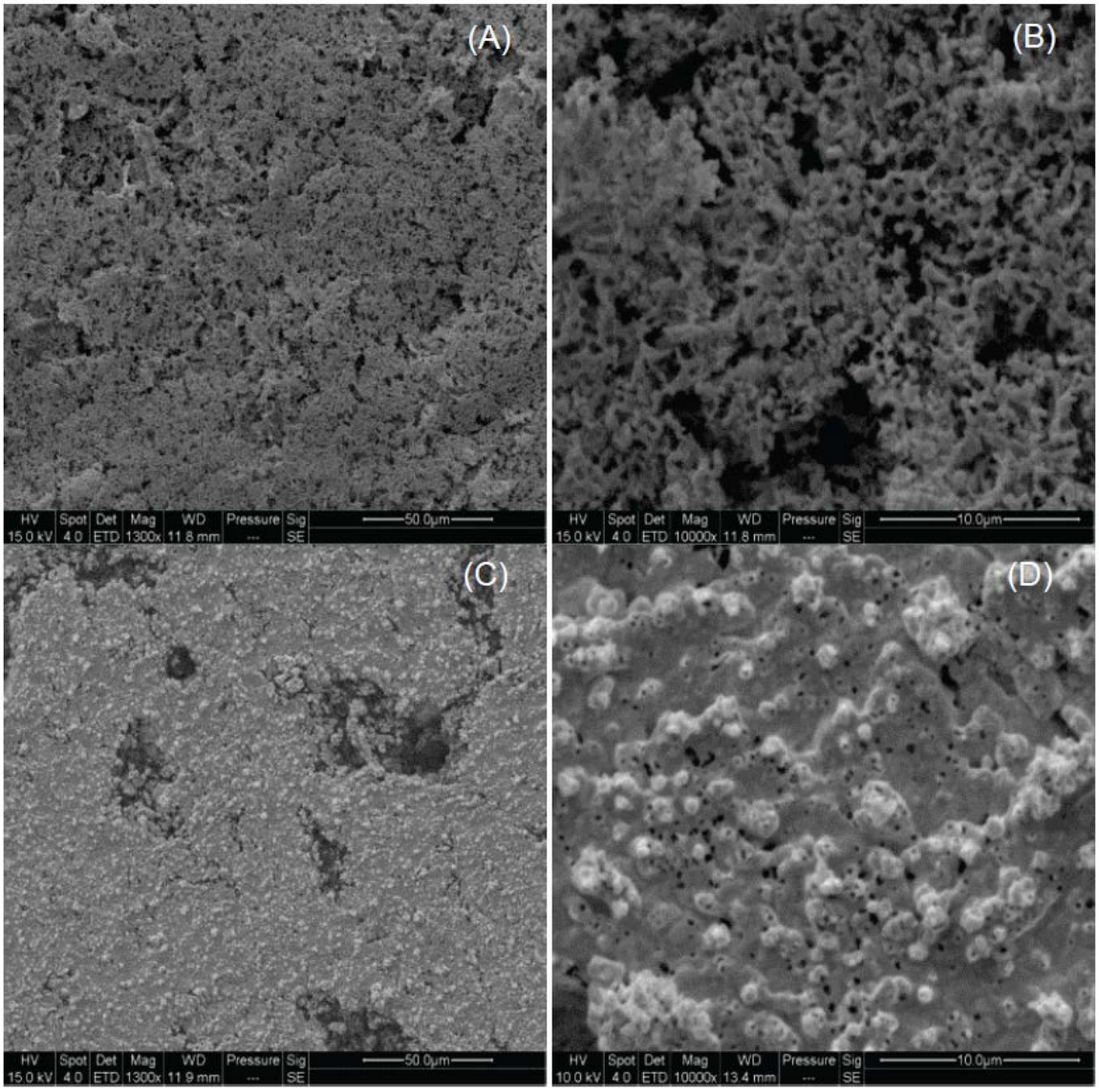

Figure 4.3. ESEM images of (A–B) a bio-templated mesoporous structure created by *G. sulfurreducens* and (C–D) an electrochemically formed structure under high (10,000 ×) and low magnification (1,300 ×).

4.7 Tables

Table 4.1. Pore volume analysis of Pd structures formed with a biotemplate or electrochemically.

	Average Surface Area (m^2/g)	Average Pore Volume (cm^3/g)	Average Pore Size (nm)	Mass of Pd (mg/cm^2)
Bio-templated	569 ± 75	1.4 ± 0.17	9.7 ± 0.1	0.23 ± 0.01
Abiotic plated	330 ± 45	0.9 ± 0.14	11.1 ± 0.3	0.35 ± 0.02
Graphite block	0.65 ± 0.05	0.001	—	—

4.8 References

1. Fendler, J.H., *Self-assembled nanostructured materials.* Chem Mater, 1996. **8**(8): p. 1616-1624.
2. Mackay, M.E., et al., *General strategies for nanoparticle dispersion.* Science, 2006. **311**(5768): p. 1740-1743.
3. Li, Y. and M.A. El-Sayed, *The effect of stabilizers on the catalytic activity and stability of Pd colloidal nanoparticles in the Suzuki reactions in aqueous solution†.* J Phys Chem B, 2001. **105**(37): p. 8938-8943.
4. Warren, S.C., et al., *Ordered mesoporous materials from metal nanoparticle–block copolymer self-assembly.* Science, 2008. **320**(5884): p. 1748-1752.
5. Wang, T., et al., *Enhanced electrocatalytic activity for hydrogen evolution reaction from self-assembled monodispersed molybdenum sulfide nanoparticles on an Au electrode.* Energ Environ Sci, 2013. **6**(2): p. 625-633.
6. Orilall, M.C. and U. Wiesner, *Block copolymer based composition and morphology control in nanostructured hybrid materials for energy conversion and storage: solar cells, batteries, and fuel cells.* Chem Soc Rev, 2011. **40**(2): p. 520-535.

7. Tominaka, S., et al., *Mesoporous PdCo sponge-like nanostructure synthesized by electrodeposition and dealloying for oxygen reduction reaction.* Journal of Materials Chemistry, 2010. **20**(34): p. 7175-7182.

8. Mabbett, A.N., et al., *Biorecovered precious metals from industrial wastes: Single-step conversion of a mixed metal liquid waste to a bioinorganic catalyst with environmental application.* Environ Sci Technol, 2005. **40**(3): p. 1015-1021.

9. Yates, M.D., R.D. Cusick, and B.E. Logan, *Extracellular palladium nanoparticle production using Geobacter sulfurreducens.* ACS Sus Chem Eng, 2013. **1**(9): p. 1165-1171.

10. Yong, P., et al., *Bioaccumulation of palladium by Desulfovibrio desulfuricans.* J Chem Technol Biot, 2002. **77**(5): p. 593-601.

11. De Windt, W., et al., *Biological control of the size and reactivity of catalytic Pd(0) produced by Shewanella oneidensis.* Anton Leeuw J Microb, 2006. **90**(4): p. 377-389.

12. Lovley, D.R., *Dissimilatory metal reduction.* Ann Rev Microbiol, 1993. **47**(1): p. 263-290.

13. Malvankar, N.S., M.T. Tuominen, and D.R. Lovley, *Biofilm conductivity is a decisive variable for high-current-density Geobacter sulfurreducens microbial fuel cells.* Energ Environ Sci, 2012. **5**(2): p. 5790-5797.

14. Cologgi, D.L., et al., *Extracellular reduction of uranium via Geobacter conductive pili as a protective cellular mechanism.* P Natl Acad Sci USA, 2011.

15. Bond, D.R., et al., *On electron transport through Geobacter biofilms.* ChemSusChem, 2012. **5**(6): p. 1099-1105.

16. Li, D., B. Mathew, and C. Mao, *Biotemplated synthesis of hollow double-layered core/shell titania/silica nanotubes under ambient conditions.* Small, 2012. **8**(23): p. 3691-3697.

17. Chen, X., et al., *Virus-enabled silicon anode for lithium-ion batteries.* ACS Nano, 2010. **4**(9): p. 5366-5372.

18. Yong, P., et al., *From bio-mineralisation to fuel cells: biomanufacture of Pt and Pd nanocrystals for fuel cell electrode catalyst.* Biotechnol Lett, 2007. **29**(4): p. 539-544.

19. Orozco, R.L., et al., *Towards an integrated system for bio-energy: hydrogen production by Escherichia coli and use of palladium-coated waste cells for electricity generation in a fuel cell.* Biotechnol Lett, 2010. **32**(12): p. 1837-1845.

20. Chen, J.J. and E. Ruckenstein, *Role of interfacial phenomena in the behavior of alumina-supported palladium crystallites in oxygen.* J Phys Chem, 1981. **85**(11): p. 1606-1612.

21. Roen, L.M., C.H. Paik, and T.D. Jarvi, *Electrocatalytic corrosion of carbon support in PEMFC cathodes.* Electrochem Solid St, 2004. **7**(1): p. A19-A22.

22. Lancaster, W.A., et al., *Metallomics of Two Microorganisms Relevant to Heavy Metal Bioremediation Reveal Fundamental Differences in Metal Assimilation and Utilization.* Metallomics, 2014.

23. Wan, Y., et al., *Ordered Mesoporous Pd/Silica−Carbon as a Highly Active Heterogeneous Catalyst for Coupling Reaction of Chlorobenzene in Aqueous Media.* Journal of the American Chemical Society, 2009. **131**(12): p. 4541-4550.

24. Yang, X., et al., *High-performance Pd–Au bimetallic catalyst with mesoporous silica nanoparticles as support and its catalysis of cinnamaldehyde hydrogenation.* Journal of Catalysis, 2012. **291**(0): p. 36-43.

Chapter 5

Biotemplated Palladium Catalysts can be Stabilized on Different Support Materials

5.1 Abstract

Sustainably biotemplated palladium catalysts generated on different carbon-based support materials were examined for durability under electrochemical (oxidative) and mechanical stress conditions. Biotemplated catalysts on carbon paper with both stresses retained 95% (at 0.6 V) of the initial catalytic activity compared to 70% for carbon cloth and 60% for graphite. Graphite electrodes retained 95% of initial catalytic activity with only a single stress. Using electrodeposited polyaniline (PANI) and polydimethylsiloxane binder increased the current density after the stress tests by 22%, compared to a 30% decrease for Nafion. In additional tests, PANI coated electrodes retained more activity than carbon paper electrodes in elevated mechanical (94% vs 70%, using glycerol) or more oxidative (175% vs. 62%, using 1 M H_2SO_4) stress tests. Biotemplated catalytic electrodes could be useful alternatives to synthetically produced catalysts for some electrochemical applications.

5.2 Introduction

Catalytic materials used in many industrial and energy conversion processes must be durable to maximize the useful lifetime of these processes, especially when expensive precious metal catalysts are utilized [1]. Conventional methods of catalyst formation typically use synthetic stabilizers and reductants to form nanostructures with high surface area and catalytic activity. Synthesized nanomaterials are then mixed with a chemical binder to form a catalyst ink that is applied to a support, often alumina [2, 3] or carbon [4, 5], for various applications [6]. The stability of the bond between the binder and support is important to keep the catalytic material in contact with the electrode support. Additionally, the durability of the ligand material is an important consideration because ligands account for the bulk of electrode manufacturing costs, largely because they cannot be captured and recycled like the catalytic metal [1].

Recently there has been increased interest in developing sustainable processes to fabricate nanoparticles and porous nanostructures with high surface areas using biological materials as supports [7-9] or biotemplates [10-12] to replace synthetically formed nanomaterials. An electroactive biofilm of *G. sulfurreducens* was recently used as a biotemplate to form a nanoporous catalytic palladium structure that was directly attached to an electrode surface using only materials naturally produced by the biofilm [13]. The biotemplated palladium structure had a higher catalytic activity than an electrodeposited palladium control electrode or electrodes coated with a palladium/Nafion catalyst ink. Electroactive bacteria offer a sustainable solution for formation of a nanoporous structure on an electrode because the biofilm effectively disperses and reduces the catalytic material directly on the electrode surface without the use of any conventional synthetic binders, increasing the sustainability of the process. However, the stability of biotemplated palladium structures has not previously been tested. While sustainable methods

of catalyst formation are desirable, the electrode durability needs to be similar or better than electrodes produced using synthetic methods.

Fuel cells and batteries are the primary applications for catalytically active electrodes. Two of the primary design considerations for electrodes in these systems are thermal [5, 14] and electrochemicall [5, 15] stability. Electrode stability of conventional catalysts is often tested by either applying a catalyst to an electrode support material before coating with a binder to ensure that the material remains on the surface during testing, or by applying a premixed binder/nanomaterial solution [16, 17]. The most common binders are proton conducting polymers, such as Nafion [18]. More recently, electrically conductive polymers, primarily polyaniline (PANI), have been used as a binder because of its ability to conduct electrons and be electropolymerized on an electrode. Pyrolyzed PANI has also been used as starting material to form catalytic electrodes [19] as well as corrosion resistant coatings [20, 21]. Catalytic materials can also be electrodeposited into PANI films on support electrodes [22] or deposited into freshly produced PANI films by soaking the film in a solution containing metal ions. PANI has been used as a conductive intermediate link for other purposes, such as movement of artificial muscles [23], highlighting its versatility as a binder.

Electrochemical (oxidative) stability is also an important factor for biotemplated electrodes, but another critical consideration is mechanical stability. Biotemplated catalyst layers do not require a chemical binder for attachment to the electrode surface, which may make the catalyst layer more susceptible to degradation by mechanical shear stresses. Mechanical stability is often overlooked in conventional electrochemical systems because either the catalysts are bound to the electrode surface with a synthetic material, the substrates are gases which have a very low viscosity (viscosity, $\mu \sim 0.02$ centipoise for air [24]), or the system is used in a stagnant electrolyte [25]. However, there are other applications with liquid electrolytes that have high viscosities, such as hydrogenation reactions or reductive dechlorination of toxic compounds in

water ($\mu \sim 1$ cP) [26]. The higher viscosity of a liquid can mean that mechanical shear forces are important to catalyst stability because the electrolyte imparts an additional stress on the electrode. This aspect of electrode mechanical durability relative to shear stress, however, has not been well-studied.

The mechanical and electrochemical durability of biotemplated nanoporous palladium catalysts on carbon supports during hydrogen oxidation was examined here using a rotating disc electrode (RDE). Graphitized carbon is a widely used support for electroactive biofilm growth because it is electrically conductive as well as inexpensive [27]. Graphite is also a good material for catalyst deposition due to delocalized pi bonds that can interact with metals to enhance the attachment of catalysts to a surface [28]. However, it is unclear how much mechanical shear stress and electrochemical oxidation these electrodes are able to withstand. Different electrode support materials (graphite, carbon cloth, and carbon paper) were therefore examined to determine the most durable electrode structure. Different readily available polymer coatings (Nafion, polydimethylsiloxane, and polyaniline) were also investigated as binders to enhance retention of the nanoporous catalytic material to the support material. Electrodes able to best withstand degradation initial stress tests were further tested under conditions of higher mechanical (using 85% glycerol as a more viscous electrolyte) and oxidative stresses (1 M H_2SO_4 electrolyte) to examine durability under harsher chemical conditions.

5.3 Materials and Methods

5.3.1 Reactor Configuration

Two-chamber reactors (duplicates) were connected by side-arms (inner diameter of 2.4 cm), sealed with an O-ring, and separated by a Nafion® 117 membrane (Fuel Cell Store, Boulder, CO,

USA) that was held with a screw clamp (35/25, VWR, Radnor, PA, USA). Each chamber had three 20 mm side ports, which were sealed with rubber stoppers and aluminum crimp seals, and a total liquid volume of 120 mL and a headspace volume of 60 mL. The stopper inserted into the middle side port of the working electrode chamber had a 5 mm diameter hole to allow insertion of a reference electrode.

The working electrode was made by attaching a titanium wire (0.81 mm, McMaster Carr) to different support materials [Graphite (McMaster Carr, USA), Carbon paper (Spectracarb 0% wet-proofed; Clean Fuel Cell Energy LLC., USA), and carbon cloth (0% wet proofed, E-TEK, USA)] cut into 1 cm diameter pieces via small holes drilled near the top of the electrode. Graphite electrodes were polished with 400 and 1500 grit sandpaper, sonicated briefly to remove loose particles, and then soaked in 1 M HCl overnight. Electrodes were then rinsed three times with deionized water and polished with Kimwipes to remove any remaining loose material. Carbon paper and carbon cloth electrodes were placed into a muffle furnace for 45 minutes at 450°C to remove any organics on the surface.[29] All electrodes had a resistance of less than 1 Ω between the wire and electrode surface. The electrode was inserted through a butyl rubber stopper, placed into the top of the reactor, and sealed with an aluminum crimp seal. A platinum wire counter electrode was inserted through a stopper in the middle side-arm in the counter electrode chamber. Electrode potentials were measured using Ag/AgCl reference electrodes (–200 ± 5 mV vs. SHE; BASi, West Lafayette, IN, USA), and all potentials reported here are versus SHE. The tip (glass frit) of the inserted reference electrode was ~2 cm away from the working electrode surface. All reactors and media were sterilized before use. Medium replacement was carried out using sterile, anaerobic techniques.

5.3.2 Culture Conditions and Reactor Operation

Geobacter sulfurreducens PCA was grown using stocks frozen at –80°C. Cells were cultured in ATCC medium 1957 with 30 mM acetate and incubated at 30°C. The anode chambers of reactors were inoculated with 1:10 ratio of mid-log phase *G. sulfurreducens* culture to ATCC 1957 medium, excluding fumarate. Anode potentials were set to –0.15 V (vs. SHE) with a potentiostat (Biologic, TN, USA) in a 30°C temperature controlled chamber. Anode chambers were stirred at ~200 rpm with a magnetic stir bar to help reduce diffusion limitations of substrate to the biofilm.

The biofilm was grown until current production began to decrease from its maximum (~6 days). The medium was exchanged for fresh ATCC medium 1957, excluding fumarate, to remove cells in suspension. Sodium tetrachloropalladate (150 mg/L final concentration; Na_2PdCl_4, Sigma-Aldrich, USA) and sodium acetate (10 mM) were added to the working electrode chamber while the working electrode was set to –0.15 V (vs. SHE). Electrodes were disconnected from the potentiostat after 40 minutes of incubation, removed from the reactor, and stored at 4°C until further processing (< 30 min). Control electrodes were not exposed to palladium, but exposed to similar conditions.

5.3.3 Electrode Processing

Electrodes were pyrolyzed in a tube furnace (Thermo Scientific, USA) under an argon atmosphere (30 mL/min flowrate). The furnace temperature was ramped at 5°C/min to 450 °C, held for 45 minutes, and then allowed to cool to ambient temperature to carbonize cell material. The carbonized cell material was then removed via thermal oxidation in a muffle furnace at 450°C in air for two hours, leaving a porous palladium catalyst.

Some graphite electrodes were coated with a polymer to stabilize the catalyst layer to the surface of the electrode to enhance attachment. Polyaniline (PANI), a conductive polymer, was electropolymerized on the electrode by electrochemically cycling (CV) the electrode at 100 mV/s between –0.1 and 1.0 V in a1 M sulfuric acid solution with 50 mM aniline monomer.[23] Different amounts of polyaniline was deposited by cycling a variable amount of times (3, 10, and 30 cycles; 30 cycles ~15 nm thickness[23]). Electrodeposition of PANI for 30 cycles results in 3.7 mg/cm^2 of polymer deposited on the electrode. Polydimethylsiloxane (PDMS) was tested as a stabilizer because of its relative durability and low cost compared to Nafion.[30] A 5% solution of PDMS added approximately 1.4 mg/cm^2 of polymer to the electrode. Solutions containing 1%, 5%, and 10% PDMS were prepared according to standard protocols in toluene[30] and were dropped onto the surface of the electrode and allowed to cure at ambient temperature for more than 2 days. Nafion was tested as a control because it is the most commonly used polymer to disperse nanoparticles and attach them to electrode surfaces.[18] A solution (10 μL) containing 1% or 5% Nafion in isopropanol was dropped using a piptettor onto the surface of the electrode and allowed to dry overnight before testing. Coating the biotemplated catalyst with a 5% solution of Nafion added approximately 0.9 mg/cm^2 of polymer on the electrode.

5.3.4 Electrode Characterization

Catalytic activity of electrodes for H_2 oxidation was evaluated using cyclic voltammetry (CV) in H_2 saturated 0.1 M H_2SO_4. The electrolyte was prepared by sparging 0.1 M H_2SO_4 for at least 30 minutes. Initial and final electrochemical performance of all catalysts was tested using a rotating disk electrode (RDE) to decrease the effect of diffusion resistance. Tests were run with continuous H_2 or N_2 sparging to differentiate the catalytic currents gained by oxidizing H_2 from the background currents. Potentials were cycled between –0.15 to 0.65 V (vs SHE) at 1 mV/s

during CVs with an electrode rotation rate of 1000 rpm to evaluate electrode performance. Current densities were normalized to the geometric surface area of the electrode. Data was recorded on a Gamry potentiostat (Gamry, USA). Pt mesh counter electrodes and Ag/AgCl (3M NaCl) reference electrodes were used in all tests. Bare electrodes were also characterized electrochemically as controls. All potential values are reported versus the Standard Hydrogen Electrode. Some support materials tested do not meet requirements for testing on a typical RDE setup. To circumvent this, all materials were tested on an electrode modified with a Teflon screw cap. The electrode was threaded to accommodate this screw cap and a stainless steel plate was fashioned to make contact with the gold current collector of the electrode. A 6mm hole was drilled into the middle of the cap and the face of the cap tapered to the edge to mimic RDE conditions as closely as possible. A schematic of this setup is shown in the Supplementaty Information (Figure C.3). The resistance between the electrode surface and the body of the electrode was less than 0.5 Ω in all cases. All electrodes were tested using this modified apparatus for consistency.

5.3.5 Mechanical and Electrochemical Durability Tests

The stability of the catalyst layer for electrochemical stress and mechanical stress was evaluated using a rotating disc electrode. The initial and final electrochemical performance was evaluated as described above. The electrochemical durability was tested using an accelerated electrochemical stability test by potential cycling of the electrode from –0.15 to –0.65 at 100 mV/s for 3000 cycles [16] in 0.1 M H_2SO_4. Enhanced electrochemical stability tests were carried out under similar conditions except 1 M H_2SO_4 or 85% glycerol was used as the electrolyte. The mechanical durability was tested by applying a shear force using the rotating disc electrode at 1000 rpm in 0.1 M H_2SO_4 for 12.5 hr for tests to isolate the effects of mechanical stresses on the

electrode. Enhanced mechanical durability tests utilized 85% glycerol as the electrolyte. All Equations for shear stress calculations are provided in the Supplementary Information.

5.3.6 Microscopic Characterization

The electrode surface structures before and after durability testing was examined using field emission scanning electron microscopy (FE-SEM, FEI Quanta 200) equipped with electron dispersive X-ray spectrometry (EDS). Elemental spectra of the electrode surfaces were obtained to verify the presence of the electrode coatings after durability testing.

5.4 Results and Discussion

5.4.1 Stability of Biotemplated Palladium Catalyst Layers on Different Carbon Support Materials

The stability of the biotemplated palladium layers varied depending on the carbon support. Carbon paper exhibited the best durability following exposure to a combination of mechanical shear (1000 rpm, shear rate of 35 s^{-1}) and accelerated oxidative stresses (cyclic voltammetry between –0.1 and 0.65 V at 100 mV/s for 3000 cycles [16] in 0.1 M H_2SO_4). Representative initial and final voltammograms for each support type showed evidence of performance degradation at potentials above ~0.4 V (Figure 5.1). Initial and final currents at 0.6 V were used as a basis of comparison here because it is above this minimum potential where catalytic degradation was first observed. Approximately 95% of the catalytic activity (2.5 ± 0.2 mA/cm^2 initial, 2.4 ± 0.15 mA/cm^2 final; at 0.6 V) was retained after the carbon paper support was subjected to a combined mechanical shear and accelerated oxidative stability stresses (Figure 5.2). Biotemplated catalysts were less stable on carbon cloth supports when subjected to the same

conditions, retaining only ~70% of the initial catalytic activity (4.6 ± 0.4 mA/cm^2 to 2.9 ± 0.2 mA/cm^2). Graphite supported biotemplated electrodes retained ~60% of the initial catalytic activity (1.6 ± 0.01 mA/cm^2 to 1.0 ± 0.3 mA/cm^2) after combined stresses. Control electrodes, prepared on a graphite surface using synthetically produced palladium black nanoparticles held with a Nafion binder, initially produced a lower current density (1.4 ± 0.01 mA/cm^2) than biotemplated palladium catalysts, and further lost ~15% of its activity when subjected to the same oxidative and mechanical stresses. Control electrodes prepared by electroplating palladium onto a graphite surface retained initially produced less current than biotemplated electrodes(1.4 ± 0.04 mA/cm^2), but retained 78% catalytic activity initially produced (1.1 ± 0.15 mA/cm^2). Support materials without palladium produced negligible current (Figure C.1).

Graphite electrodes did not maintain performance under these combined stresses, but they were adequate supports when only electrochemical or mechanical stress was applied (Figure 5.2). There was a minimal decrease in catalytic activity (1.7 ± 0.05 mA/cm^2 initial, 1.7 ± 0.08 mA/cm^2 final; 0.6 V) when only the mechanical shear force was applied. Approximately 94% of the catalytic activity (1.7 ± 0.04 mA/cm^2 to 1.6 ± 0.04 mA/cm^2) was maintained during oxidative stability tests with no rotation. Plain graphite electrodes were also tested using chronoamperometry at 0.2 V or 0.6 V with mechanical stress (1000 rpm) for 12.5 hr to assess the catalyst stability at different levels of oxidative stress. Catalytic activity of electrodes decreased by 36% (1.8 to 1.1 mA/cm^2) at a set potential of 0.6 V, compared to a 17% increase in activity (1.8 to 2.0 mA/cm^2) for electrodes set at 0.2 V. These results confirm that a combination of an oxidizing environment with mechanical shear produced electrode failure. The increase in catalytic activity for the electrode held at 0.2 V was likely due to the conditioning of the palladium catalyst in the hydrogen atmosphere, which could increase the number of active sites [31]. To verify that this conditioning of the electrode was occurring, a graphite electrode with a palladium catalyst layer was placed in a hydrogen sparged electrolyte for 12.5 hours, and rotated at 1000 rpm. The

catalytic activity of the palladium layer increased by 35% (Figure 5.2) after being exposed to hydrogen sparging, suggesting that optimization of this biotemplated catalyst formation process is still needed.

5.4.2 Electrode Surface Characterization

Biotemplated palladium catalysts formed on carbon cloth and carbon paper supports produced higher current densities than on graphite supports, even though they had the same projected surface area. Carbon paper and cloth are made of carbon fibers [14] that give an increased surface area for biofilm growth and formation of the palladium catalyst layer, compared to the smooth graphite surface (Figure 5.3). The catalytic activities of all support materials without palladium were approximately the same (0.07 ± 0.03 mA/cm^2) indicating that there was no intrinsic effect of the support material on the catalytic activity. Therefore, the increase in current density was due to an increased available surface area for catalyst attachment.

The carbon paper electrode may have outperformed the other support materials because of its more rigid structure, which enabled greater resistance to support deformation, in combination with the high surface areas of the layers of carbon fibers (Figure 5.3). Carbon paper electrodes had palladium nanostructures formed primarily along the carbon fibers, but palladium films that interconnected the fibers were also observed. Some of these interconnecting film structures were also observed below the top layer of the support, suggesting activity extended beyond the surface plane. More catalytic structures were apparent on the surface of carbon paper supports after stability testing, but this change in catalyst morphology did not affect the overall performance.

Carbon cloth electrodes had palladium nanostructures primarily along carbon fibers. However, there were no observed films interconnecting different carbon fibers. One possibility for its reduced durability compared to the paper is that the cloth is not rigid and therefore is more

easily deformed under the mechanical stress conditions. Deformation of the support could make the palladium catalyst layers susceptible to fracture and detachment, decreasing the catalytically active area of the electrode.

Graphite blocks offer a rigid support for the catalyst layer, but the smooth, solid surface offers less surface area for the biotemplate to form on. The flat surface results in a palladium layer that is formed only on the surface of the electrode, in one cohesive layer, whereas the paper and cloth could have biotemplated catalyst deposited deeper in the material which would be more resistant to surface shear. Large areas of the bare support were seen on uncoated graphite electrodes after the combined mechanical and oxidative stresses, suggesting that the decrease in catalytic activity was a result of detachment of the material from the surface support (Figure 5.3).

5.4.3 Stabilizing Palladium Layers on Graphite with Different Polymers

Three different commonly used binders (polyaniline, polydimethylsiloxane, and Nafion) were tested as coatings to stabilize the biotemplated palladium catalyst layer to the graphite electrodes. Although the addition of synthetic polymers to biotemplated materials decreases the sustainability of the overall process, as chemical polymers are used, the improvement in catalyst stability may be a more important factor for applications under harsh electrochemical or mechanical stress conditions.

Polyaniline (PANI) was the most effective stabilizer of the three polymers tested (Figure 5.4). A PANI coating approximately 15 nm thick [23] (30 electrodeposition cycles) over the palladium layer increased the catalytic activity of the electrode by ~22% (1.8 ± 0.02 mA/cm^2 initial, 2.2 ± 0.2 mA/cm^2 final; 0.6 V) after exposure to electrochemical and mechanical stress, suggesting that the polyaniline layer stabilized the biotemplated layer on the electrode. The increase in catalytic current was due to the conditioning of the palladium catalyst in the hydrogen atmosphere.

Catalysts coated with less polyaniline (1.5 and 5 nm thick layers) did not maintain their initial activity after testing (67% and 75% activity retained), likely because the polymer layer was not thick enough to provide a strong bond between the catalyst and the support. The palladium electrode tested here performed similarly, on the basis of mA cm^{-2} mg Pd^{-1}, to a PANI film with palladium nanoparticles reduced inside the film [32]. However, the electrode was previously synthesized by casting a stabilized nanoparticle solution and aniline mixture onto an electrode using a chemical reductant before testing. The method presented here is a simpler method for formation of a palladium catalyst on an electrode, it uses less polyaniline to bind the catalyst to the surface, and it avoids the use of nanoparticles stabilized with synthetic materials. Biotemplated electrodes could be coated with a variety of electroactive polymers to tailor the electrode to different applications with this method.

Poly(dimethylsiloxane) (PDMS) was also tested as a catalyst stabilizer because it was previously shown to be an effective, low cost binder material for microbial fuel cell cathodes [30]. Catalysts coated in PDMS (10%, 5%, and 1% w/w) all had an initial activity (1.4 ± 0.07 mA/cm^2) below that of an uncoated electrode (1.7 ± 0.1 mA/cm^2). However, after stability tests the catalysts coated with 10% (1.7 ± 0.1 mA/cm^2) or 5% (1.8 ± 0.1 mA/cm^2) PDMS had activities similar to the average uncoated electrode. The catalysts coated with only 1% PDMS lost ~66% of the initial activity, likely because there was not enough polymer to effectively maintain binding of the catalyst layer to the support. The overall current densities were lower when PDMS was used, compared to PANI, likely because PDMS is an insulating polymer.

Nafion was tested, as a control, because it is the most commonly used binder for electrode materials [18] due to its proton conduction properties, but it is expensive [33]. However, Nafion was not found to be suitable as a stabilizing polymer for the biotemplated palladium catalyst layer. Catalysts coated with 5% or 1% Nafion had a lower initial catalytic activity (1.4 ± 0.02 mA/cm^2) than the uncoated electrode. The catalytic activity decreased for all Nafion coated

electrodes by ~30% (1.0 ± 0.05 mA/cm^2). Degradation of Nafion coated electrodes was assumed to be more a result of mechanical than oxidative stress due to the good chemical stability of Nafion in acidic environments. The decrease in activity was more pronounced than that obtained with electrodes coated with a palladium black and a Nafion suspension, likely because there was less direct contact between the Nafion and the carbon support.

Electrodeposited PANI is advantageous as a stabilizer not only because it can stabilize the catalyst layer on the electrode, but also because it can be electrodeposited directly on the electrode after the formation of the catalyst layer, which results in more control over the thickness of the polymer layer [34]. The other polymers tested had to be applied by a drop-cast method onto the support, which afforded less control over the thickness of the polymer film. Additionally, PANI is a conductive material in acidic solutions due to pi-pi stacking [34], which is advantageous for electrochemical applications such as fuel cells. One disadvantage of PANI compared to PDMS is its cost. A PANI layer ~15 nm thick costs ~5.2 \$/m^2 (based on 72 \$/500 g of aniline monomer), which is approximately 3 times more than the cost of PDMS (1.5 \$/m^2; 50 \$/500 g) [30]. However, this cost difference is not likely to be prohibitive based on the advantages afforded by PANI as a stabilizer, especially since both of these polymers are two orders of magnitude less expensive than Nafion (667 \$/m^2; based on 200\$ for 100 mL of 5% Nafion solution).

The microscopic structure of the catalysts stabilized with PANI and PDMS was similar to the uncoated palladium nanostructure formed on the graphite surface [13] (Figure C.2). The catalyst layer coated with Nafion could not be observed due to the inability of the electron beam to penetrate the Nafion layer without destroying it.

5.4.4 Enhanced Durability Tests of Select Conditions

Biotemplated palladium catalyst layers on carbon paper supports and on graphite blocks coated with PANI (15 nm) were further tested under increased shear stress and more oxidative conditions (Figure 5.5). Electrodes were tested under the same physical conditions as above (1000 rpm and 100 mV/s cyclic voltammetry for 3000 cycles), except the electrolyte solution was switched to an 85% glycerol solution to increase the viscosity (μ = 110 cP [35]), increasing the shear stress to 4 Pa compared to 0.1 Pa in 0.1 M H_2SO_4 (μ = 3 cP [36]). Initial and final current densities were obtained in CV tests in the 0.1 M H_2SO_4 electrolyte to provide conditions consistent with previous tests. The PANI coated electrode retained 94% of its initial catalytic activity under these conditions (1.7 ± 0.02 mA/cm^2 initial, 1.6 ± 0.05 mA/cm^2 final; 0.6 V). The carbon paper support, however, only retained ~70% of the initial catalytic activity under the increased mechanical shear (2.8 ± 0.02 mA/cm^2 to 2.1 ± 0.2 mA/cm^2). Glycerol electro-oxidation was minimal since the glycerol oxidation peak occurs at ~0.8 V [37] and the maximum potential used here was 0.65 V. These results suggest that under conditions of high shear stresses, stabilization of the catalyst support using PANI or another electroactive polymer is beneficial.

These two electrodes were also subjected to increased oxidative stress by conducting CVs in a 1 M H_2SO_4 electrolyte. The PANI coated graphite electrode increased in activity by ~75% (1.7 mA/cm^2 to 3.0 mA/cm^2) after testing. This increase was likely due to complete protonation and reduction of the PANI layer in the highly acidic solution, which gives better electron transport properties [38] while also preventing catalyst detachment from the electrode surface. PANI is a known to be a corrosion resistant polymer [21], which could have protected the electrode from dissolution under the highly oxidative stresses in the system. The catalytic activity of the PANI coating also increased the overall catalytic activity of the electrode after treatment in the highly acidic solution. Initially, the PANI coated electrode produced a current density of 0.1 mA/cm^2 in

a nitrogen atmosphere. After testing in 1 M H_2SO_4, the activity increased to 1.68 mA/cm^2 in the same nitrogen atmosphere, likely as a result of full protonation and reduction of the PANI layer. The carbon paper electrodes retained only ~40% of their initial activity (2.3 mA/cm^2 to 1.0 mA/cm^2) during stability testing in the increased corrosive environment. Although the carbon paper performance declined in the enhanced stress tests, findings reported by others suggest that stability could be improved by increased graphitization and nitrogen doping of the support material [5].

5.4.5 Mechanical Shear Calculations for Relevant Catalytic Applications

The mechanical shear force in hydrogen fuel cells is negligible due to a very low substrate viscosity of gases ($\mu \sim 0.02$ cP for air [24]). However, in other systems that use a liquid electrolyte, such as formic acid fuel cells or water treatment applications, the shear stress in the system becomes a more important consideration for system performance and longevity.

The average shear rate and shear stresses used in RDE tests here (35 s^{-1}; 0.1 Pa in 0.1 M H_2SO_4 and 4 Pa for 85% glycerol) [39] were similar to or higher than shear stresses that would be encountered in applications where biotemplated catalysts could be used. One possible application of biotemplated catalysts is their use on electrodes in direct formic acid fuel cells. If the anode flow pattern is approximated to be a pipe with a diameter of 0.36 a flow rate of 1 mL/min [39], the average wall shear rate (18 s^{-1}) and shear stress [0.03 Pa; μ (formic acid) = 1.5 cP [40]] is less than the shear rate here that resulted in electrode failure, implying that biotemplated electrodes without a binder should be durable in this system.

Removal of harmful contaminants from water streams is another application that uses catalysts. Flow of contaminated water flow through a packed bed reactor is a typical geometry for water treatment systems. Values for particle diameter and reactor cross section are taken from a

previous study that used palladium coated Al_2O_3 beads and a hydrogen infuser for reductive dechlorination of chlorinated contaminants [26]. The shear rate is calculated to be approximately 10 times higher (360 s^{-1}) through the packed bed than the shear stress imparted to the biotemplated electrodes by the RDE in 0.1 M H_2SO_4. However, when the viscosity of water is taken into account [μ (H_2O) = 1 cP [36]], the shear stress in the packed bed (0.3 Pa) is similar to the shear stress on the biotemplated electrodes in 0.1M H_2SO_4. The shear stress experienced by electrodes tested in 85% glycerol is 10 times larger than either of these applications, implying that biotemplated catalysts may be able to be used directly in many cases and that a binder would only have to be added under harsh conditions. The results of these calculations show that biotemplated catalysts could likely be used in other applications based on their durability to shear conditions in these reactors.

5.5 Conclusions

The oxidative and mechanical durability of biotemplated nanoporous palladium catalysts was tested using different support materials and polymer coatings. A thin layer of polyaniline electrodeposited over the palladium catalyst on graphite block supports greatly increased the durability of the electrode, even when subjected to increased electrochemical and mechanical stress. Although addition of polymer over a sustainably formed catalyst detracts from their environmental sustainability, there may be conditions where addition of this material is warranted. Carbon paper was the best support material, likely because its rigid, but highly porous structure provided accessible recessed layers of carbon fibers protected from surface shear stress. Additionally, the carbon fiber layers provided increased surface area for biofilm formation and subsequent palladium reduction. Estimates of shear stress in various possible electrode applications suggest that a biotemplated catalyst structure could be sufficiently stable to replace

synthetically formed catalysts in these applications. The results demonstrate that biotemplated catalyst electrodes could be good alternatives to electrodes prepared by synthetic methods.

5.6 Figures

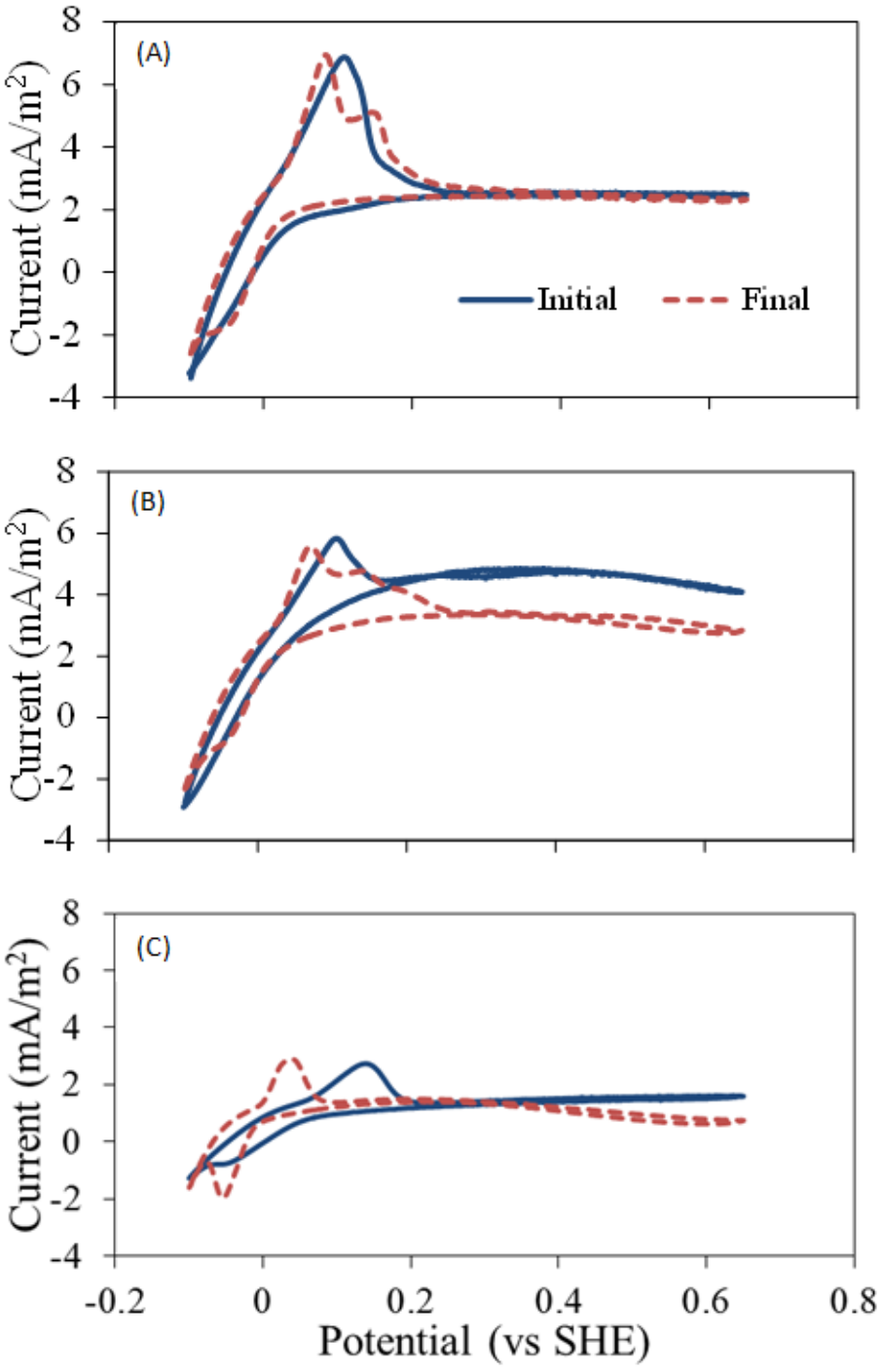

Figure 5.1. Representative cyclic voltammograms before and after durability testing of biotemplated palladium catalysts on (A) carbon paper (CP), (B) carbon cloth (CC), and (C) graphite (G).

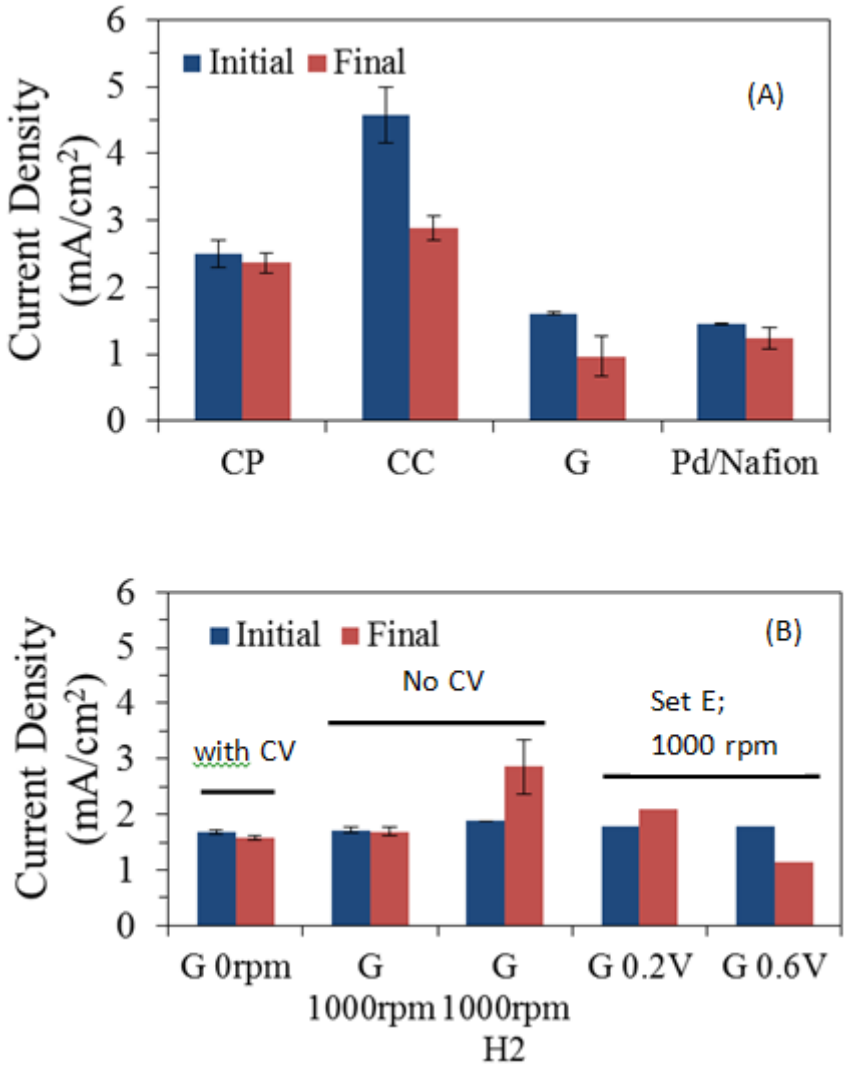

Figure 5.2. Initial and final current densities of palladium catalysts supported on different carbon materials. (A) Combined electrochemical and mechanical durability tests on different supports (CP = Carbon Paper; CC = Carbon Cloth; G= Graphite). (B) Durability tests on biotemplated catalysts on graphite under single stress conditions or at set potentials with mechanical stress. Pd/Nafion is a graphite electrode coated with a catalyst ink composed of Nafion and palladium black. All current densities are taken at a potential of 0.6 V.

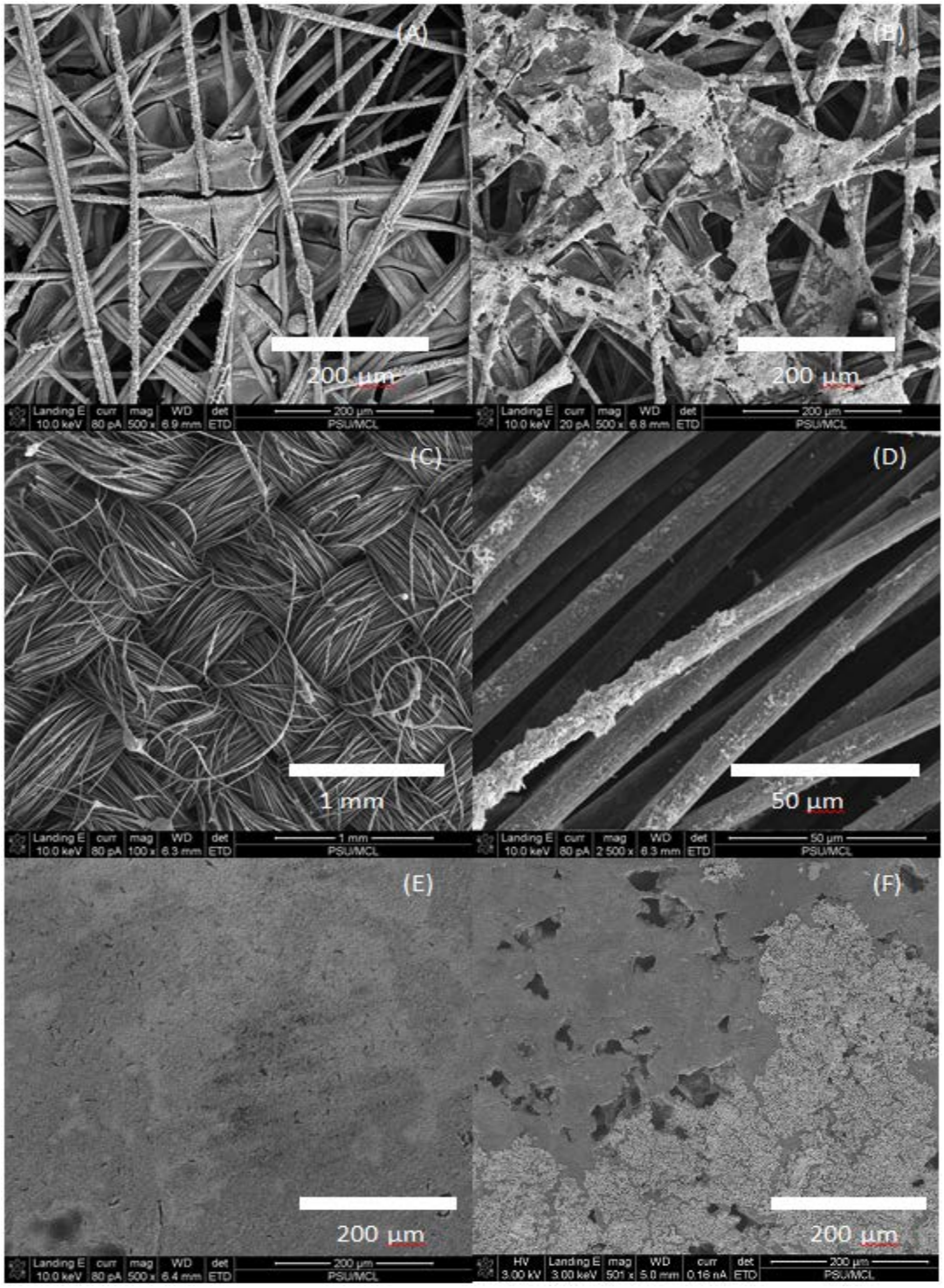

Figure 5.3. SEM images of palladium catalyst layers formed on different support materials: Carbon paper (A) before and (B) after stability testing, (C-D) carbon cloth before stability testing, and graphite electrodes (E) before and (F) after stability testing showing detachment of palladium after durability testing.

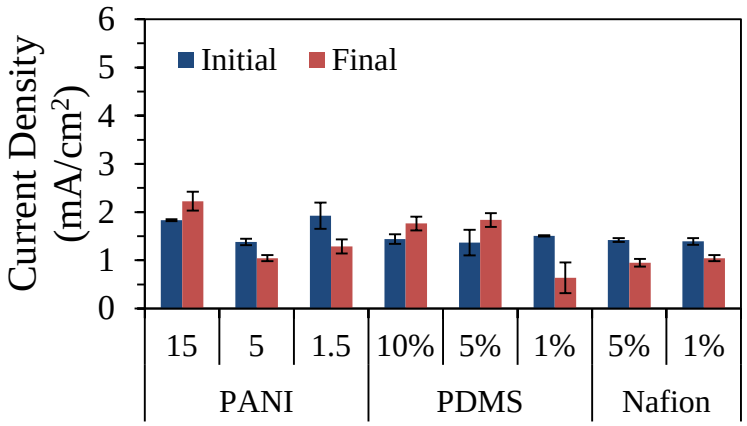

Figure 5.4. Initial and final current densities of palladium catalysts supported on graphite and coated with different stabilizing polymers. All stability tests were conducted with combined electrochemical and mechanical stress in 0.1 M H_2SO_4. Polyaniline shows the most promise as a stabilizer for coating catalytically active electrodes.

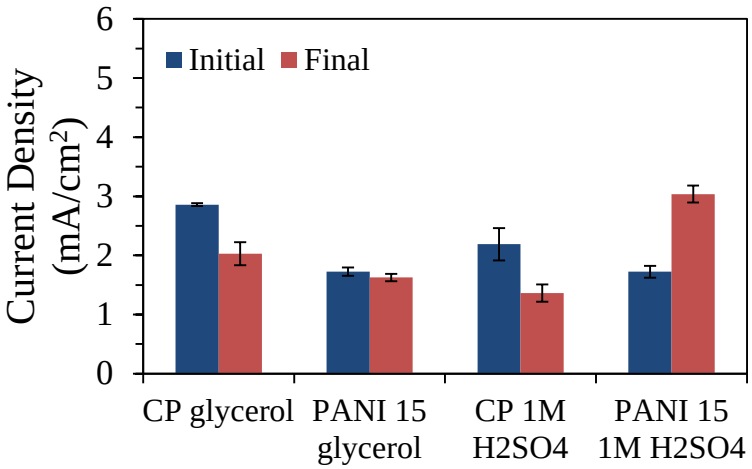

Figure 5.5. Initial and final current densities for carbon paper electrodes and graphite electrodes coated with polyaniline subjected to increased mechanical stress (1000 rpm in 85% glycerol solution) and electrochemical stress (long-term operation in highly oxidative conditions).

5.7 References

1. *The role of the chemical sciences in finding alternatives to critical resources: A workshop summary*. 2012: The National Academies Press.
2. Persson, K., et al., *Stability of palladium-based catalysts during catalytic combustion of methane: The influence of water.* Appl Catal B-Environ, 2007. **74**(3–4): p. 242-250.
3. Yang, S., et al., *Methane combustion over supported palladium catalysts: I. Reactivity and active phase.* Appl Catal B-Environ, 2000. **28**(3–4): p. 223-233.
4. Toebes, M.L., J.A. van Dillen, and K.P. de Jong, *Synthesis of supported palladium catalysts.* J Mol Catal A-Chem, 2001. **173**(1–2): p. 75-98.
5. Wang, X.X., et al., *Carbon nanocages: A new support material for Pt catalyst with remarkably high durability.* Sci Rep, 2014. **4**.
6. Gooding, J.J., *Nanostructuring electrodes with carbon nanotubes: A review on electrochemistry and applications for sensing.* Electrochim Acta, 2005. **50**(15): p. 3049-3060.
7. Hennebel, T., et al., *Biocatalytic dechlorination of trichloroethylene with bio-palladium in a pilot-scale membrane reactor.* Biotechnol Bioeng, 2009. **102**(4): p. 995-1002.
8. Windt, W.D., P. Aelterman, and W. Verstraete, *Bioreductive deposition of palladium (0) nanoparticles on Shewanella oneidensis with catalytic activity towards reductive dechlorination of polychlorinated biphenyls.* Environ Microbiol, 2005. **7**(3): p. 314-325.
9. Mabbett, A.N., et al., *Biorecovered precious metals from industrial wastes: Single-step conversion of a mixed metal liquid waste to a bioinorganic catalyst with environmental application.* Environ Sci Technol, 2005. **40**(3): p. 1015-1021.

10. Li, D., B. Mathew, and C. Mao, *Biotemplated synthesis of hollow double-layered core/shell titania/silica nanotubes under ambient conditions.* Small, 2012. **8**(23): p. 3691-3697.

11. Liu, Y., et al., *Tin coated viral-nanoforests as sodium-ion battery anodes.* ACS Nano, 2013. **7**(4): p. 3627-3634.

12. Shim, H.-W., et al., *Highly reversible lithium storage in Bacillus subtilis-directed porous Co_3O_4 nanostructures.* ACS Nano, 2010. **5**(1): p. 443-449.

13. Yates, M.D., et al., *Exoelectrogenic biofilm as a template for sustainable formation of a catalytic porous structure.* Biotechnol Bioeng, 2014.

14. Mench, M., E. Kumbur, and T. Veziroglu, *Polymer Electrolyte Fuel Cell Degradation*. 2012: Elsevier, Inc.

15. Huang, S.-Y., P. Ganesan, and B.N. Popov, *Electrocatalytic activity and stability of titania-supported platinum–palladium electrocatalysts for polymer electrolyte membrane fuel cell.* ACS Catal, 2012. **2**(5): p. 825-831.

16. Chen, W.-F., et al., *Biomass-derived electrocatalytic composites for hydrogen evolution.* Energ Environ Sci, 2013. **6**(6): p. 1818-1826.

17. Zhu, Y., Z. Khan, and R.I. Masel, *The behavior of palladium catalysts in direct formic acid fuel cells.* J Power Sources, 2005. **139**(1–2): p. 15-20.

18. De Almeida, N.E. and E.B. Easton, *Nafion/sulfonated silica composite membranes for PEM fuel cells.* ECS Transactions, 2010. **28**(27): p. 29-38.

19. Wu, G., et al., *High-performance electrocatalysts for oxygen reduction derived from polyaniline, iron, and cobalt.* Science, 2011. **332**(6028): p. 443-447.

20. Joseph, S., et al., *Polyaniline and polypyrrole coatings on aluminum for PEM fuel cell bipolar plates.* J Power Sources, 2008. **177**(1): p. 161-166.

21. Rout, T.K., et al., *Development of conducting polyaniline coating: a novel approach to superior corrosion resistance.* Surf Coating Technol, 2003. **167**(1): p. 16-24.

22. Kost, K.M., et al., *Electrodeposition of platinum microparticles into polyaniline films with electrocatalytic applications.* Anal Chem, 1988. **60**(21): p. 2379-2384.

23. Detsi, E., P. Onck, and J.T.M. De Hosson, *Metallic muscles at work: High rate actuation in nanoporous gold/polyaniline composites.* ACS Nano, 2013. **7**(5): p. 4299-4306.

24. Incropera, F., et al., *Fundamentals of heat and mass transfer*. 6th ed. 2007: John Wiley and Sons.

25. Wang, C., et al., *Self-healing chemistry enables the stable operation of silicon microparticle anodes for high-energy lithium-ion batteries.* Nat Chem, 2013. **5**: p. 1042-1048.

26. McNab, W.W., R. Ruiz, and M. Reinhard, *In-situ destruction of chlorinated hydrocarbons in groundwater using catalytic reductive dehalogenation in a reactive well: Testing and operational experiences.* Environ Sci Technol, 1999. **34**(1): p. 149-153.

27. Logan, B.E. and J.M. Regan, *Microbial fuel cells—challenges and applications.* Environ Sci Technol, 2006. **40**(17): p. 5172-5180.

28. Coloma, F., et al., *Preparation of platinum supported on pregraphitized carbon blacks.* Langmuir, 1994. **10**(3): p. 750-755.

29. Feng, Y., et al., *Treatment of graphite fiber brush anodes for improving power generation in air-cathode microbial fuel cells.* J Power Sources, 2010. **195**: p. 1841-1844.

30. Zhang, F., et al., *Novel anti-flooding poly(dimethylsiloxane) (PDMS) catalyst binder for microbial fuel cell cathodes.* J Power Sources, 2012. **218**(0): p. 100-105.

31. Zhu, Y., S.Y. Ha, and R.I. Masel, *High power density direct formic acid fuel cells.* J Power Sources, 2004. **130**(1–2): p. 8-14.

32. Park, J.-E., et al., *Electrochemical and chemical interactions between polyaniline and palladium nanoparticles.* Synthetic Met, 2004. **141**(3): p. 265-269.

33. Casciola, M., et al., *On the decay of Nafion proton conductivity at high temperature and relative humidity*. J Power Sources, 2006. **162**(1): p. 141-145.

34. Ćirić-Marjanović, G., *Recent advances in polyaniline composites with metals, metalloids and nonmetals.* Synthetic Met, 2013. **170**(0): p. 31-56.

35. Sheely, M.L., *Glycerol viscosity tables.* Ind Eng Chem, 1932. **24**(9): p. 1060-1064.

36. Rhodes, F.H. and C.B. Barbour, *The viscosities of mixtures of sulfuric acid and water.* Ind Eng Chem, 1923. **15**(8): p. 850-852.

37. Kwon, Y. and M.T.M. Koper, *Combining voltammetry with HPLC: Application to electro-oxidation of glycerol.* Anal Chem, 2010. **82**(13): p. 5420-5424.

38. Ray, A., et al., *Polyaniline: Doping, structure and derivatives.* Synthetic Met, 1989. **29**(1): p. 141-150.

39. Munson, B., et al., *Fundamentals of Fluid Mechanics, Sixth Edition*. 6th ed. 2009: John Wiley and Sons.

40. Cases, A.M., et al., *Density, viscosity, and refractive index of formamide, three carboxylic acids, and formamide + carboxylic acid binary mixtures.* J Chem Eng Data, 2001. **46**(3): p. 712-715.

Chapter 6

Hydrogen Evolution Catalyzed by Viable and Non-Viable Cells on Biocathodes

6.1 Abstract

The presence of microorganisms on cathodes has been shown to enhance the hydrogen evolution reaction (HER), but a requirement for viable cells has not been sufficiently examined. HER was examined using live or killed biocathodes of exoelectrogenic (*Geobacter sulfurreducens*) and non-exoelectrogenic (*Escherichia coli*) bacteria, and a hydrogenotrophic methanogen (*Methanosarcina barkeri*). Electrodes at a set potential of –0.6 V (versus a standard hydrogen electrode) containing *G. sulfurreducens* biofilms or killed controls produced hydrogen at a similar rates (118±15 nmol/d-mL) over 5 months. Electrodes containing cell extracts produced hydrogen at approximately half this rate (56±6 nmol/d-mL). Biocathodes fed lactate produced only 14±2 nmol/d-mL. Electrodes inoculated with *M. barkeri* produced hydrogen at a rate (120±18 nmol/d-mL) similar to the *G. sulfurreducens*, but no methane was recovered after the initial inoculation cycle. Non-exoelectrogenic *E. coli* cells and extracts produced hydrogen at a slower rate (13±1 and 4±1 nmol/d-mL, over 3 cycles). Electrodes exposed to viable cells that were examined after 5 months had increased levels of in nitrogen, sulfur, iron, nickel, cobalt (%wt), and peptides (possibly remnants of hydrogenases and other oxidoreductases) relative to uninoculated controls, and no intact cells. These results show that enhanced HER can result from cell debris and that living cells are not required.

6.2 Introduction

Fossil fuels are currently the primary feedstock for hydrogen production, producing large amounts of CO_2. A sustainable alternative for hydrogen production is water electrolysis. However, water electrolyzers often use expensive precious metal catalysts to reduce electrode overpotentials. The overpotential is defined as the off-set potential needed to achieve a measurable catalytic effect compared to the theoretical potential obtained from the Nernst equation. Precious metal catalysts, such as platinum, are expensive and they are readily poisoned by trace concentrations of contaminants, such as carbon monoxide [1], alcohols [2], and sulfides [3].

Biocatalysts provide an alternative method of hydrogen production that avoids the use of precious metals. Hydrogenases are the most studied biocatalysts for hydrogen production. They are produced by microorganisms from diverse phylogenetic classifications, including methanogenic archaea [4], fermentative bacteria [5], and dissimilatory metal reducing bacteria [6], among others [7]. Hydrogenases are defined as oxidoreductases that have a redox potential at the same potential of the H_2/H^+ redox couple (E = –410 mV vs. a standard hydrogen electrode [SHE]) at ambient standard conditions (25°C, atmospheric pressure, all concentrations 1 M except for the pH of 7). They contain an inorganic catalytic center (NiFe, FeFe, or NiFeSe [8]) surrounded by 2 protein subunits with a chain of iron sulfide clusters (4Fe–4S or 2Fe–2S) that can transfer electrons to and from the enzyme surface [9]. Purified hydrogenases have been attached to electrodes (commonly oxidized graphite) for hydrogen production [8], but the enzymes become inactive over relatively short periods of time due to protein desorption [10] or unfolding [11], especially under highly oxidative conditions [12]. Other proteins involved in electron transport, such as ferredoxins, are also able to produce hydrogen from protons and electrons provided by chemical reducing agents [13, 14]. Despite being pivotal for methanogenic

metabolism, hydrogen producing proteins of methanogens have not been investigated for biohydrogen production.

The use of purified enzymes is currently untenable for industrial scale hydrogen production primarily because hydrogenases are difficult to stabilize on electrodes. However, whole cells of mixed or pure cultures of actively growing microorganisms represent an economical alternative because they do not require any purification steps [15]. Pure and mixed cultures have been previously investigated for biocathodic hydrogen production. Pure culture *Geobacter sulfurreducens* biocathodes produced hydrogen at different rates over a range of potentials from –0.6 to –0.8 V (vs. SHE) [16]. Additionally, pure cultures of *Desulfovibrio* sp. grown on a cathode increased the hydrogen production rate compared to an abiotic control [17] at an electrode potential of –0.9 V vs. SHE. *Desulfovibrio* sp. were also identified as the dominant species in a mixed community biocathode producing hydrogen at an electrode potential of –0.7 V vs. SHE [18]. Other recent studies observed hydrogen production using mixed culture biocathodes under mesophilic [19, 20] and thermophilic [21] conditions, and using a dechlorinating consortium [22].

While the mechanism of enhanced hydrogen production by these different biocathodes is unknown, it is clear that biofilm growth on the electrode decreases overpotentials [22, 23]. The presence of the microorganisms could cause a reduction in overpotential through excreted material, enhanced corrosion, or by electron flow through the cells. Mechanisms for hydrogen production that rely only on catalytic cell materials (i.e. non-viable cells) have not been sufficiently evaluated. In addition, the long-term stability of hydrogen producing cathodes has not been well assessed. Here, the use of electrical current for hydrogen gas production with biocatalytic cell material was investigated with either live or killed pure cultures of *G. sulfurreducens*, *Methanosarcina barkeri*, or *Escherichia coli* on graphite electrodes. Reactors were run for an extended period of time (5 months) to investigate the sustainability of hydrogen production over time. Electrode surfaces were characterized spectroscopically and

microscopically to identify proteins and elemental surface changes to elucidate possible reasons for enhanced hydrogen production.

6.3 Materials and Methods

6.3.1 Reactor Construction and Operation

Two-chamber reactors (duplicate) were connected by side-arms (inner diameter of 2.4 cm), sealed with an O-ring, and separated by a Nafion® 117 membrane (Fuel Cell Store, Boulder, CO, USA) that was held with a screw clamp (35/25, VWR, Radnor, PA, USA). Each chamber had three 20 mm side ports, which were sealed with rubber stoppers and aluminum crimp seals, and a liquid volume of 120 mL and a headspace volume of 60 mL. A stopper was inserted into the middle side port of the working electrode chamber with a 5 mm diameter hole to allow insertion of a reference electrode.

The working electrode was made by attaching a titanium wire (0.8 mm, McMaster Carr, Cleveland, OH, USA) to graphite blocks (1 cm × 2 cm) via small holes drilled near the top of the electrode. Graphite electrodes were polished with 400 and 1500 grit sandpaper, sonicated briefly to remove loose particles, and then soaked in 1 M HCl overnight. Electrodes were then rinsed three times with deionized water and polished with tissue (Kim® wipes) to remove any remaining loose material. The electrode was inserted through a butyl rubber stopper, placed into the top of the reactor, and sealed with an aluminum crimp seal. A platinum wire counter electrode was inserted through a stopper in the middle side-arm in the counter electrode chamber. Electrode potentials were measured using reference electrodes (Ag/AgCl, –200 ± 5 mV vs. SHE; BASi, West Lafayette, IN, USA), and all potentials reported here are vs. SHE. All reference electrodes were replaced at the end of each batch cycle using new or refurbished electrodes. Reference

electrodes were refurbished by cleaning the electrode with concentrated HCl, forming a new silver-chloride layer with a 5% hypochlorite solution, replacing the 3 M NaCl solution, and attaching a new frit. The tip (molseive, 3A, 3-4 mm diameter, Alfa Aesar, Ward Hill, MA, USA) of the inserted reference electrode was ~2 cm away from the working electrode surface. The reactors used for the incubation experiments with *Methanosarcina acetivorans* did not have side-arms in the chambers, as described in a previous study [23]. All reactors and media were sterilized before use. Media replacement was carried out using sterile, anaerobic techniques. Current uptake by the electrodes at –0.6 V was measured and recorded using a potentiostat (MPG2 , Biologic Inc, Grenoble, France). Coulombic recoveries (CRs) were calculated as the ratio between measured charge transferred, and charge recovered as hydrogen or methane.

Reactors were inoculated with *G. sulfurreducens* cells and anode potentials set to –0.15 V to stimulate biofilm growth. After the biofilm developed over 14 days, the working electrode solution was changed and the potential was dropped step-wise to –0.6 V in order to examine hydrogen evolution as previously described [16]. Cycle 1 was started once the potential reached –0.6 V. Reactors containing only *M. barkeri* or *E. coli* cells, and abiotic controls, were directly set to –0.6 V. Two *G. sulfurreducens* reactors were inoculated with *M. barkeri* cells after two cycles of hydrogen production. A cycle was defined as a change in headspace hydrogen content (molar basis) of less than 10% (~ 2 weeks for cycles 1 and 2; ~1 month for cycles 3, 4, and 5). After the first inoculation cycle, the solution of the reactors with the two strains was completely replaced, while for *M. barkeri* 10% of the medium was left in the reactor to prevent complete cell washout as little biofilm was observed on the electrode surface.

6.3.2 Media Compositions and Culturing

G. sulfurreducens strain PCA was obtained from frozen stocks (–80°C), and cultured in ATCC medium 1957 at 30°C. Cells were grown to an OD_{610} = 0.5 (mid-log phase), washed 3 times by centrifugation in sterile anaerobic growth medium (to remove acetate and fumarate), and then used to inoculate reactors.

M. barkeri (DSM 804) was obtained from the Deutsche Sammlung für Mikroorganismen und Zellkulturen (DSMZ), and cultured as previously described [24] with 1 mM methanol and 10 mM cysteine. The culture headspace was filled with 80% hydrogen prior to inoculation. Cells were harvested during mid-log growth, concentrated to an OD_{610} = 0.5, and washed 3 times in sterile anaerobic ATCC 1957 medium containing 10 mM cysteine, and then added to the reactors. *M. barkeri* was also cultured using ATCC medium 1957 with 1 mM methanol, 10 mM cysteine, and a headspace concentration of 80% hydrogen and 20% CO_2 to verify its ability to grow in the reactor medium. ATCC medium 1957 was used for both *G. sulfurreducens* and *M. barkeri* reactors to eliminate possible differences due to the medium.

E. coli strain K12 was obtained from frozen stocks (–80°C), and cultured overnight at 30°C in sterile, anaerobic tryptic soy broth supplemented with 1 g/L glucose. Cells were grown to an OD_{610} = 0.5 and washed 3 times before inoculation into reactors.

M. acetivorans strain C2A (DSM 2834), donated by James Ferry of the Pennsylvania State University, was cultured as previously described [25]. Despite its phylogenetic similarity to *M. barkeri*, *M. acetivorans* expresses genes only for acetoclastic growth; hydrogen utilization genes are not expressed [4].

6.3.3 Reactor Medium Preparation

The medium used for all experiments contained (final concentration in g/L): $NaHCO_3$ 2.5; NH_4Cl 1.5; NaH_2PO_4 0.6 and KCl 0.1. Anaerobic, filter-sterilized vitamins and trace elements (10 mL/L each; see Supporting Information) were added after autoclaving and flushing the headspace of the hot medium with 80% N_2/ 20% CO_2 (to remove trace oxygen). Sterile, anaerobic sodium lactate (4 mM) was added to some *G. sulfurreducens* reactors to determine the effect of adding a carbon source to the medium [26]. Additionally, duplicate *G. sulfurreducens* biofilms were killed by soaking in 70% ethanol for 45 minutes to investigate differences in hydrogen production between a living or killed biofilm. Anaerobic, filter-sterilized cysteine (10 mM) was added to reactor medium after *M. barkeri* inoculation. Medium was changed in a biological safety cabinet using sterile, anaerobic techniques. The headspace of both chambers was purged with sterile 20% CO_2 / 80% N_2 each cycle after the medium was changed.

6.3.4 Control Reactors

Abiotic deconstruction control reactors (duplicates) were built and operated as described above for the same period of time to rule out factors that did not contribute to hydrogen production, and to distinguish between biotic (viable cells) and abiotic (non-viable organic or inorganic matter) hydrogen formation. The basal medium used here was the same as described above excluding vitamins and minerals. Controls tested include the basal medium with addition of only: vitamins and minerals (10 mL/L), cysteine (10 mM), *M. barkeri* cell extract, *G. sulfurreducens* cell extract, or yeast extract (0.1% w/v). A combination of cysteine (10 mM), *M. barkeri* cell extract, and *G. sulfurreducens* cell extract was also used to test possible interactions between the non-viable components. *E. coli* cells and cell extracts were utilized as a non-

exoelectrogenic control [27]. Cell extract was produced by sonicating concentrated cell suspensions (OD_{610} = 0.8) for three, 10 minute intervals. An open circuit control reactor was operated for each abiotic control to ensure that hydrogen production was only produced in set potential reactors.

M. barkeri cells were also grown in an open circuit, two-chamber reactor with methanol and hydrogen in the headspace to ensure that the cells could grow in the reactor. Hydrogen production by *M. acetivorans* was also tested on a graphite electrode poised at –0.6 V.

6.3.5 Chemical Measurements

Bi-weekly measurements of hydrogen and methane concentration in the reactor headspace were conducted using a gastight syringe (Vici, Baton Rouge, LA, USA) and sterilized needles. Samples were analyzed using a gas chromatograph (SRI 310C, SRI Instruments, Torrance, CA, USA) with a 6-foot long molsieve-column at an oven temperature of 80˚C. Rates of gas production were calculated by linear regression of hydrogen gas concentrations over the entire batch cycle, and normalized by medium volume or electrode surface area. Error bars indicate high and low values of duplicate reactors. Electrodes were removed after 5 cycles for spectroscopic and microscopic characterization or protein analysis. The cathodes subjected to spectroscopic characterization were re-inserted into the reactors with fresh medium to determine if the hydrogen production rate could be recovered.

Concentrations of formic, acetic, propionic and butyric acids were determined during the final cycle using a high performance liquid chromatograph (HPLC; CTO-20A UFLC; Shimadzu, Columbia, MD, USA) equipped with an autosampler (SIL-20A HT, Shimadzu, Columbia, MD, USA). The mobile phase was 50 mM KH_2PO_4 adjusted to a pH of 2.3 using H_3PO_4. The column (250 × 4.6 mm “Allure Organic Acids”, 5 μm particle size; Restek, Bellefonte, PA, USA)

temperature was held at 40°C, and each run lasted 50 min. Samples and standards were filtered using 0.2 µm syringe filters prior to analyses.

6.3.6 Protein Characterization

Proteins attached to electrode surfaces were identified for reactors with cell extracts of *G. sulfurreducens* or *M. barkeri* and reactors inoculated with live cells of *G. sulfurreducens* and *M. barkeri*. Electrodes were washed three times with a 6 M urea and 1% SDS solution in a 100 mM Tris buffer (pH 8.1) at 30°C for 10 minutes each to disrupt non-covalent bonds and linearize proteins. Electrodes were then washed three times in an 8 g/L ammonium bicarbonate solution (pH 8) at 30°C for 10 minutes each to remove the urea/SDS/Tris buffer. Pierce trypsin protease (5 µg/mL; Thermo Scientific, Pittsburgh, PA, USA) was added to the solution and allowed to react overnight at 30°C to partially digest proteins attached to the surface. The enzymatic digest was then reduced with 10 mM dithiothreitol (DTT) in 8 g/L ammonium bicarbonate in a hot water bath to break sulfhydryl bonds and alkylated with 15 mM iodoacetamide (IAA) in 8 g/L ammonium bicarbonate for 30 minutes in the dark to prevent reforming of bonds. The resulting solution was re-digested with 5 µg/mL Pierce trypsin protease for 3 hours at 30°C to ensure proteins were fully digested. The digested product was stored at 4°C until further analysis in a LTQ Orbitrap Velos ETD with Dionex UltiMate 3000 nano-flow 2D LC system (Thermo Scientific, Pittsburgh, PA, USA). The peptide sequences generated by the LTQ Orbitrap were matched to known protein sequences using the SEQUEST search algorithm.

6.3.7 Surface Characterization

Electrodes were prepared for SEM analysis by fixing overnight at 4°C in 5 mL of a phosphate buffer solution (pH 7.2) containing 2.5% glutaraldehyde and 1.5% paraformaldehyde. Electrodes were then sequentially dried in ethanol-water series of 50%, 70%, 85%, 90%, 95%, and 100% ethanol and stored in fresh 100% ethanol at 4°C in the dark. Prior to electron microscopy, electrodes were critical point CO_2-dried and stored in a desiccator until analyzed with an environmental scanning electron microscope (E-SEM; FEI Quanta 200 instrument, FEI company, Hillsboro, OR, USA) equipped with electron dispersive X-ray spectroscopy (EDX).

X-ray photoelectron spectroscopy (XPS; Kratos Analytical Ultra, Kratos, UK) was used to characterize the elemental composition of the electrode surface. Three survey scans were performed on different parts of the electrode. Approximate weight percent values were obtained based on these triplicate survey scans.

6.4 Results

6.4.1 Hydrogen Production Rates from Viable Cells

Hydrogen gas was produced in all reactors inoculated with living cells at set cathode potential of –0.6 V. Biocathodes pre-enriched with a *G. sulfurreducens* biofilm produced hydrogen gas at 120 ± 2 nmol d^{-1} mL^{-1} of catholyte during the first cycle (after the switch from anodic to cathodic conditions; Fig. 1). Ethanol-killed *G. sulfurreducens* biofilms initially produced hydrogen at a higher rate (145 ± 3 nmol d^{-1} mL^{-1}) after sterilization, but this decreased (120 ± 15 nmol d^{-1} mL^{-1}) in the last cycle (5 months for all five cycles) to a rate similar to the biotic reactors. Hydrogen gas production was much lower over the same period of time when lactate was added (11 ± 5

nmol d^{-1} mL^{-1} initially and 20 ± 17 nmol d^{-1} mL^{-1} during the final cycle) to the biotic reactors. Sterile controls produced very little hydrogen gas (4 ± 2 nmol d^{-1} mL^{-1}).

Reactors inoculated with *M. barkeri* cells, produced hydrogen during the final cycle (119 nmol d^{-1} mL^{-1}) at a rate similar to reactors with *G. sulfurreducens*, despite initially producing less hydrogen (72 ± 7 nmol d^{-1} mL^{-1}). There was also an increase in hydrogen production after inoculation (Fig. 1) of *M. barkeri* into reactors with a *G. sulfurreducens* biofilm on the electrode (90% increase; 36 ± 20 nmol d^{-1} mL^{-1}). Electrodes containing *G. sulfurreducens* biofilms that were not inoculated with *M. barkeri* exhibited a slightly a smaller increase of 30% in the hydrogen production rate (12 ± 2 nmol d^{-1} mL^{-1}) over the same number of cycles. During the final cycle, hydrogen production rates from reactors with pure cultures of *M. barkeri* (119 nmol d^{-1} mL^{-1}) or *G. sulfurreducens* (118 ± 15 nmol d^{-1} mL^{-1}) were similar to each other, and to reactors inoculated with both cultures (Fig. 1).

Reactors inoculated with *E. coli* initially produced hydrogen at a slightly slower rate (95 ± 6 nmol d^{-1} mL^{-1}) than reactor inoculated with *M. barkeri* and *G. sulfurreducens* (both pure and co-cultures). After three cycles, the hydrogen production rate decreased to 13 ± 1 nmol/d-mL.

Methanosarcina acetivorans, an acetoclastic methanogen, was used to examine possible HER by a methanogen unable to grow on hydrogen. However, reactors inoculated with *M. acetivorans* produced hydrogen at a similar rate (4.0 ± 0.4 nmol d^{-1} mL^{-1}) as the sterile control (4 ± 2 nmol d^{-1} mL^{-1}) over a period of 90 days, indicating no enhanced HER using this methanogen.

6.4.2 Hydrogen Production from Cell Extracts

Approximately 50 to 60% of the hydrogen production rate of viable cells was achieved using cell extracts (Fig. 1) of both *G. sulfurreducens* and *M. barkeri*. Hydrogen production rates by the duplicates were initially different (88 and 2 nmol d^{-1} mL^{-1}), but converged over time, producing

52 and 58 nmol d^{-1} mL^{-1} hydrogen in cycle 5. *E. coli* extracts initially produced hydrogen at a rate (81 ± 5 nmol d^{-1} mL^{-1}) that was ~80% of that obtained using whole cells. However, the hydrogen production rate decreased to (4 ± 1 nmol d^{-1} mL^{-1}) after 3 cycles. The rate of hydrogen production with yeast extract (3 ± 1 nmol d^{-1} mL^{-1}) was similar to *E. coli* extracts and sterile controls lacking any additional organic matter (Fig. 1). These results demonstrated that the hydrogen production rate was dependent on the specific microorganism used, and not just the presence of cell material in the reactors.

Medium components were also tested for hydrogen production in reactors at set potentials of –0.6 V (Fig. 1). Reactors amended with trace vitamins and minerals produced very little hydrogen gas (0.9 ± 0.3 nmol d^{-1} mL^{-1} to 3 ± 1 nmol d^{-1} mL^{-1}), as did reactors containing cysteine (no vitamins or trace metals, 5 ± 2 nmol d^{-1} mL^{-1} for all cycles) or all of these components (3 nmol d^{-1} mL^{-1}). These low hydrogen production rates from the medium components effectively eliminated them as the sole reason for enhanced hydrogen production in these systems.

6.4.3 Elemental Surface Characterization

In order to explore possible reasons for enhanced HER by electrodes inoculated with viable or non-viable cells, we screened the cathode surfaces for cells, metals, and proteins. Examination of the surfaces of the electrodes using scanning electron microscopy (SEM) did not reveal any cell-shaped structures after 5 months of incubation. This was also the case on electrodes that initially supported a *G. sulfurreducens* biofilm (Fig 2). However, material that appeared to be remnants of biological material was found on both electrode surfaces. The initial presence of *G. sulfurreducens* biofilms on the electrode was shown by the characteristic pink color of the electrode which is due to the abundance of expressed cytochromes by these cells [28]. Electrodes exposed to *M. barkeri* were not initially examined for the presence of cells on the surface.

The elemental composition of the material adhered to the surface was identified using XPS. There was an increase in nitrogen and sulfur, as well as cobalt, nickel, iron, and zinc, on the electrode surfaces exposed to cells, compared to controls (not exposed to cells; Fig. 3). The enrichment of these elements on electrodes exposed to cells supported the idea that material attached to the surface of the electrode was likely derived from cells and could be contributing to hydrogen production (Fig. 3).

6.4.4 Coulombic Recoveries

Coulombic recoveries were near or greater than 100% for most cycles in reactors inoculated with viable cells (Fig. 1, outlined bars) and increased during cycles that cells were added into the reactor (during the initial cycle for the *G. sulfurreducens* reactors, and again when *M. barkeri* was added). Coulombic recoveries for reactors inoculated with *G. sulfurreducens* were initially the largest (1400 ± 80%), but they gradually decreased over time to 110 ± 22% during cycle 5. *G. sulfurreducens* reactors fed lactate for all cycles exhibited a net positive current (oxidation state) and a negative Coulombic recovery during the initial cycle (–41± 23%), followed by an increase every cycle to a final value of 40 ± 35%, suggesting that living cells produced relatively little hydrogen in these systems. Coulombic recoveries of *M. barkeri* inoculated reactors decreased every cycle, but remained greater than 100% (342 ± 20%) throughout the experiment. Coulombic recoveries were initially greater than 100% for reactors inoculated with *E. coli* (2100 ± 300%), but decreased to 63 ± 6% during the final cycle.

Abiotic reactors with medium components (vitamins and minerals, cysteine, and all three combined) exhibited no clear trend in Coulombic recovery (initial 39 ± 37 %, final 37 ± 22%) but there overall hydrogen production rate was very low (Fig. 1B). The reactors with cell extracts added exhibited a trend similar to viable cells of a decrease over time, with a Coulombic recovery

of 210 ± 36% during cycle 2 that decreased to 125 ± 45% during cycle 5 (Fig. 1A). The first cycle was excluded from Fig. 1 because the variability between duplicates was high (231% and 18% CR).

6.4.5 Presence of Peptides on the Electrode Surface

Reactors inoculated with pure cultures were analyzed for peptides attached to the cathode surface after 5 months (Table 1). Peptides originating from different ferredoxin oxidoreductases were identified in extracts from electrode surfaces exposed to *G. sulfurreducens*. These enzymes are involved in electron transfer processes in hydrogen production/utilization pathways. Peptides related to dehydrogenases, which are involved in the transfer of hydrogen groups in different cellular processes, and biosynthetic enzymes were also found in extracts from the electrode surface.

In the reactors inoculated with *M. barkeri*, peptides originating from proteins involved in methanogenesis pathways were identified in the electrode extracts (Table 1). These included, for example, methanol–corrinoid proteins utilized in the pathway for methanol conversion to methane. Peptides similar to methyl coenzyme M reductase subunits, an enzyme with a nickel cofactor for catalyzing the final step of methanogenesis, were also identified in the extracts. 5,10-methylenetetrahydromethanopterin (MP4T) reductase, an oxidoreductase without a metal center involved in hydrogenotrophic methane production [29], peptides were identified as well. A full list of identified peptides can be found in Table 1.

6.4.6 VFA Production Rates

Acetate was produced in all reactors with viable cells (87 ± 3 nmol d^{-1} mL^{-1}; Table 2), but not in any abiotic control reactors with or without cell extracts. Formate was only detected in low concentration in one sterile reactor (0.5 nmol/d-mL), and no propionate or butyrate was detected. *M. barkeri* cell suspensions are able to produce acetate from CO_2 explaining the observed acetate accumulation [30]. VFA production has also been reported in previous studies using biocathodes but its origin (electrode material or CO_2 reduction) was unclear [23].

6.5 Discussion

6.5.1 Hydrogen Production by Live versus Dead Cells

Cells and cell extracts from two distinct microorganisms produced hydrogen at a similar rate (except during cycle 2), indicating that inactivated cells catalyzed proton reduction in these biocathodic systems. *G. sulfurreducens* [31] is unable to fix CO_2, so this microorganism was unable to grow in these reactors when no organic carbon source was provided over the 5 month duration of the experiments. It is possible some cells entered a long term survival state and remained viable, but not active [32, 33], but tests with the cell extracts makes it clear that neither active or growing cells were needed for enhanced H_2 gas production. In addition, when reactors inoculated with *G. sulfurreducens* were supplied with lactate, an electron donor that can be used by this strain [26], they produced ~10× less hydrogen than without lactate throughout the experiment. Thus, the presence of growing cells was actually detrimental to enhanced H_2 gas production. Lactate-fed cultures (4.0 ± 1.5 C) consumed less current than abiotic controls (–1.5 ± 0.9 C) through the first two cycles, indicating that the electrode did not provide electrons to the cells when set at –0.6 V. Although the positive current suggests operation as an anode, the

produced current was relatively minimal. The suppressed hydrogen production by reactors with lactate added indicates that hydrogen was primarily catalyzed by abiotic cell material on the electrode surfaces.

Initial rates of hydrogen gas production by *G. sulfurreducens* biocathodes were approximately similar to previously reported rates at –0.6 V for this microorganism when normalized to electrode surface area (3.5 $\mu mol^{-1}\ d^{-1}\ cm^{-2}$ by others [16], compared to 2.9 ± 1.2 $\mu mol^{-1}\ d^{-1}\ cm^{-2}$ here), although rates were different when compared on a volumetric basis due to different electrode surface area to reactor volume ratios (66.7 m^2/m^3 compared to 4 m^2/m^3 here). Mixed culture biocathodes have recently been shown to catalyze hydrogen formation at slightly higher rates than those obtained here using pure cultures, but more negative electrode potentials or higher incubation temperatures were used. Batlle-Vilanova *et al.*[19] reported a mixed culture biocathode that produced 900 nmol $d^{-1}\ mL^{-1}$ (1.3 m^2/m^3) at a cathode potential of –0.9 V under mesophilic conditions (22°C). A dechlorinating consortium on a biocathode at a more positive set potential of –0.75 V produced 1400 nmol $d^{-1}\ mL^{-1}$ (2.7 m^2/m^3) of hydrogen gas [22]. At a set potential (–0.65 V) only slightly larger than that used here, Fu *et al*. [21] reported that a mixed thermophilic consortium, incubated at 55°C, produced 600 nmol $d^{-1}\ mL^{-1}$ (26.6 m^2/m^3). These hydrogen production rates were calculated over much shorter periods of time (10 h to 12 d) than the 5 months of operation examined here. Hydrogen may have been produced by viable cells during the timescale of previous reports. However, the results here show that the inactivation of the viable cells does not hinder hydrogen production and alleviates the requirement for cell maintenance with exogenous carbon sources. Electrode corrosion may also have contributed to hydrogen evolution, as further discussed below.

Reactors inoculated with *E. coli*, a non-exoelectrogenic bacterium [27], produced ~10× less hydrogen than *G. sulfurreducens* or *M. barkeri* inoculated reactors, suggesting that the type of microorganisms in the system affected hydrogen production rates. The high initial rate of

hydrogen production from *E. coli* cells compared to *G. sulfurreducens* and *M. barkeri* suggested that hydrogen could initially be produced from autolytic cell material, but the reduction in this rate over time showed this effect could not be sustained with this microorganism.

Hydrogen production was sustained for 3 consecutive months from reactors inoculated with *M. barkeri*. Methane was detected in the first cycle with for reactors inoculated with *M. barkeri* (13 ± 7 nmol d^{-1} mL^{-1}). However, the methane production was negligible (0.5 ± 0.02 nmol d^{-1} mL^{-1}) in cycle 2, and below detection limit of ~1000 ppm) in cycle 3 and subsequent cycles. It can be assumed, based on the lack of methane production, that the reactors did not contain active or growing cells. Therefore, elevated rates of hydrogen gas production were due to the cell material and not active cells of this microorganism. *M. barkeri* can grow autotrophically [34] at a local hydrogen partial pressure of 40 Pa or more [35]. The hydrogen partial pressure in the headspace after the first 2 weeks of cycle 2 (10 ± 4 kPa) was well above this threshold, which therefore could have enabled growth. A culture of *M. barkeri* inoculated into an open circuit reactor containing 80% hydrogen in the headspace was able to produce methane (Fig SI1). Thus the lack of growth was not due to some aspect of reactor construction, oxygen leakage, or toxic compounds in the medium. While reasons for a lack of growth in the presence of hydrogen gas were not identified, it is possible that toxic products were formed or released from the polarized electrode, such as hydroxyl radicals. In contrast, *M. barkeri* respiration was maintained in a biocathodic system in a previous study over multiple cycles [36], possibly due to differences medium composition.

The similar hydrogen production rate using viable or non-viable cells from two phylogenetically distinct microorganisms (*G. sulfurreducens* and *M. barkeri*) suggests that hydrogen production from cell material is not specific to a certain group of microorganisms. However, the lack of hydrogen production from *E. coli* cells indicates that enhanced hydrogen gas production cannot be obtained from all microorganisms. Thus, there is some dependence of

cell type on catalytic activity. Since sterile graphite electrodes did not produce appreciable hydrogen, intact cells or cell debris must have been responsible for the elevated rates of hydrogen production compared to uninoculated controls. Our experiments demonstrated that HER on biologically conditioned graphite cathodes could be sustained for 5 months without further addition of a carbon source or any additional materials to the reactors. This biotic conditioning of the electrodes produced hydrogen gas at rates as high as 3 ± 0.3 μmol^{-1} d^{-1} cm^{-2}, compared to controls (0.09 ± 0.03 μmol^{-1} d^{-1} cm^{-2}), although these are much lower than those possible using precious metal catalysts such as platinum (170 μmol^{-1} d^{-1} cm^{-2}) [23].

6.5.2 Peptides and elements on electrode surfaces

Electrode surfaces were characterized for the presence of peptides and enrichment of different elements in order to investigate these components as possible explanations for the increase in hydrogen production by reactors inoculated with cells. It cannot be concluded, however, that the presence of these molecules is proof of their catalytic activity. Most peptides extracted from the electrode surfaces were derived from metalloenzymes that are involved in cellular electron transfer processes (Table 1). The presence of metals (Fe, Ni, Co, Zn), typical for catalytic centers of identified metalloenzymes, was verified using XPS (Fig. 3). Increased sulfur and nitrogen content is consistent with the presence of proteins. Enzymes that act as oxidoreductases were extracted from all electrodes exposed to live cells. Oxidoreductases facilitate electron transfer from reducing equivalents (e.g. NADH, FADH etc.) to available electron acceptors, usually other proteins in the electron transport chain. However, oxidoreductases can utilize protons as an electron acceptor if no alternative acceptor is available [37].

Nickel and cobalt were found in all reactors exposed to viable cells. These metals have been used as catalysts for HER when attached to an electrode using synthetic ligands [38, 39]. Peptides originating from metalloenzymes binding nickel or cobalt cofactors, such as methanol–corrinoid proteins with cobalamin prosthetic groups [40], were found attached to a poised electrode and could therefore provide a route for electrochemical hydrogen production. Catalytic centers of metalloenzymes could be structurally supported on the electrode surface by protein remnants, which no longer perform their original function. However, the lack of hydrogen production by *M. acetivorans*, a close relative of *M. barkeri* with silenced hydrogenase genes [4], suggests that proteins involved in the utilization of hydrogen were important for hydrogen production from an electrode.

Simple “hydrogenase mimics” consisting of a metallic catalytic center surrounded by stabilizing ligands [41, 42] have been synthetically created, suggesting that only basic requirements must be met to form a catalytically active, hydrogen producing protein-like structure able to accept electrons supplied from an electrode. The peptide sequences identified on the electrode surfaces were derived from proteins that have such requisite catalytic centers, such as FeS [43], and supporting ligands required for hydrogen production similar to these simple synthetic proteins. However, additional work is needed to examine if these are relevant to enhanced hydrogen evolution from these cell materials.

Even though not all of the metals identified are naturally present in the proteins attached to the electrode, such as cobalt for reactors inoculated with *G. sulfurreducens* electrodes, some peptides were derived from proteins with metal binding domains that could facilitate the precipitation of metals present in the trace elements solution on the electrode surface. An alkalinity gradient surrounding the electrode alone cannot explain metal precipitation because the elemental surface composition of sterile controls was not altered by metals in the same way (Fig 3).

The high oxygen content of electrodes (Fig. 3), as observed in XPS spectra, suggests that electrode surfaces were oxidized and contained functional groups which likely facilitated attachment of organic matter such as amino acids, peptides, proteins, and fatty acids. Polarizing graphite electrodes can result in the formation of surface functional groups [44], which are commonly used to attach proteins, such as hydrogenases, to electrodes for hydrogen production/oxidation [8]. Increased attachment of amino acids via surface functional groups could facilitate increased hydrogen production.

6.5.3 Corrosion evidenced by Coulombic recoveries

Coulombic recoveries were calculated to quantify the contribution of electrons derived from the electrode to hydrogen production. When the Coulombic recovery was greater than 100% additional coulombs were used for hydrogen production that could only come from autolytic cell material, or electrode decomposition (corrosion). A similar trend of initially high Coulombic recoveries (1200 ± 500%) followed by a decrease over time to ~100% was observed previously for mixed culture methanogenic biocathodes [23]. The large Coulombic recovery was the result of cells utilizing other reduced compounds in the system, as an alternative electron source for methane formation that was not supplied in the form of current [23]. The number of coulombs obtained from the electrical circuit increased over time, as measured by current uptake (Fig. SI3), suggesting that initially the majority of electrons was obtained from other sources. However, the system adapted over time to use electrons from the electrical circuit as the primary electron source for hydrogen production. Corrosion was enhanced by the use of a highly negative set potential, as there was no hydrogen gas production in open circuit controls.

6.6 Conclusions

Enhanced hydrogen gas evolution was demonstrated using biologically derived cell components of some microorganisms, showing that viable or growing cells are not required from cathodes containing microorganisms in bioelectrochemical systems. Reactors inoculated with viable or non-viable cells from two different phylogenetic classifications produced hydrogen at a higher rate over an extended period of time (5 months) compared to cells provided with a source of organic carbon but no electron acceptor. Intact cells were not detected on any electrode surface after 5 months using SEM. Several different peptides were extracted from electrodes inoculated with live cells, but it was not clear whether these peptides, or other metals identified on the electrode surface using XPS, were responsible for enhanced rates of hydrogen gas production relative to uninoculated controls. Although the precise mechanism was not determined, these results provide insight into reasons for enhanced hydrogen production using biocatalysts and have implications for previously reported conclusions of hydrogen generation from biocathodes.

6.7 Figures

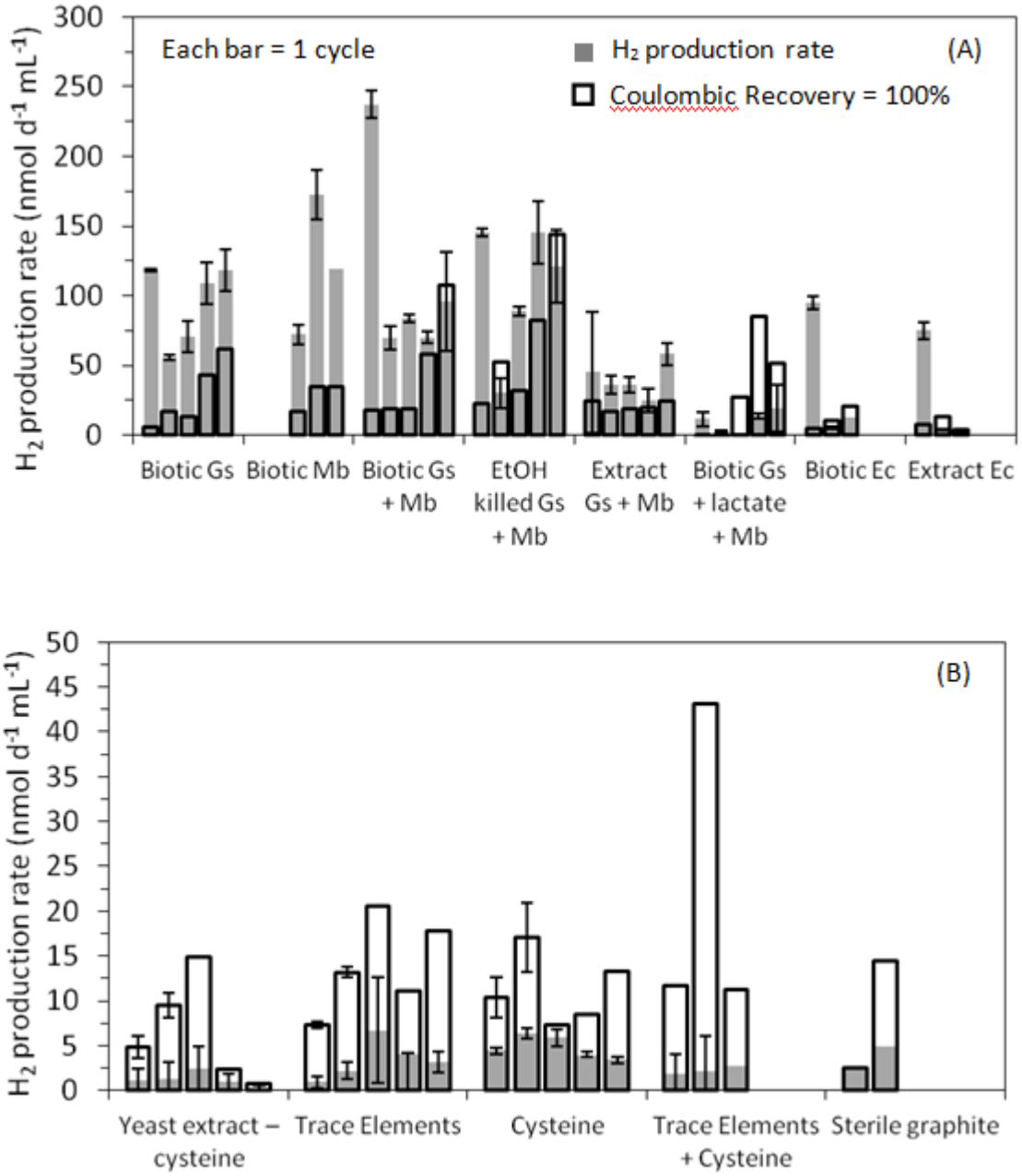

Figure 6.1. Hydrogen and methane production rates from reactors inoculated with (A) pure cultures or synthetic components and (B) biotic and killed cells under different conditions. Gs = *G. sulfurreducens*; Mb = *M. barkeri*; EtOH= Ethanol. Each bar represents 1 cycle (~1 month). Cell extracts were obtained by sonicating cell suspensions for 30 minutes. Methane was not reported as it was negligible after the *M. barkeri* inoculation cycle. *M. barkeri* was inoculated during cycle 3 of the *G. sulfurreducens* reactors for co-culture experiments. The outlined bar

chart represents the hydrogen production rate that would give a Coulombic Recovery of CR=100%. Therefore, rates higher than the outline have a CR>100%. CR values are given in Figure D.3.

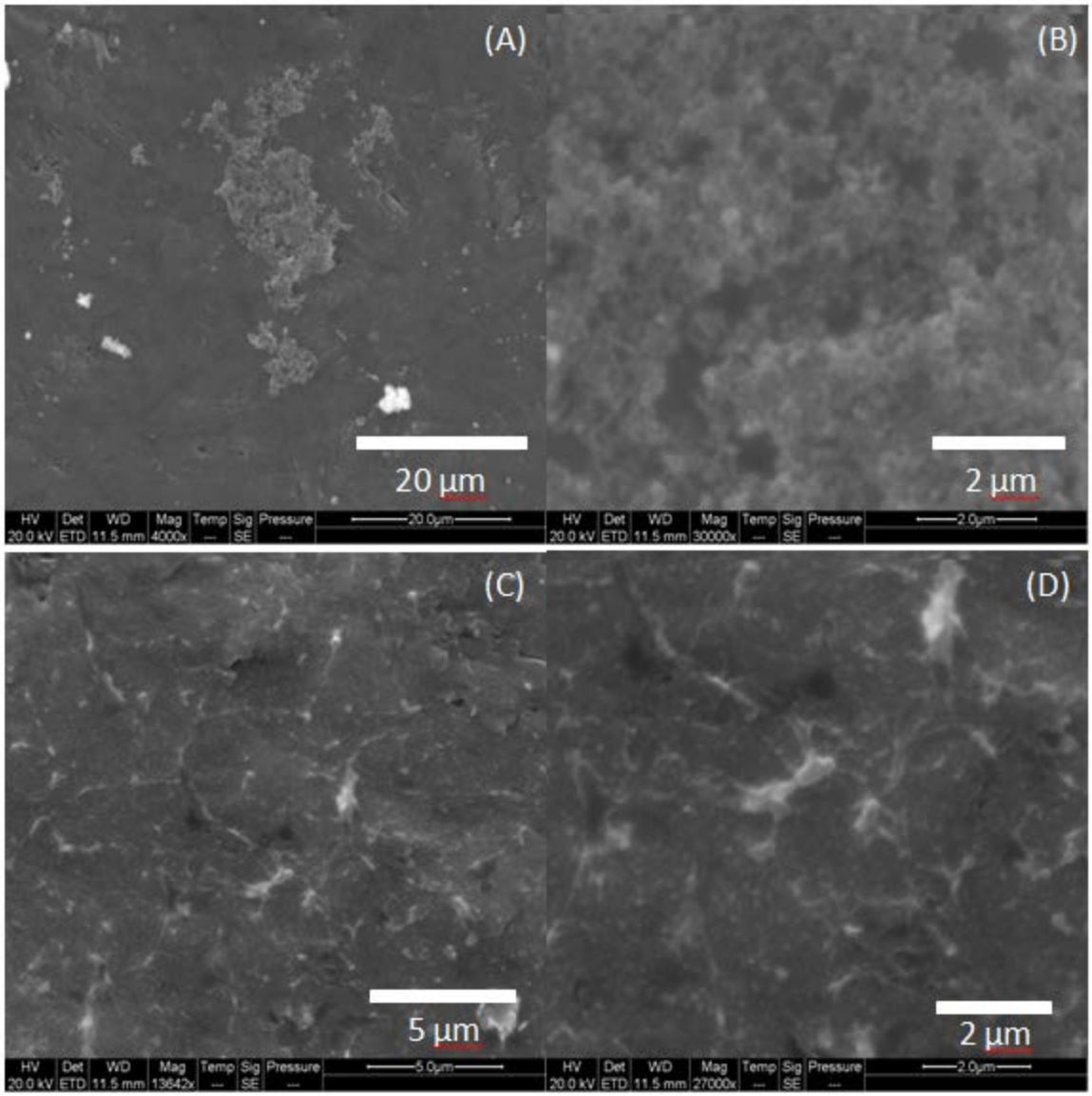

Figure 6.2. Images of the electrode surface of reactors inoculated with (A-B) *M. barkeri* and (C-D) *G. sulfurreducens* obtained using scanning electron microscopy (SEM).

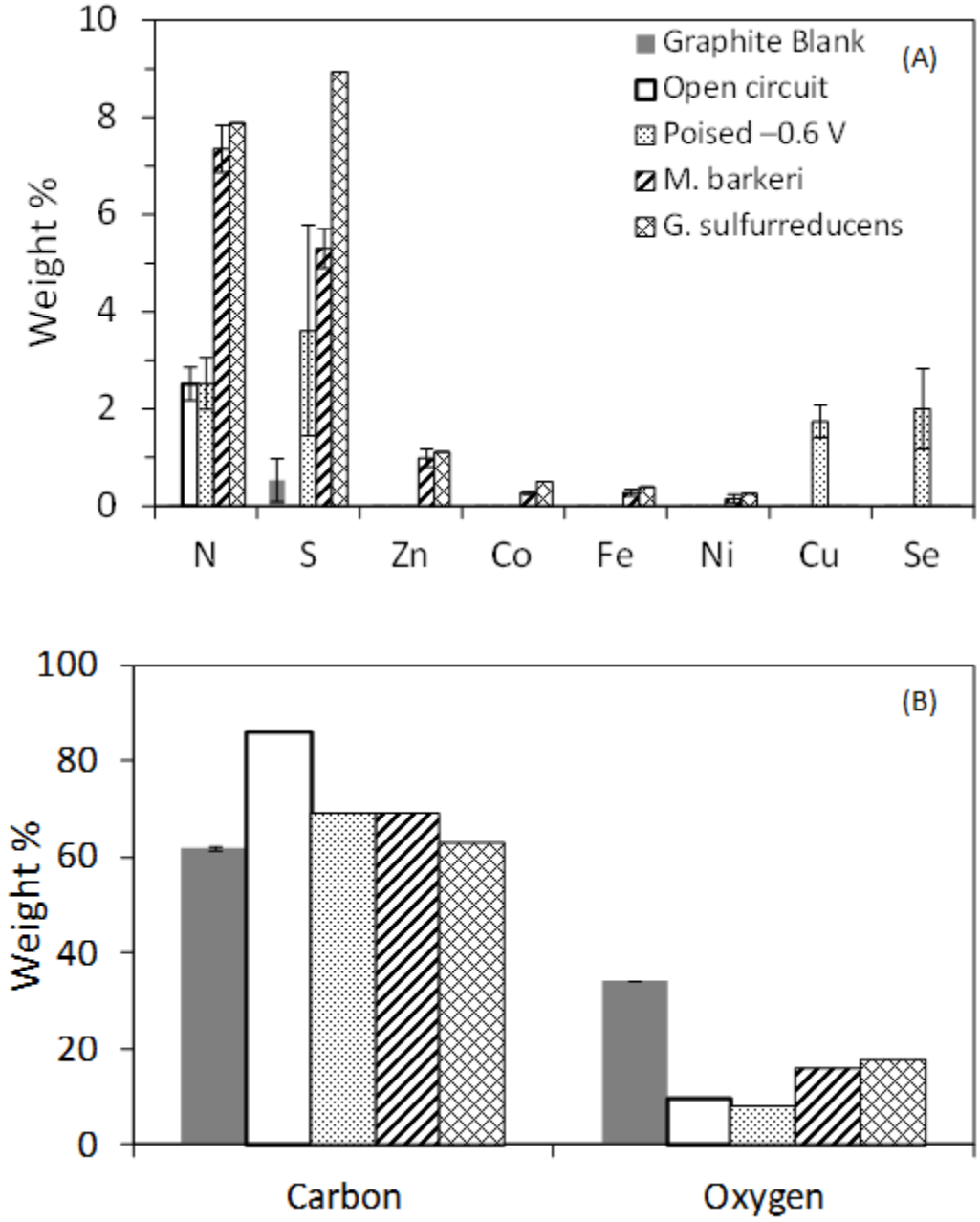

Figure 6.3. Identification of (A) minor elements and (B) carbon and oxygen contents from the electrode surfaces using X-ray photoelectron spectroscopy (XPS). Electrodes exposed to live cells exhibited an increase in elements such as iron, nickel, cobalt, sulfur, and zinc, many of which are present in catalytic centers of enzymes.

6.8 Tables

Table 6.1. Peptides attached to electrode surfaces exposed to different cell types.

Reactor	Protein	Characteristics	Reference[a]
G. sulfurreducens	Ferredoxin oxidoreductase	Reduces ferredoxins which can produce H_2 Contains three 4Fe-4S groups	[45, 46]
	Pyruvate-ferredoxin oxidoreductase	4Fe-4S binding domain Reduces ferredoxins which can produce H_2 Related to integral ferredoxin-like subunits in *H. pylori*	[45, 47]
	Malate dehydrogenase	Proton accepting domain NADH binding domain Membrane associated isoforms	[48]
	Isocitrate dehydrogenase	Metal binding domain (Mn^{2+} and Mg^{2+}) Some membrane associated forms (primarily cytoplasmic)	[45, 49]
	Thioredoxin	Dithiol/disulfide reductase Primarily in cytoplasm	[50]
	2-isopropylmalate synthase	Metal binding domain (Zn^{2+})	[45, 51]
	ABC transporter, periplasmic		
M. barkeri	Methyl-coenzyme M reductase	Contains active nickel cofactor	[52]
	Methanol-corrinoid protein	Contains active cobalt cofactor Zinc required for activity Contain Fe-S groups	[53]
	5,10-MP4T reductase	Hydrogenase-like Without nickel or FeS cofactor	[29]
	Enolase	Metalloenzyme (Mg^{2+} cofactor) Exosomal protein	[54]
	Uncharacterized protein	73.5 kDa	
	Uncharacterized protein	15.9 kDa	

[a]Reference refers to the study(s) where the protein was identified and/or characterized

Table 6.2. Average volatile fatty acid production rate (nmol d^{-1} mL^{-1}) during the final cycle.

	Formate	Acetate
M. barkeri	ND[1]	ND
G. sulfurreducens + EtOH + M. barkeri	6 ± 6	83 ± 8
G. sulfurreducens	0	88 ± 4
G. sulfurreducens + lactate	0	89 ± 17
G. sulfurreducens; No *M. barkeri*	ND	ND
Cysteine	0	0
M. barkeri extract	0	0
G. sulfurreducens extract	0.5 ± 0.5	0
Mixed extract	0	0
Open circuit control	0	0

[1]ND = Not determined.
[2]Propionate and butyrate were not detected in any sample.
[3] Tests in duplicate.

6.9 References

1. Papageorgopoulos, D.C., et al., *CO tolerance of Pd-rich platinum palladium carbon-supported electrocatalysts: Proton exchange membrane fuel cell applications.* J Electrochem Soc, 2002. **149**(11): p. A1400-A1404.
2. Ide, M.S., D.D. Falcone, and R.J. Davis, *On the deactivation of supported platinum catalysts for selective oxidation of alcohols.* J Catal, 2014. **311**(0): p. 295-305.
3. Chin, D.-T. and P.D. Howard, *Hydrogen sulfide poisoning of platinum anode in phosphoric acid fuel cell electrolyte.* J Electrochem Soc, 1986. **133**(12): p. 2447-2450.
4. Guss, A.M., G. Kulkarni, and W.W. Metcalf, *Differences in hydrogenase gene expression between Methanosarcina acetivorans and Methanosarcina barkeri.* J Bacteriol, 2009. **191**(8): p. 2826-2833.

5. Calusinska, M., et al., *The surprising diversity of clostridial hydrogenases: a comparative genomic perspective.* Microbiology, 2010. **156**(6): p. 1575-1588.

6. Madigan, M.T. and J.M. Martinko, *Brock Biology of Microorganisms*. Eleventh ed. 2006, Upper Saddle River, NJ: Pearson Eductation Inc.

7. Wu, L.-F. and M.A. Mandrand, *Microbial hydrogenases: primary structure, classification, signatures, and phylogeny*. FEMS Microbiol Rev, 1993. **104**: p. 243-270.

8. Armstrong, F.A., et al., *Dynamic electrochemical investigations of hydrogen oxidation and production by enzymes and implications for future technology.* Chem Soc Rev, 2009. **38**(1): p. 36-51.

9. Fontecilla-Camps, J.C., et al., *Structure/function relationships of [NiFe]- and [FeFe]-hydrogenases.* Chem Rev, 2007. **107**(10): p. 4273-4303.

10. Lojou, E., *Hydrogenases as catalysts for fuel cells: Strategies for efficient immobilization at electrode interfaces.* Electrochim Acta, 2011. **56**(28): p. 10385-10397.

11. Baffert, C., et al., *Covalent attachment of FeFe hydrogenases to carbon electrodes for direct electron transfer.* Anal Chem, 2012. **84**(18): p. 7999-8005.

12. Coremans, J.M.C.C., J.W. van der Zwaan, and S.P.J. Albracht, *Distinct redox behaviour of prosthetic groups in ready and unready hydrogenase from Chromatium vinosum.* BBA-Protein Struct M, 1992. **1119**(2): p. 157-168.

13. Jungermann, K., et al., *Ferredoxin mediated hydrogen formation from NADPH in a cell-free system of Clostridium kluyveri.* FEBS Lett, 1969. **3**(2): p. 144-146.

14. Thauer, R.K., et al., *Hydrogen formation from NADH in cell-free extracts of Clostridium kluyveri: Acetyl coenzyme A requirement and ferredoxin dependence.* FEBS Lett, 1969. **4**(2): p. 108-112.

15. Sané, S., et al., *Using planktonic microorganisms to supply the unpurified multi-copper oxidases laccase and copper efflux oxidases at a biofuel cell cathode.* Bioresource Technol, 2014. **158**(0): p. 231-238.

16. Geelhoed, J.S. and A.J.M. Stams, *Electricity-assisted biological hydrogen production from acetate by Geobacter sulfurreducens.* Environ Sci Technol, 2010. **45**(2): p. 815-820.

17. Aulenta, F., et al., *Linking bacterial metabolism to graphite cathodes: Electrochemical insights into the H_2-producing capability of Desulfovibrio sp.* ChemSusChem, 2012. **5**(6): p. 1080-1085.

18. Croese, E., et al., *Analysis of the microbial community of the biocathode of a hydrogen-producing microbial electrolysis cell.* Appl Microbiol Biotechnol, 2011. **92**(5): p. 1083-1093.

19. Batlle-Vilanova, P., et al., *Assessment of biotic and abiotic graphite cathodes for hydrogen production in microbial electrolysis cells.* Int J Hydrogen Energ, 2014. **39**(3): p. 1297-1305.

20. Rozendal, R.A., et al., *Hydrogen production with a microbial biocathode.* Environ Sci Technol, 2008. **42**(2): p. 629-634.

21. Fu, Q., et al., *Bioelectrochemical analyses of a thermophilic biocathode catalyzing sustainable hydrogen production.* Int J Hydrogen Energ, 2013. **38**(35): p. 15638-15645.

22. Villano, M., et al., *Bioelectrochemical hydrogen production with hydrogenophilic dechlorinating bacteria as electrocatalytic agents.* Bioresource Technol, 2011. **102**(3): p. 3193-3199.

23. Siegert, M., et al., *Comparison of non-precious metal cathode materials for methane production by electromethanogenesis.* ACS Sus Chem Eng, 2014.

24. Murray, P.A. and S.H. Zinder, *Nutritional requirements of Methanosarcina sp. strain TM-1.* Appl Environ Microbiol, 1985. **50**(1): p. 49-55.

25. Sowers, K.R., S.F. Baron, and J.G. Ferry, *Methanosarcina acetivorans sp. nov., an acetotrophic methane-producing bacterium isolated from marine sediments.* Appl Environ Microbiol, 1984. **47**(5): p. 971-978.

26. Call, D.F. and B.E. Logan, *Lactate oxidation coupled to iron or electrode reduction by Geobacter sulfurreducens PCA.* Appl Environ Microbiol, 2011.

27. Sugnaux, M., et al., *Probing electron transfer with Escherichia coli: A method to examine exoelectronics in microbial fuel cell type systems.* Bioresource Technology, 2013. **148**(0): p. 567-573.

28. Leang, C., et al., *Engineering Geobacter sulfurreducens to produce a highly cohesive conductive matrix with enhanced capacity for current production.* Energy & Environmental Science, 2013. **6**(6): p. 1901-1908.

29. Kates, M., D. Kushner, and A. Matheson, *The Biochemistry of Archaea (Archaebacteria)*. 1993: Elsevier. 592.

30. Kenealy, W.R. and J.G. Zeikus, *One-carbon metabolism in methanogens: Evidence for synthesis of a two-carbon cellular intermediate and unification of catabolism and anabolism in Methanosarcina barkeri.* J Bacteriol, 1982. **151**(2): p. 932-941.

31. Speers, A.M. and G. Reguera, *Electron donors supporting growth and electroactivity of Geobacter sulfurreducens anode biofilms.* Appl Environ Microbiol, 2012. **78**(2): p. 437-444.

32. Helmus, R.A., et al., *Growth advantage in stationary-phase (GASP) phenotype in long-term survival strains of Geobacter sulfurreducens.* FEMS Microbiology Ecology, 2012. **79**(1): p. 218-228.

33. Finkel, S.E., *Long-term survival during stationary phase: evolution and the GASP phenotype.* Nature Reviews. Microbiology, 2006. **4**(2): p. 113-20.

34. Blaut, M., *Metabolism of methanogens.* Anton Leeuw, 1994. **66**(1-3): p. 187-208.

35. Boone, D.R., et al., *Effects of hydrogen pressure during growth and effects of pregrowth with hydrogen on acetate degradation by Methanosarcina species.* Appl Environ Microbiol, 1987. **53**(1): p. 83-87.

36. Lohner, S.T., et al., *Microbial electrosynthesis by direct uptake and metabolism of cathodic electrons by the Archaeon Methanococcus maripaludis.* ISME J, 2014. **in press**.

37. Sapra, R., K. Bagramyan, and M.W.W. Adams, *A simple energy-conserving system: Proton reduction coupled to proton translocation.* Proc Natl Acad Sci USA, 2003. **100**(13): p. 7545-7550.

38. Stewart, M.P., et al., *High catalytic rates for hydrogen production using nickel electrocatalysts with seven-membered cyclic diphosphine ligands containing one pendant amine.* J Am Chem Soc, 2013. **135**(16): p. 6033-6046.

39. Sun, Y., et al., *Electrodeposited cobalt-sulfide catalyst for electrochemical and photoelectrochemical hydrogen generation from water.* J Am Chem Soc, 2013. **135**(47): p. 17699-17702.

40. Nelson, D.L. and M.M. Cox, *Lehninger Principles of Biochemistry*. 5th ed, ed. W.H. Freeman. 2008.

41. Li, C.-B., et al., *Interface-directed assembly of a simple precursor of [FeFe]-H_2ase mimics on CdSe QDs for photosynthetic hydrogen evolution in water.* Energ Environ Sci, 2013. **6**(9): p. 2597-2602.

42. Nann, T., et al., *Water splitting by visible light: A nanophotocathode for hydrogen production.* Angew Chem Int Edit, 2010. **49**(9): p. 1574-1577.

43. Holm, R.H., P. Kennepohl, and E.I. Solomon, *Structural and functional aspects of metal sites in biology.* Chem Rev, 1996. **96**(7): p. 2239-2314.

44. Sloan, F.E. and J.B. Talbot, *Corrosion of graphite-fiber-reinforced composites I — Galvanic coupling damage.* Corrosion, 1992. **48**(10): p. 830-838.

45. Nagarajan, H., et al., *De novo assembly of the complete genome of an enhanced electricity-producing variant of Geobacter sulfurreducens using only short reads.* PLoS ONE, 2010. **5**(6): p. e10922.

46. Dörner, E. and M. Boll, *Properties of 2-oxoglutarate:ferredoxin oxidoreductase from Thauera aromatica and its role in enzymatic reduction of the aromatic ring.* J Bacteriol, 2002. **184**(14): p. 3975-3983.

47. Hughes, N.J., et al., *Helicobacter pylori porCDAB and oorDABC genes encode distinct pyruvate:flavodoxin and 2-oxoglutarate:acceptor oxidoreductases which mediate electron transport to NADP.* J Bacteriol, 1998. **180**(5): p. 1119-1128.

48. Methe, B.A., et al., *Genome of Geobacter sulfurreducens: Metal reduction in subsurface environments.* Science, 2003. **302**(5652): p. 1967-1969.

49. Möller-Zinkhan, D. and R. Thauer, *Membrane-bound NADPH dehydrogenase- and ferredoxin: NADP oxidoreductase activity involved in electron transport during acetate oxidation to CO_2 in Desulfobacter postgatei.* Arch Microbiol, 1988. **150**(2): p. 145-154.

50. Arnér, E.S.J. and A. Holmgren, *Physiological functions of thioredoxin and thioredoxin reductase.* Eur J Biochem, 2000. **267**(20): p. 6102-6109.

51. Koon, N., C.J. Squire, and E.N. Baker, *Crystal structure of LeuA from Mycobacterium tuberculosis, a key enzyme in leucine biosynthesis.* Proc Natl Acad Sci USA, 2004. **101**(22): p. 8295-8300.

52. Ermler, U., et al., *Crystal structure of methyl-coenzyme M reductase: The key enzyme of biological methane formation.* Science, 1997. **278**(5342): p. 1457-1462.

53. Sauer, K. and R.K. Thauer, *Methanol: coenzyme M methyltransferase from Methanosarcina barkeri.* Eur J Biochem, 1997. **249**(1): p. 280-285.

54. Maeder, D.L., et al., *The Methanosarcina barkeri genome: Comparative analysis with Methanosarcina acetivorans and Methanosarcina mazei reveals extensive rearrangement within Methanosarcinal genomes.* J Bacteriol, 2006. **188**(22): p. 7922-7931.

Appendix A

Extracellular Palladium Nanoparticle Production Using *Geobacter sulfurreducens*

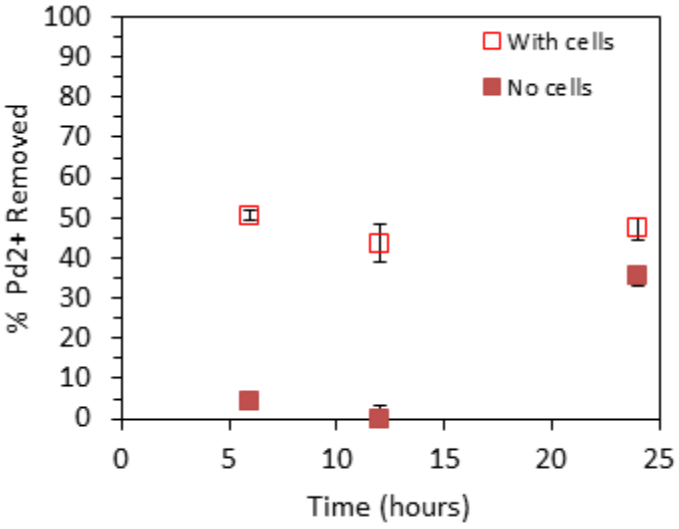

Figure A.1. Palladium reduction with and without cells incubated for different lengths of time with 1% H_2 in the headspace. Starting concentration of palladium was 100 mg/L Pd(II). Six hours was chosen as the incubation time for subsequent tests because it gave low abiotic reduction and similar removal to other time points.

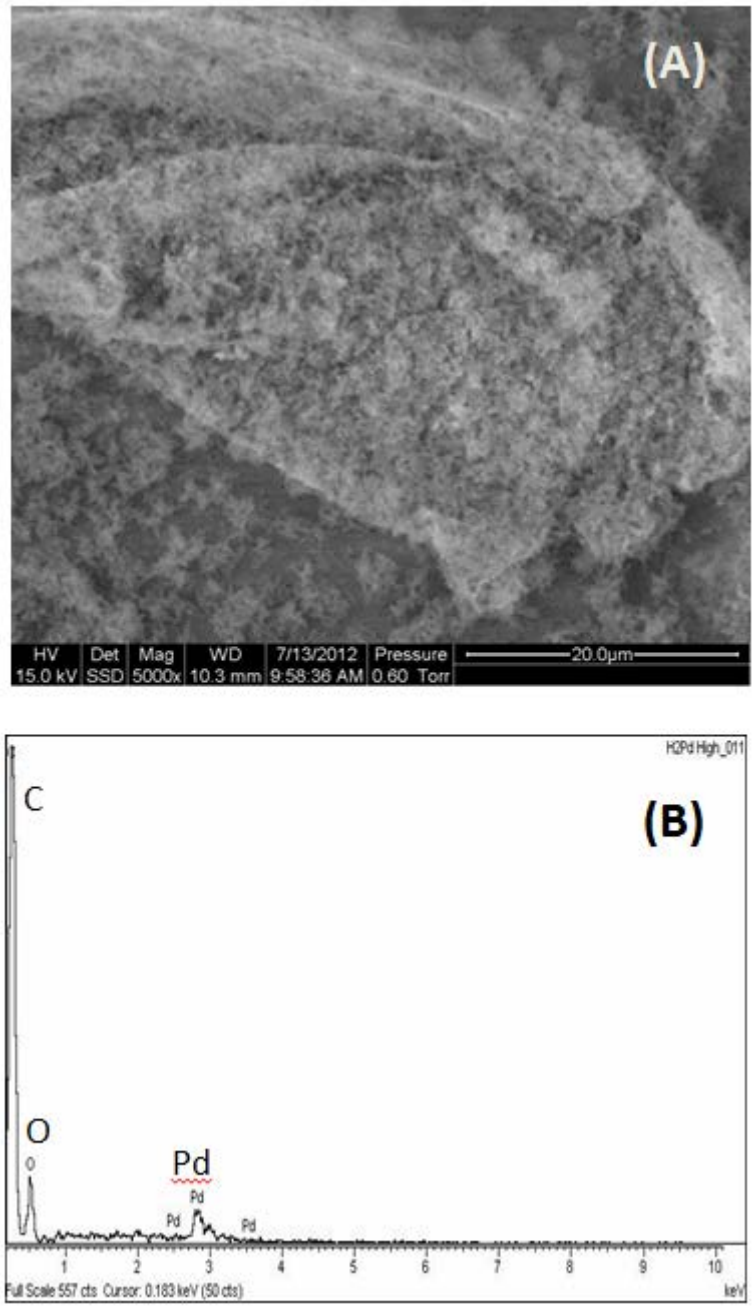

Figure A.2. (A) SEM of *G. sulfurreducens* aggregate with palladium reduction on the surface of the cells. (B) EDS spectrum of culture confirming that the particles on surface are palladium.

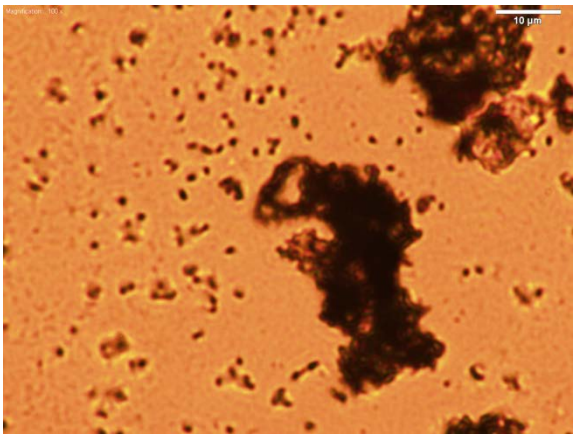

Figure A.3. Image of Pd(0) reduced abiotically. Particles are approximately 1 µm and aggregates are larger than 10 µm. Increased size and aggregation of palladium decreases the available catalytic surface area.

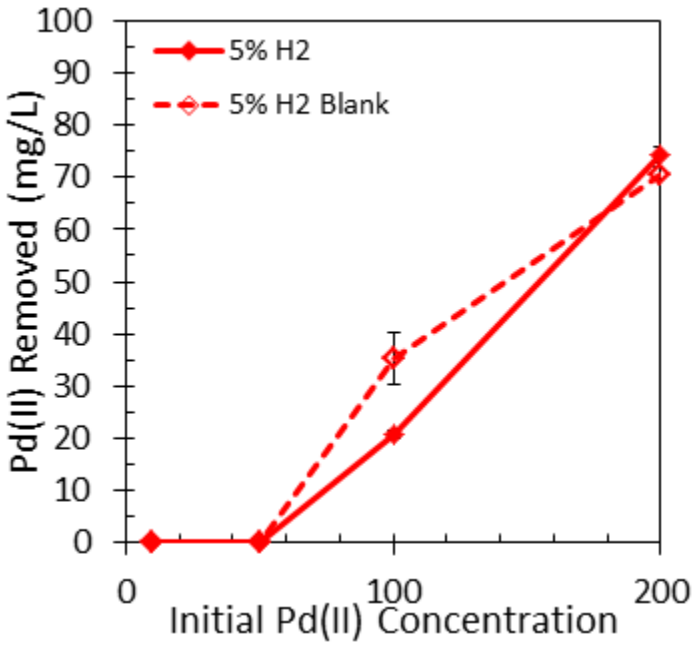

Figure A.4. Palladium removal with 5% H_2 in the headspace. Removal by *G. sulfurreducens* suspensions were less than or equal to abiotic controls leading to uncontrolled abiotic growth of palladium particles.

Appendix B

Exoelectrogenic Biofilm as a Template for Sustainable Formation of a Catalytic Mesoporous Structure

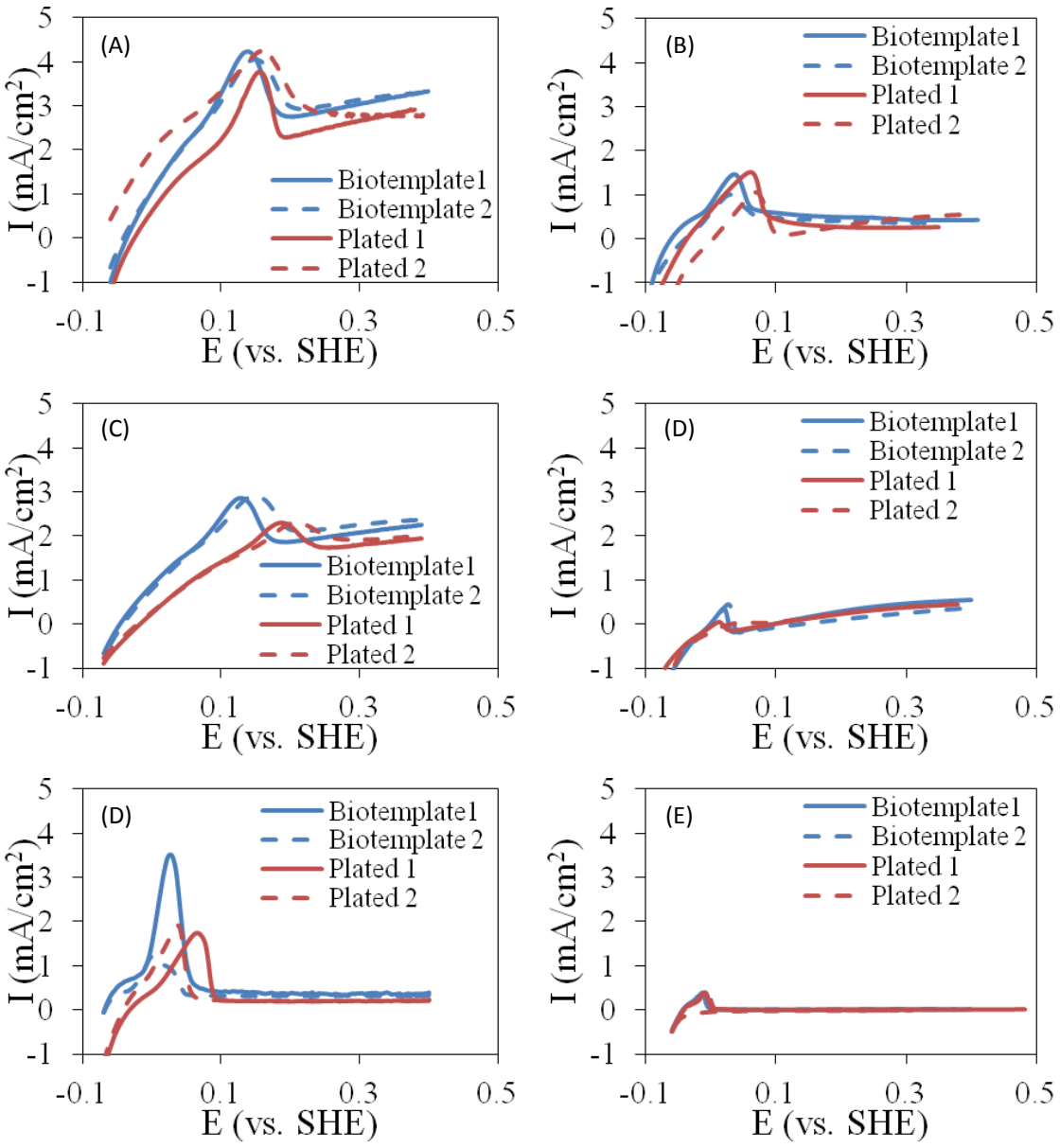

Figure B.1. Current density of individual electrodes during RDE tests at 2000 rpm sparged with (A) hydrogen and (B)nitrogen; 1000 rpm sparged with (C) hydrogen and (D) nitrogen; and 0 rpm sparged with (D) hydrogen and (E) nitrogen.

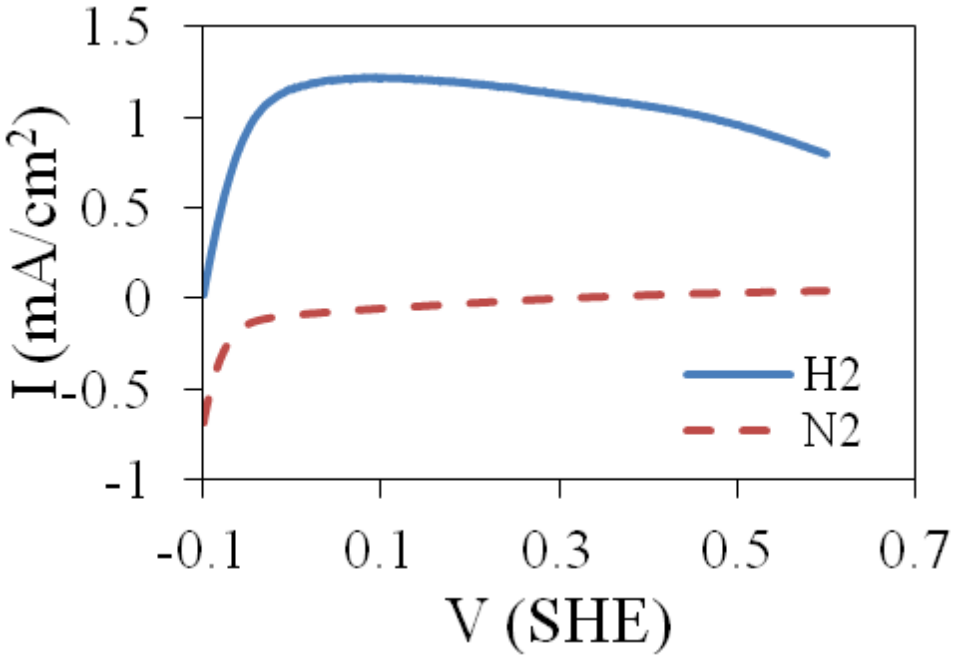

Figure B.2. Voltammograms of biotemplated electrodes that were pyrolyzed, but did not undergo the subsequent oxidation step generated with an RDE at 1000 rpm in 0.1 M H_2SO_4. Oxidation of the carbon within the structure is important and results in approximately double the current density (2.3 mA/cm^2).

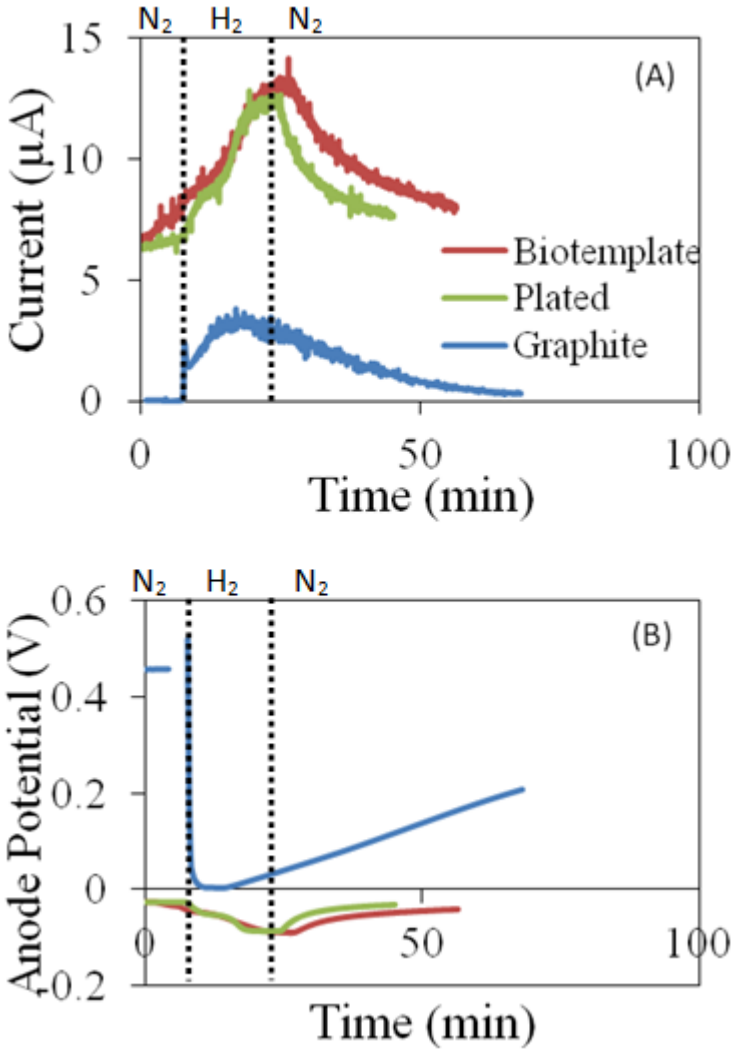

Figure B.3. (A) Current across a 1 kΩ resistor and (B) anode potential (vs. SHE) of electrodes operated in a hydrogen fuel cell without potentiostatic control to test electrical connectivity between the palladium layer and the graphite support. Reactors were alternately sparged with nitrogen and hydrogen to show the catalytic response of the reactors in the presence and absence of hydrogen. Electrons liberated during hydrogen oxidation were transferred through the circuit to the cathode showing that the palladium layer is electrically connected to the graphite support.

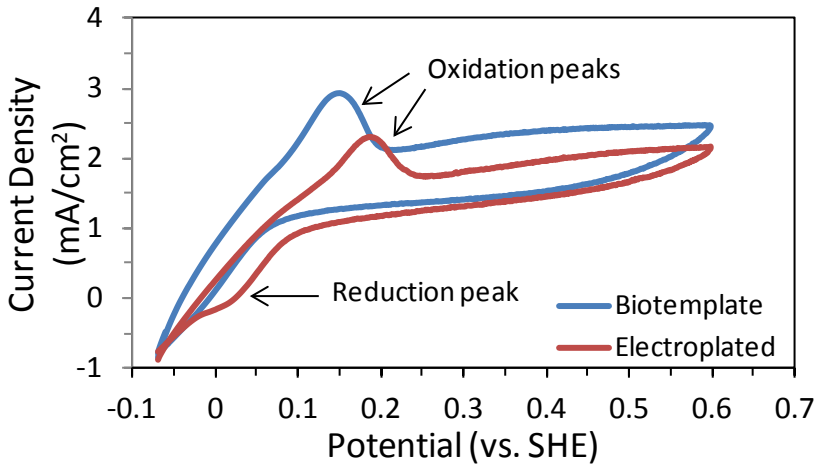

Figure B.4. Cyclic voltammograms of a biotemplated and electroplated electrode. The absence of pronounced reduction peak in the reverse scan suggests that the non-catalytic oxidative peak is due to corrosion and not a redox reaction. Curves were generated at 1mV/s scan rate and 1000 rpm in 0.1 M H_2SO_4.

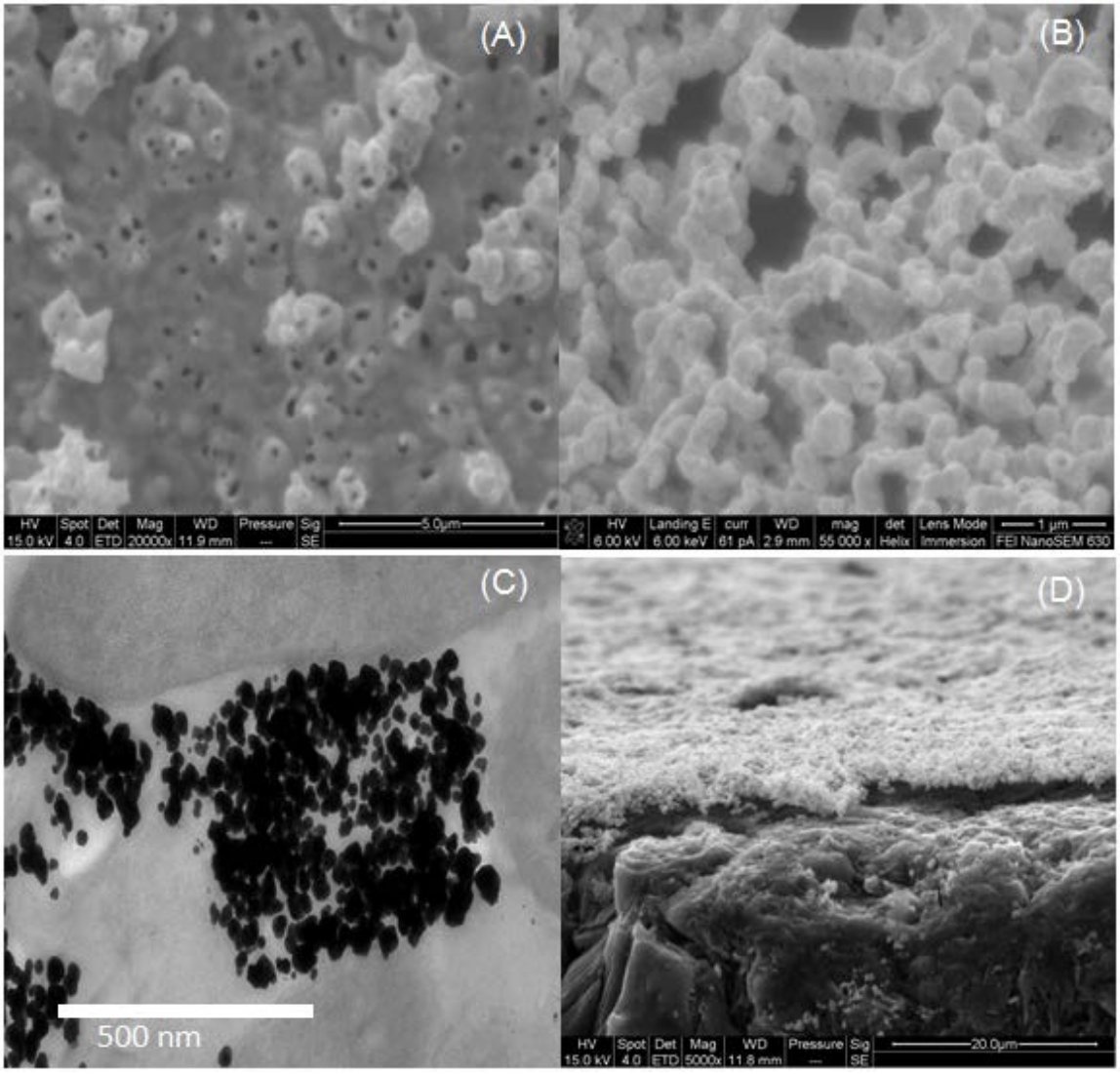

Figure B.5. High magnification images of (A) electrochemically formed structure (20,000 ×) and (B) biotemplated mesoporous structure (55,000 ×). (C) TEM image of an ultra-microtomed (70 nm) *G. sulfurreducens* biofilm showing palladium reduction within the biofilm as a precursor for mesoporous structure formation. (D) Low maginification image of the mesoporous palladium layer on the graphite support post-processing.

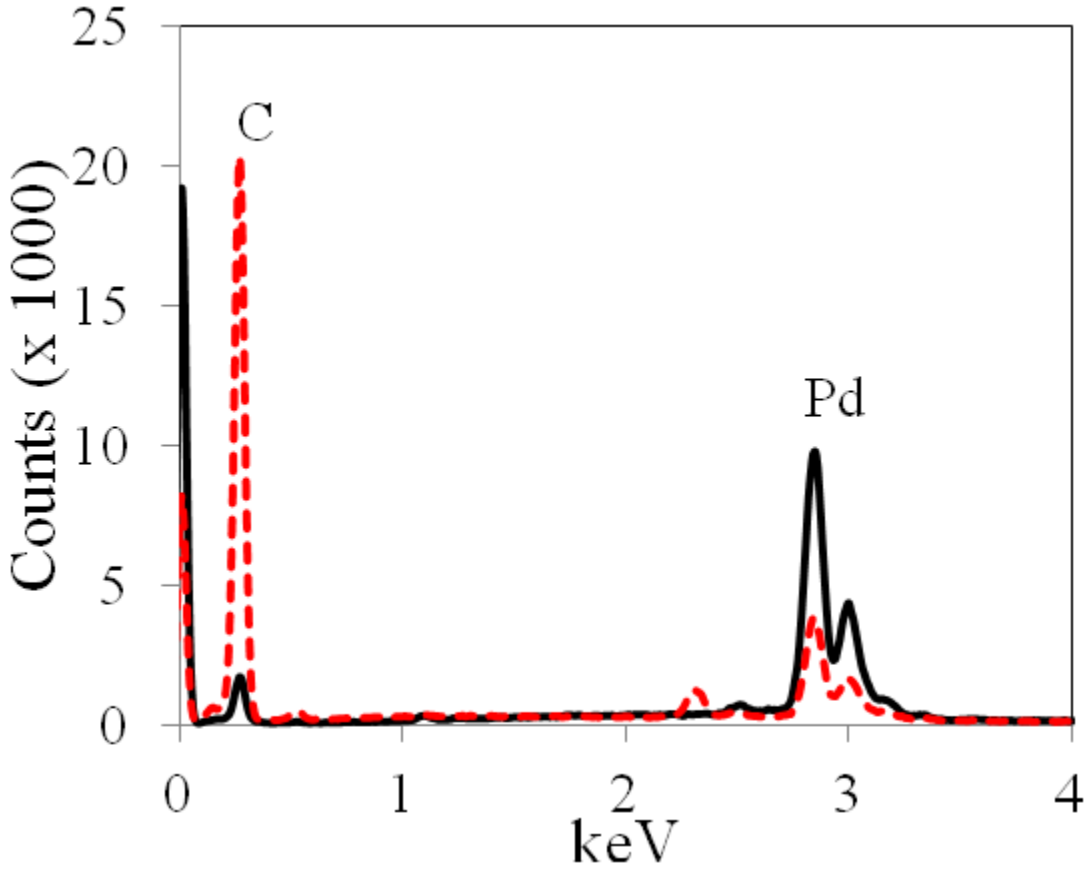

Figure B.6. Energy dispersive x-ray spectroscopy (EDS) spectra of biotemplated Pd structure composed of 50% Pd and 50% C after pyrolysis alone at 450°C (-------) and composed of 97% Pd after pyrolysis at 450°C and oxidation at 450°C in air for 2 hours (———). The oxidation step is important to remove excess carbon formed from cell material during pyrolysis and expose more catalytically active Pd.

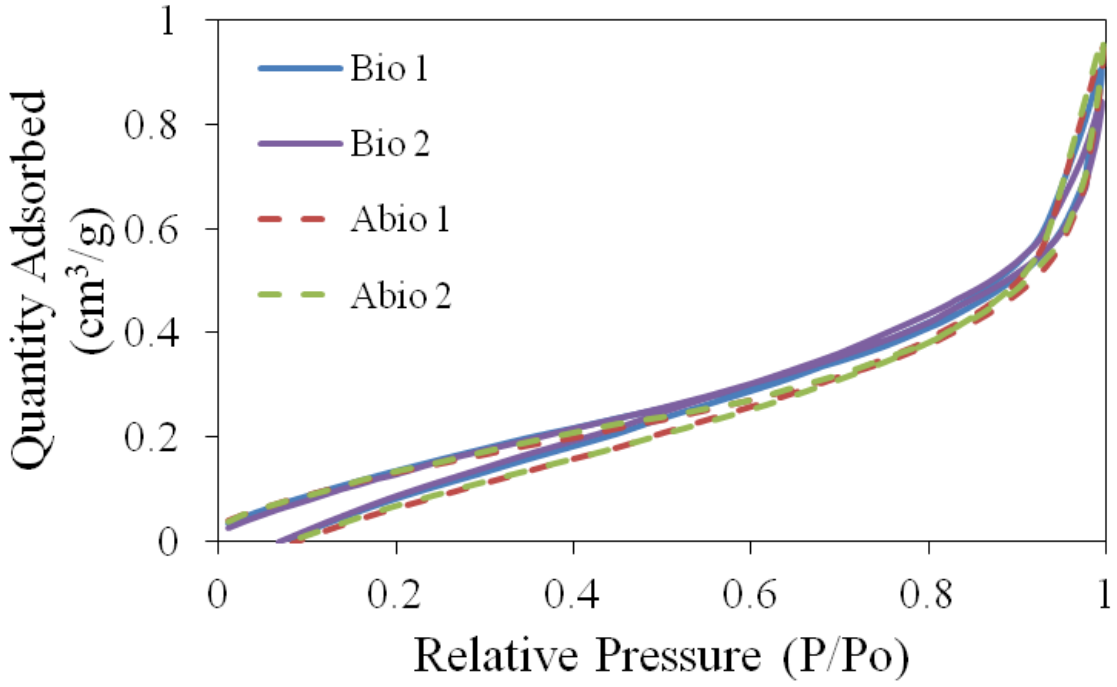

Figure B.7. BET nitrogen adsorption isotherms for the different samples.

Appendix C

Biotemplated Palladium Catalysts can be Stabilized on Different Support Materials

C.1 Shear Stress Calculations

The shear stress imparted by a rotating disc electrode used in these experiments is calculated as [1]:

$$\Gamma_{avg} = \frac{\tau_{avg}}{\mu} = \frac{du}{dz} = \frac{\omega R}{3Z} \qquad \text{Equation (1)}$$

where R is the radius of the disk (m), Z is the height above the bottom of the electrochemical cell (m), and ω is the angular velocity (rad/s).

The wall shear stress of fluid flowing by a pipe is calculated as[1]:

$$\Gamma_{avg} = \frac{32Q}{\pi} D^3 \qquad \text{Equation (2)}$$

where Q is the volumetric flowrate (m^3/s), and D is the pipe diameter (m). A formic acid fuel cell constructed for high power densities[2] was operated with a flowrate of and had an active surface area of $5cm^2$ (2.23 cm x 2.23 cm). Assuming a total chamber volume of 0.25 cm^3 and a length of 2.23 cm, the effective diameter of a pipe of similar volume would be 0.36 cm.

The shear stress through porous media is described by[3]:

$$\Gamma_{avg} = \frac{3n+1}{4n} \frac{12G}{\rho\sqrt{150k\varepsilon}} \qquad \text{Equation (3)}$$

$$G = \rho V_0 \qquad \text{Equation (4)}$$

$$k = \frac{D_p^2 \varepsilon^3}{(150-\varepsilon)^2} \qquad \text{Equation (5)}$$

where ρ is the density of water, ε is the fractional void volume, V_0 is the apparent velocity in the system, k is the permeability, and D_p is the particle diameter. The fluid is assumed to be Newtonian, so the power law coefficient, n, is assumed to be 1 in Eq 3. The fractional void volume was assumed to be 0.7.

Shear stress (τ) is calculated by multiplying the shear rate by the dynamic viscosity, μ (kg/s-m).

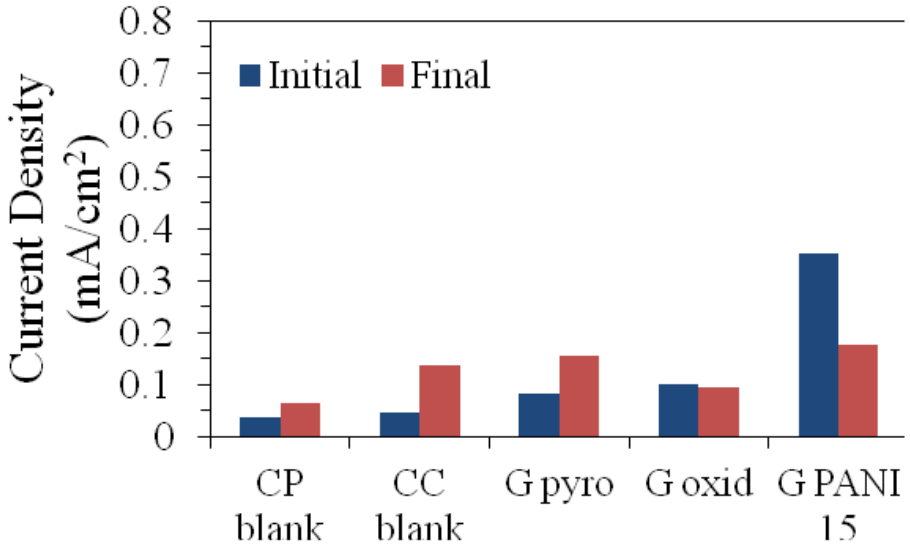

Figure C.1. Current densities produced by support materials without palladium at 0.6 V. The scale here is ten times smaller than when palladium was used.

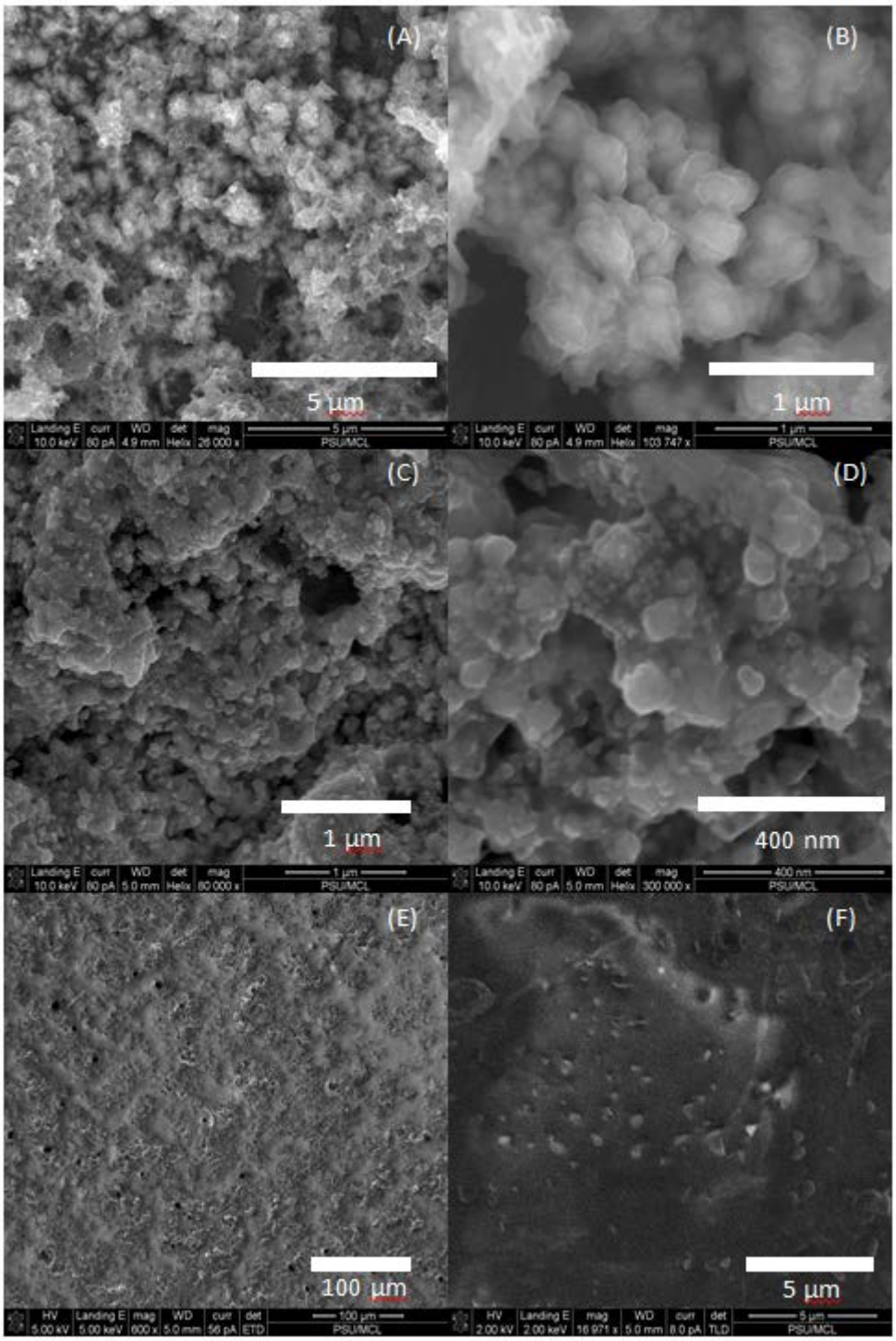

Figure C.2. Porous palladium structures formed on graphite electrodes and coated with (A-B) PANI 15, (C-D) PDMS 5%, (E-F) Nafion 5%. The catalyst layer could not be examined when coated by the 5% Nafion solution due to the inability of the electron beam to penetrate the layer without destroying it.

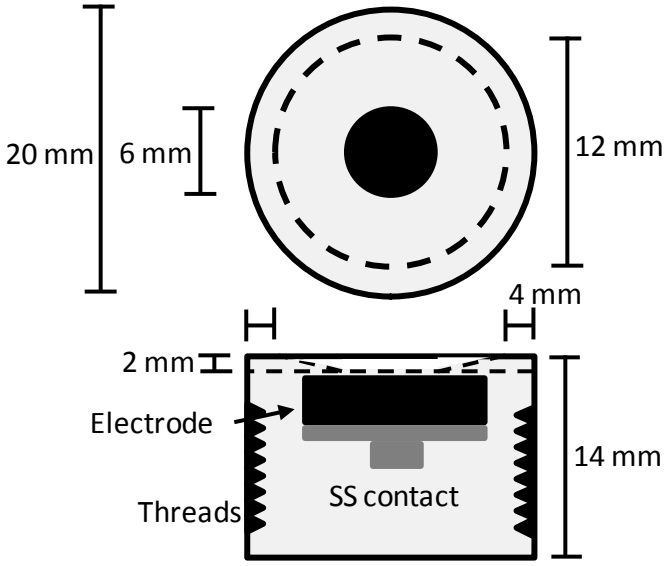

Figure C.3. Schematic of modified RDE to allow direct testing of different support materials. The cap is made from Teflon and the contact between the electrode and the RDE is made from stainless steel. The resistance between the surface of the electrode and the RDE is less than 1 Ω for all tests.

1. Munson, B., et al., *Fundamentals of Fluid Mechanics, Sixth Edition*. 6th ed. 2009: John Wiley and Sons.

2. Zhu, Y., S.Y. Ha, and R.I. Masel, *High power density direct formic acid fuel cells.* J Power Sources, 2004. **130**(1–2): p. 8-14.

3. Marshall, R.J. and A.B. Metzner, *Flow of viscoelastic fluids through porous media.* Ind Eng Chem Fund, 1967. **6**(3): p. 393-400.

Appendix D

Hydrogen Evolution Catalyzed by Viable and Non-Viable Cells on Biocathodes

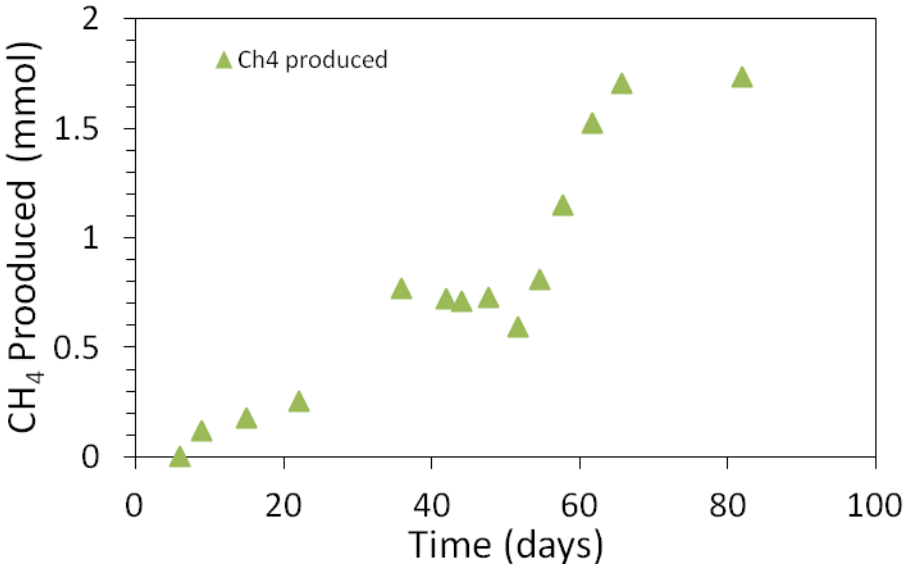

Figure D.1. Methane production of *M. barkeri* cultured in an unpoised reactor with 80% (v/v) hydrogen in the headspace to ensure that cells were able to grow in the reactor configuration used in this study.

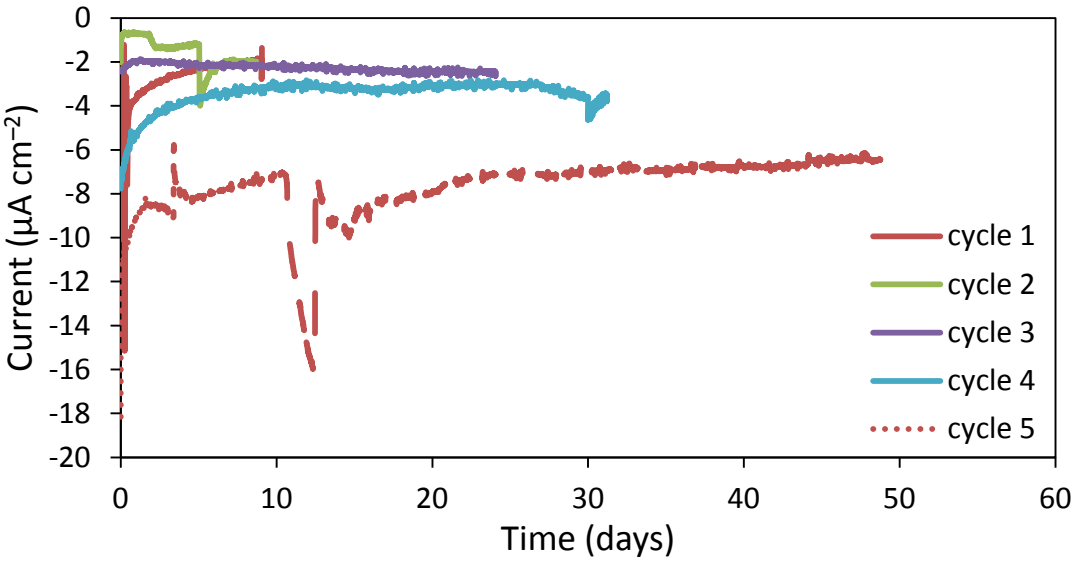

Figure D.2. Current uptake by *G. sulfurreducens* reactors during each cycle. The current being taken from the reactor for hydrogen production decreases between cycle 1 and 2, but then steadily increases for the duration of the experiment.

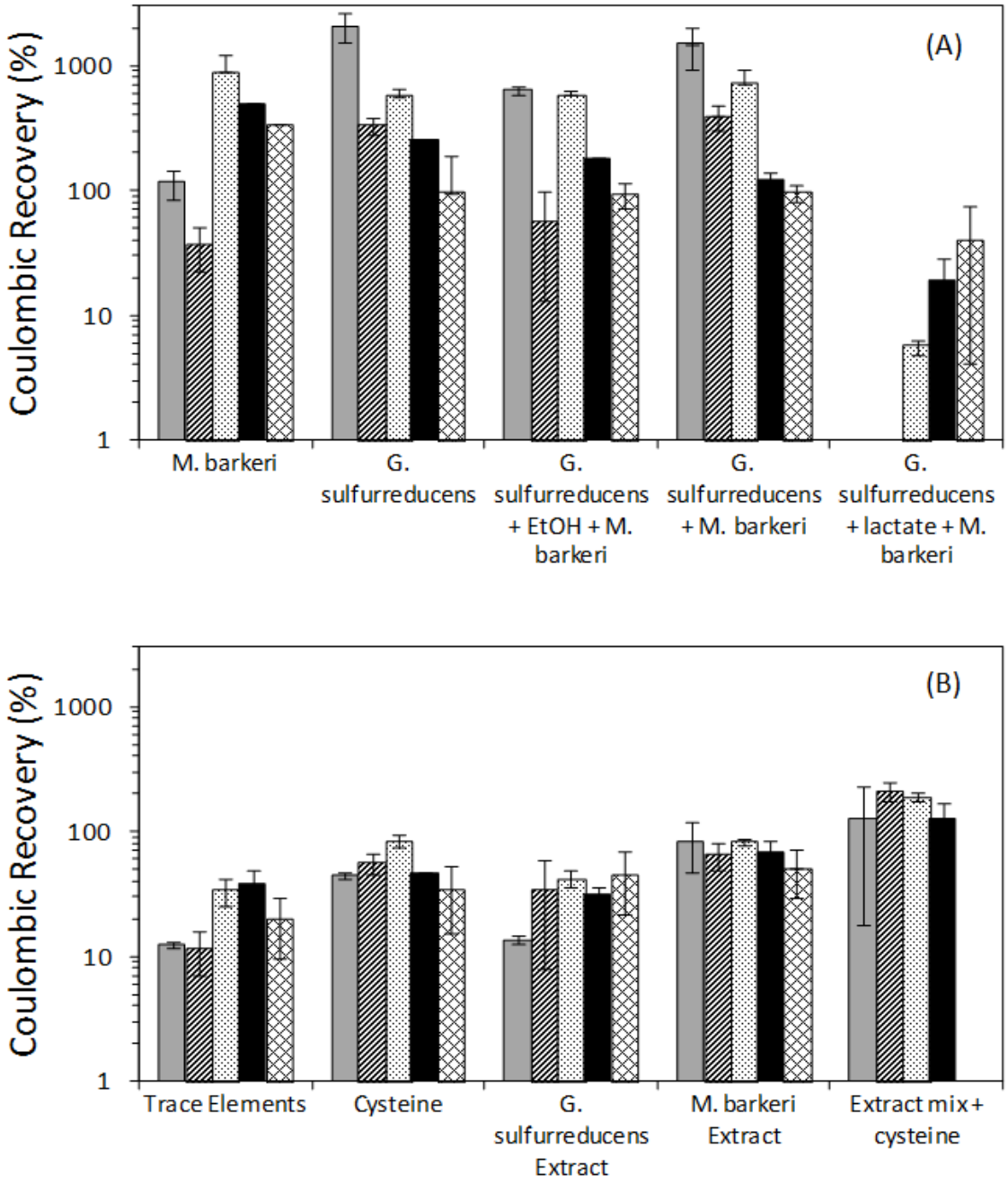

Figure D.3. Coulombic recoveries from reactors (A) inoculated with *G. sulfurreducens* and/or *M. barkeri* and (B) killed or no microorganisms. Recoveries were calculated based on the ratio of Coulombs contained in the headspace gas and the Coulombs of current taken up at the electrode, as measured by the potentiostat. CRs in reactors inoculated with living cells far exceed 100% during an inoculation cycle, but decreased to ~100% after the fifth cycle due to an increase in current uptake at the electrode. The hydrogen production rate remained steady independent of the Coulombic recovery (Figure 6.1A).

VITA

Matthew D. Yates

Doctor of Philosophy in Environmental Engineering, Department of Civil and Environmental Engineering, The Pennsylvania State University, University Park, PA, 08/2011 – 08/2014 (expected). Advisor: Dr. Bruce E. Logan

Master of Science in Environmental Engineering, Department of Civil and Environmental Engineering, The Pennsylvania State University, University Park, PA, 08/2009 – 08/2011 Advisor: Dr. Bruce E. Logan

Bachelor of Science in Biological Systems Engineering, Department of Biological and Agricultural Engineering, The University of California, Davis, Davis, CA, 09/2005 – 05/2009.

AWARDS

- National Science Foundation Graduate Research Fellowship, 2010-2013
- Outstanding Undergraduate student in Biological and Agricultural Engineering at the University of California, Davis, June 2009
- Howard R Murphy Scholarship for Biological Systems Engineers at the University of California, Davis, 2009